CHEMOPREVENTIVE PROPERTIES OF OKINAWAN BIORESOURCES

沖縄産生物資源の化学的予防機能に関する研究

MD. SHAHINOZZAMAN

2019

Chemopreventive Properties of Okinawan Bioresources

沖縄産生物資源の化学的予防機能に関する研究

A dissertation submitted to

The United Graduate School of Agricultural Sciences,

Kagoshima University, Japan

under the requirements for the Degree of

Doctor of Philosophy

MD. SHAHINOZZAMAN

March, 2019

ACKNOWLEDGEMENTS

I would like to express the deepest gratitude to Prof. Shinkichi Tawata who was the reason for the success of this study which was impossible without his financial support and supervision. I am also thankful to my advisor Prof. Md. Amzad Hossain for his encouragement and comprehensive advice until this work came to existence. Special gratitude to Associate Prof. Takahiro Ishii who extended immense support to accomplish all the experiments successfully. My heartfelt thanks and gratitude to Prof. Hisanori Tamaki, Kagoshima University for making fruitful comments and providing encouragement every time to proceed my researches duly.

I am also grateful to Prof. Ryo Takano and Associate Prof. Masakazu Fukuta, University of the Ryukyus. Sincere thanks to the thesis reviewers Prof. De-Xing Hou, Kagoshima University, and Prof. Kensaku Takara, University of the Ryukyus. My appreciation also goes to Mr. Shinichi Gima, Drs. Mohammad A. Halim, Nozomi Taira, Binh C. Q. Nguyen, and Md. Zahorul Islam for their invaluable help during this study.

My thankfulness to the office staffs of Faculty of Agriculture, University of the Ryukyus and the United Graduate School of Agricultural Sciences, Kagoshima University.

Finally, I would like to convey heartfelt thanks and gratitude to my parents, younger brother, and sister. They all keep me going ahead for getting the success in my life. Special thanks to my wife, Most. Rozina Parvin, and our only daughter, Shantuma Shahin Ridha, who accompany and inspire me always with their beloved support.

TABLE OF CONTENTS

Acknowledgements……..iii
Table of Contents……iv
List of Tables…….....vi
List of Figures……viii
Abbreviations……xiv
Abstract in English……...xviii
Abstract in Japanese…….....xx

Chapter I: General Introduction 1–28

1.1. Natural resource: A novel reservoir of wonder drugs 1

1.2. Therapeutic applications of natural products: A practical perspective 3

1.3. Bioresources in Okinawa: Terrestrial and marine products 5

1.4. Health-promoting benefits of Okinawan bioresources 7

1.5. Inflammation and its role in human health and diseases 10

1.6. Inducible nitric oxide synthase (iNOS) and cyclooxygenase-2 (COX-2): Two major pro-inflammatory enzymes 12

1.7. Melanogenesis 15

1.8. P21-activated kinase 1 (PAK1) 16

1.9. Type 2 diabetes 17

1.10. Alzheimer's disease 19

1.11. Computational approaches in modern drug discovery 21

1.12. Molecular docking: A powerful tool for structure-based drug design 23

1.13. Motivation and objective of this study 27

Chapter II: Anti-inflammatory and Anti-melanogenic Effects of *Alpinia zerumbet* Leaf-derived Major Components 29–54

2.1. Summary 29

2.2. Introduction 30

2.3. Materials and methods 32

2.4. Results and discussion 40

2.5. Conclusion 46

Chapter III: Cytotoxic and Anti-inflammatory Bioactive Compounds from the Leaves of *Ardisia sieboldii* 55–82

3.1. Summary 55

3.2. Introduction 56

3.3. Materials and methods 57

3.4. Results and discussion 65

3.5. Conclusion 71

Chapter IV: Cytotoxic Desulfated Saponin from *Holothuria atra* Predicted to Have Inhibitory Effects on PAK1 83–107

4.1. Summary 83

4.2. Introduction 83

4.3. Materials and methods 85

4.4. Results and discussion 91

4.5. Conclusion 95

Chapter V: Anti-inflammatory, Anti-diabetic, and Anti-Alzheimer's Effects of Prenylated Flavonoids from Okinawa Propolis 108–142

5.1. Summary 108

5.2. Introduction 109

5.3. Materials and methods 111

5.4. Results and discussion 119

5.5. Conclusion 127

Chapter VI: General Conclusion 143

Literature Cited 145

LIST OF TABLES

Table No.	Title	Page No.
2.1.	Effects of different compounds on cell proliferation, melanin content, tyrosinase activity in B16F10 cells.	54
3.1.	Cytotoxic effects of different fractions and purified compounds of *Ardisia sieboldii*.	79
3.2.	LC-ESI-MS identification of the major compounds in fraction 3 and fraction 6 prepared from *Ardisia sieboldii* leaves.	80
3.3.	Effects of different compounds on cell viability and nitrite inhibition in lipopolysaccharide-induced RAW 264.7 cells.	81
3.4.	Binding free energy, type of interactions of compounds **1**–**3** with the cycloxygenase-2 protein.	82
4.1.	Cytotoxic effects of different sea cucumber extracts/crude saponin.	103
4.2.	Cytotoxic effects of different fractions of *Holothuria atra* crude saponin.	104
4.3.	Anti-proliferative effects of desulfated echinoside B and frondoside A.	105
4.4.	Binding affinity and non-bonding interaction of saponins with the catalytic domain of PAK1 obtained using AutoDock vina.	106
4.5.	Non-bonding interactions of ligands with the catalytic domain of PAK1 obtained after 20 ns molecular dynamics simulation.	107
5.1.	IC_{50} values of nitrite inhibition by different compounds. NA: nymphaeol-A; NB: nymphaeol-B; NC: nymphaeol-C; INB: isonymphaeol-B; GN: 3′-geranyl-naringenin.	137
5.2.	Binding affinity and binding interactions of Okinawa propolis (OP) compounds with α-glucosidase (PDB ID: 3A4A) and acetylcholinesterase (PDB ID: 4EY7) proteins.	138

LIST OF TABLES

Table No.	Title	Page No.
5.3.	Physicochemical properties of the compounds for good oral bioavailability.	140
5.4.	Toxicological properties of the compounds.	141
5.5.	Results of quantum chemical calculations and thermodynamic properties of the compounds.	142

LIST OF FIGURES

Figure No.	Title	Page No.
1.1.	Strategy to search for promising drug leads from natural resources.	2
1.2.	Two first purified natural product drugs. Morphine was isolated from *Papaver somniferum* (opium poppy), and salicin was purified from *Salix alba* (white willow). Salicin is involved in the origin of semi-synthetic non-steroidal anti-inflammatory drug, aspirin.	4
1.3.	Inflammation and human diseases. Inflammation includes acute and chronic types. Acute inflammation leads to the healing process, whereas chronic inflammation is associated with various human diseases.	12
1.4.	Inflammatory cascade showing the induction of iNOS (inducible nitric oxide synthase) and COX-2 (cyclooxygenase-2) by different stimuli and further development of inflammation through generating cardinal signs.	14
1.5.	PAK1, as a central node, facilitates cross-talk among different important signaling pathways. MITF: Microphthalmia-associated transcription factor; LIMK: LIM kinase; PI3K: Phosphatidylinositol 3 kinase; VEGF: Vascular endothelial growth factor.	18
1.6.	Schematic representation of drug discovery and development process through using computational approaches.	24
1.7.	Basic steps of molecular docking simulation.	25

LIST OF FIGURES

Figure No.	Title	Page No.
2.1.	HPLC chromatograms and the chemical structures of 5,6-dehydrokawain (DK) (**a**), dihydro-5,6-dehydrokawain (DDK) (**b**), (*E*)-5-methoxy-8-(4-methoxy-2-oxo-2*H*-pyran-6-yl)-7-phenyl-1-styryl-2-oxabicyclo[4.2.0]oct-4-en-3-one (AS-2) (**c**), kaempferol 3-*O*-*β*-D-glucuronide (KOG) (**d**), and quercetin 3-*O*-*β*-D-glucuronide (QOG) (**e**).	48
2.2.	Protein denaturation inhibition effects (**a**) and proteinase inhibitory activities (**b**) of the compounds. Each data point represents mean ± SE (n = 6).	49
2.3.	Cytotoxic effects of *Alpinia zerumbet* leaf compounds on RAW 264.7 cells (**a**), brine shrimps (**b**), and on 3T3-L1 fibroblast cells (**c**). The results are mean ± SE, and the asterisks denote significant differences compared to the control group (* $p < 0.05$; ** $p < 0.01$).	50
2.4.	Inhibitory effects of the compounds on nitrite accumulation (**a**) and PGE_2 production (**b**) in lipopolysaccharide (LPS)-induced RAW 264.7 cells. After seeding, the cells were incubated with LPS (500 ng/ml) and varying concentrations (μM) of the tested compounds for 24 h. Data are shown as mean ± SE of two experiments. Asterisks indicate significant differences compared to the LPS-treated control group (* $p < 0.05$; ** $p < 0.01$).	51
2.5.	Effects of the compounds on mushroom tyrosinase activity *in vitro*. Each bar represents mean ± SE of three experiments. The different letters indicate significant differences among compounds by DMRT at 5% probability level.	52

LIST OF FIGURES

Figure No.	Title	Page No.
2.6.	Role of PAK1 in melanogenic and inflammatory signaling pathways, and the probable inhibitory actions of *Alpinia zerumbet* components on inflammation and melanogenesis.	53
3.1.	Schematic representation of the extraction method of *Ardisia sieboldii* leaves. Si-Gel CC: Silica gel column chromatography; Fr: Fraction; TLC: Thin-layer chromatography; LC-ESI-MS: Liquid chromatography-electrospray ionization-mass spectrometry; Comp: Compound.	72
3.2.	Structures of the compounds **1** {2-methyl-5-(8*Z*-heptadecenyl) resorcinol}, **2** {5-(8*Z*-heptadecenyl) resorcinol}, and **3** (ardisiaquinone A).	73
3.3.	Cytotoxic effects of two extracts on different cancer cells. Each bar represents mean ± SE of three independent experiments in triplicate. * $p < 0.05$ *vs.* others in the same group; ns = non-significant; 7EE = 70% ethanol extract; 7ME = 70% methanol extract.	74
3.4.	Total ion chromatograms of fraction 3 (**A**) and fraction 6 (**B**) prepared from the 70% methanol extract of *Ardisia sieboldii* leaves.	75
3.5.	Effects of compounds on the viability of brine shrimps. The results are mean ± SE of three independent experiments. Asterisks indicate statistically significant differences between the control and treatment. * $p < 0.05$, ** $p < 0.01$, *** $p < 0.001$.	76
3.6.	Inhibitory effects of the compounds on albumin denaturation (**A**), and COX-2 (cyclooxygenase-2) activity (**B**). Each data point represents mean ± SE of three independent experiments.	77

LIST OF FIGURES

Figure No.	Title	Page No.
3.7.	Binding orientations of the compounds inside the cycloxygenase-2 (COX-2) protein. Compounds **1**, **2**, and **3** were demonstrated in magenta, green, and red color, respectively. Blue circle represents the position of the active site of COX-2.	78
4.1.	Sea cucumber species after dissection and drying. (**A**) *Holothuria atra*; (**B**) *H. leucospilota*; (**C**) *Parastichopus nigripunctatus*.	97
4.2.	Chemical structures of desulfated echinoside B (DEB) (**A**) and frondoside A (FRA) (**B**).	98
4.3.	Total ion chromatogram of crude saponin of *Holothuria atra* showing the mass spectrum (MS) values of major components.	99
4.4.	Predicted pose from the docking analysis shows binding orientation of DEB (Desulfated echinoside B) (blue) and FRA (Frondoside A) (yellow) in the allosteric site of PAK1 kinase domain (**A**). Non-bonding interactions of DEB and FRA to the allosteric site residues (**B**, **C**). Representative hydrogen bonds between ligand and receptor are shown with lines (pink).	100
4.5.	The time series of root mean square deviations of backbone atoms for DEB (Desulfated echinoside B) and FRA (Frondoside A) complex (**A**, **B**). Structural modification of protein by means of root mean square deviations (RMSD) and root mean square fluctuations (RMSF) for DEB and FRA complex (**C**, **D**).	101

LIST OF FIGURES

Figure No.	Title	Page No.
4.6.	Ligand-protein complex poses after 20 ns molecular dynamics (MD) simulation compared to that of docked complexes. Receptor after molecular docking simulation: yellow; Receptor after 20 ns MD simulation: pink; Ligand after molecular docking simulation: green; Ligand after 20 ns MD simulation: blue; (**A**) DEB (Desulfated echinoside B)-PAK1 complex; (**B**) FRA (Frondoside A)-PAK1 complex.	102
5.1.	Chemical structures of the purified compounds from Okinawa propolis. (**A**) Nymphaeol-A (NA), (**B**) nymphaeol-B (NB), (**C**) nymphaeol-C (NC), (**D**) isonymphaeol-B (INB), and (**E**) 3′-geranyl-naringenin (GN).	129
5.2.	Inhibitory effects of Okinawa propolis (OP) compounds on albumin denaturation *in vitro*. Ketorolac (Ket) was used as a control, and asterisks indicate significant differences compared to the positive control (** $p < 0.01$).	130
5.3.	Effects of different compounds on RAW 264.7 cell viability (**A**) and on nitrite formation (**B**) in lipopolysaccharide (LPS)-stimulated RAW 264.7 cells. Ketorolac (Ket) was used as a standard drug. Asterisks indicate significant differences compared to the control (* $p < 0.05$; ** $p < 0.01$).	131
5.4.	Cycloxygenase-2 (COX-2) inhibitory effects of Okinawa propolis (OP) compounds. Results are expressed as means ± SE of three repeated experiments. Indomethacin (Ind) was used as a standard inhibitor. Asterisks indicate significant differences compared to the positive control (* $p < 0.05$; ** $p < 0.01$).	132

LIST OF FIGURES

Figure No.	Title	Page No.
5.5.	The α-glucosidase (**A**) and acetylcholinesterase (**B**) inhibitory effects of different Okinawa propolis (OP) compounds. Data represent means ± SE of three experiments. Asterisks indicate significant differences compared to the positive control (* $p < 0.05$; ** $p < 0.01$).	133
5.6.	Binding orientations of Okinawa propolis (OP) compounds within α-glucosidase (PDB ID: 3A4A) and acetylcholinesterase (PDB ID: 4EY7) protein receptors. (**A**) Binding orientation within 3A4A (nymphaeol-A (NA) = yellow; nymphaeol-B (NB) = green; nymphaeol-C (NC) = cyan; isonymphaeol-B (INB) = blue; 3′-geranyl-naringenin (GN) = magenta), and (**B**) binding orientation within 4EY7 (NA = yellow; NB = green; NC = cyan; INB = blue; GN = magenta).	134
5.7.	Non-bonded interactions of the best-docked compounds with α-glucosidase (PDB ID: 3A4A) and acetylcholinesterase (PDB ID: 4EY7) proteins. (**A**) Nymphaeol-A (NA) with 3A4A, (**B**) nymphaeol-C (NC) with 3A4A, (**C**) isonymphaeol-B (INB) with 3A4A, (**D**) NA with 4EY7, (**E**) nymphaeol-B (NB) with 4EY7, and (**F**) 3′-geranyl-naringenin (GN) with 4EY7.	135
5.8.	Visualization of frontier molecular orbitals of Okinawa propolis (OP) compounds. **A**, **B** – HOMO and LUMO of nymphaeol A (NA); **C**, **D** – HOMO and LUMO of nymphaeol B (NB); **E**, **F** – HOMO and LUMO of nymphaeol C (NC); **G**, **H** – HOMO and LUMO of isonymphaeol B (INB); **I**, **J** – HOMO and LUMO of 3´-geranyl-naringenin (GN). HOMO = highest occupied molecular orbital; LUMO = lowest unoccupied molecular orbital	136

ABBREVIATIONS

ACh: Acetylcholine

AChE: Acetylcholinesterase

AD: Alzheimer's disease

ADMET: Absorption, distribution, metabolism, excretion, and toxicity

Alpinia: *Alpinia zerumbet* var. *excelsa*

AGIs: α-Glucosidase inhibitors

AS-2: (*E*)-5-Methoxy-8-(4-methoxy-2-oxo-2*H*-pyran-6-yl)-7-phenyl-1-styryl-2-oxabicyclo[4.2.0]oct-4-en-3-one

ATCC: American type culture collection

Aβ: Amyloid beta

B3LYP: Becke's three-parameter hybrid model, Lee–Yang–Parr

CADD: Computer-aided drug design

CAPE: Caffeic acid phenethyl ester

CI: Chronic inflammation

COX-1: Cyclooxygenase-1

COX-2: Cyclooxygenase-2

CS: Newborn calf serum

CTBP1: C-terminal binding protein 1

CXCR4: C–X–C chemokine receptor 4

DDK: Dihydro-5,6-dehydrokawain

DEB: Desulfated echinoside B

DFT: Density functional theory

DK: 5,6-dehydrokawain

DM: Diabetes mellitus

DMEM: Dulbecco's Modified Eagle Medium

DMRT: Duncan's multiple range test

ABBREVIATIONS

DMSO: Dimethyl sulfoxide

ESI-MS: Electrospray ionization mass spectrometry

EtOAc: Ethyl acetate

EtOH: Ethanol

FBS: Fetal bovine serum

FRA: Frondoside A

GC: Gas chromatography

GCMS: Gas chromatography mass spectrometry

hERG: Human ether-a-go-go-related gene

HOMO: Highest occupied molecular orbital

HPLC: High performance liquid chromatography

IC_{50}: Half maximal inhibitory concentration

IL-1: Interleukin 1

Ind: Indomethacin

iNOS: Inducible nitric oxide synthase

Ket: Ketorolac

KOG: Kaempferol 3-*O*-β-D-glucuronide

L-DOPA: L-3,4-dihydroxyphenylalanine

Labdadiene: 12-Labdadiene-15,16-dial

LBDD: Ligand-based drug design

LC-ESI-MS: Liquid chromatography-electrospray ionization-mass spectrometry

LC-MS: Liquid chromatography-mass spectrometry

LD_{50}: Median lethal dose

LPS: Lipopolysaccharide

LUMO: Lowest unoccupied molecular orbital

m/z: Mass-to-charge ratio

ABBREVIATIONS

MAPK: Mitogen-activated protein kinase

MD: Molecular dynamics

MeOH: Methanol

MITF: Microphthalmia-associated transcription factor

MS: Mass spectrum

MTD: (1*E*,3*E*,5*E*)-6-Methoxyhexa-1,3,5-trien-1-yl)-2,5-dihydrofuran

MTT: 3-(4,5-Dimethylthiazol-2-yl)-2,5-diphenyl-tetrazolium bromide

NA: Nymphaeol A

NB: Nymphaeol B

NC: Nymphaeol C

NF-κB: Nuclear factor kappa B

NMR: Nuclear magnetic resonance

NO: Nitric oxide

NPs: Natural products

NSAID: Non-steroidal anti-inflammatory drug

OP: Okinawa propolis

PAK1: p21-activated kinase 1 / RAC/CDC42-activated kinase 1

PAKs: p21-activated kinases

PBC: Periodic boundary condition

PBS: Phosphate buffer saline

PDB / pdb: Protein data bank

PDB ID: Protein data bank identifier

PDGF: Platelet derived growth factor

PGE_2: Prostaglandin E2

PKs: Pharmacokinetic properties

PNPG: *p*-Nitrophenyl-α-D-glucopyranoside

ABBREVIATIONS

QOG: Quercetin 3-*O*-*β*-D-glucuronide

QSAR: Quantitative structure-activity relationship

RCSB: The Research Collaboratory for Structural Bioinformatics

RMSD: Root mean square deviation

RMSF: Root mean square fluctuation

RNS: Reactive nitrogen species

ROS: Reactive oxygen species

SBDD: Structure-based drug design

SE: Standard error

SNAI1: Snail homologue 1

T2D: Type 2 diabetes

TIC: Total ion chromatogram

TIP3P: Transferable intermolecular potential3 points

TLC: Thin-layer chromatography

TMOQ: (*E*)-2,2,3,3-Tetramethyl-8-methylene-7-(oct-6-en-1-yl)octahydro-1*H*-quinolizine

TMS: Trimethylsilyl

TNFα: Tumor necrosis factor alpha

TPSA: Topological polar surface area

TRP: Tyrosinase related protein

UV: Ultra violet

α-MSH: α-Melanocyte stimulating hormone

εHOMO: Energy of the highest occupied molecular orbital

εLUMO: Energy of the lowest unoccupied molecular orbital

ABSTRACT

A wide spectrum of bioresource from Okinawan terrestrial and marine sources is routinely used by indigenous people as traditional foods and medicines. They have promising health benefits leading to prevent chronic diseases/disorders and thus, they contribute to human health and lifespan. Accumulated data revealed that the bioactive natural compounds can function as chemopreventive agents and increase the quality of life and health since they are non-toxic and easy to exploit. This investigation was carried out with several Okinawan bioresources such as terrestrial medicinal plants, marine sea cucumbers, and bee propolis to explore their chemopreventive properties on different chronic diseases including inflammatory disorders, cancer, type 2 diabetes, and Alzheimer's disease.

In the first experiment with terrestrial medicinal plants, leaves of *Alpinia zerumbet* var. *excelsa* (*Alpinia*) and *Ardisia sieboldii* were investigated for their potential inhibitory effects on inflammation, skin-pigmentation, and cancer. Five major compounds from *Alpinia* leaves, 5,6-dehydrokawain (DK), dihydro-5,6-dehydrokawain (DDK), (*E*)-5-methoxy-8-(4-methoxy-2-oxo-2*H*-pyran-6-yl)-7-phenyl-1-styryl-2-oxabicyclo[4.2.0]oct-4-en-3-one (AS-2), kaempferol 3-O-*β*-D-glucuronide (KOG), and quercetin 3-O-*β*-D-glucuronide (QOG), exhibited promising anti-inflammatory effects *via* inhibiting albumin denaturation and proteinase activity *in vitro* and reducing the formation of inflammatory mediators, NO (nitric oxide) and PGE_2 (prostaglandin E2), in lipopolysaccharide (LPS)-treated RAW 264.7 cells. All compounds reduced melanin production and tyrosinase enzyme activity in B16F10 cells, clearly demonstrating that *Alpinia* leaf-derived compounds can function as potent skin depigmenting agents. On the other hand, three compounds purified from the leaves of *A. sieboldii*, 2-methyl-5-(8*Z*-heptadecenyl) resorcinol, 5-(8*Z*-heptadecenyl) resorcinol, and ardisiaquinone A, showed potential cytotoxic

effects on both cancer cells and brine shrimps. They were also found to have inhibitory effects on albumin denaturation *in vitro*, NO production in LPS-stimulated RAW 264.7 cells, and COX-2 (cyclooxygenase-2) enzyme activity.

Secondly, sea cucumber species *Holothuria atra*, a marine natural resource, was found to have cytotoxic on different cancer cell lines due to having special saponin ingredients. Desulfated echinoside B (DEB), a desulfated saponin, from *H. atra* showed promising effects on cancer cell proliferation and brine shrimps' viability as does frondoside A (FRA), a sulfated anti-cancer saponin purified from *Cucumaria frondosa*. Molecular docking and molecular dynamics simulation demonstrated that DEB, compared to FRA, has high binding interactions and stability with the oncogenic kinase PAK1 (p21-activated kinase 1).

Finally, a special bioresource Okinawa propolis (OP) was utilized in this study and its major components, nymphaeol-A (NA), nymphaeol-B (NB), nymphaeol-C (NC), isonymphaeol-B (INB), and 3′-geranyl-naringenin (GN), exhibited significant anti-inflammatory effects through suppressing *in vitro* albumin denaturation, nitrite accumulation, and COX-2 enzyme activity in LPS-induced RAW 264.7 cells. They were also found to have strong inhibitory actions on α-glucosidase and acetylcholinesterase enzymes responsible for type-2 diabetes and Alzheimer's disease, respectively.

As described above, the findings reveal that the purified bioactive compounds from *Alpinia, A. sieboldii*, sea cucumbers, and OP, have chemopreventive and therapeutic properties as anti-inflammatory, anti-melanogenic, anti-cancer, anti-diabetic, and anti-Alzheimer's herbal medicines. Thus, they could be commercially utilized in the future for developing herbal supplements or functional foods as a source of different chemopreventive agents.

ABSTRACT (*In Japanese*)

陸上および海洋を含め広範囲にわたる沖縄の生物資源は、伝統的な食品および薬として地元で日常的に使用されている。それらは、慢性的な疾患・障害の予防につながる有望な手助けをし、人々の健康および寿命に寄与している。過去の蓄積データより、天然由来の生物活性物質は無毒で利用しやすいことから、生活の質（QOL）と健康を増進する化学的予防剤として機能することが明らかとなっている。したがって、本研究は、炎症性疾患、癌、2 型糖尿病およびアルツハイマー病を含む様々な慢性疾患に対する化学的予防機能を検証するために、陸上薬用植物、ナマコ、および蜜蜂由来プロポリスなど種々の沖縄産生物資源を用いて検討を行った。

陸上薬用植物を用いた最初の実験では、ゲットウ（*Alpinia zerumbet* var. *excelsa*）およびモクタチバナ（*Ardisia sieboldii*）の葉について、炎症、皮膚色素沈着、癌に対する阻害効果を検証した。ゲットウ葉由来の 5 つの主要な化合物｛5,6-デヒドロカワイン（DK）、ジヒドロ-5,6-デヒドロカワイン（DDK）、(*E*)-5-methoxy-8-(4-methoxy-2-oxo-2*H*-pyran-6-yl)-7-phenyl-1-styryl-2-oxabicyclo[4.2.0]oct-4-en-3-one （AS-2）、ケンフェロール 3-*O*-*β*-D-グルクロニド（KOG）、そしてケルセチン 3-*O*-*β*-D-グルクロニド（QOG）｝は、*in vitro* でアルブミン変性およびプロテアーゼ活性を阻害し、リポ多糖（LPS）で処理した RAW 264.7 細胞中の炎症性メディエータである NO（一酸化窒素）および PGE_2（プロスタグランジン E2）の形成を減少させることにより、有望な抗炎症効果を示した。

また、全ての化合物は、B16F10 細胞におけるメラニン産生およびチロシナーゼ酵素活性を減少させたことから、ゲットウの葉に含まれる化合物が色素沈着防止機能を有することが明らかとなった。一方、モクタチバナの葉から精製した 3 つの化合物｛2-methyl-5-(8*Z*-heptadecenyl) resorcinol、5-(8*Z*-heptadecenyl) resorcinol、そして ardisiaquinone A｝は、癌細胞およびブライン

シュリンプの両方に潜在的な細胞毒性効果を示した。それらはまた、*in vitro* におけるアルブミン変性、LPS で刺激した RAW 264.7 細胞における NO 産生、および COX-2 (cyclooxygenase-2) 酵素活性に対しても阻害効果を有することが見出された。

次に、海洋天然資源のクロナマコ（*Holothuria atra*）が含有する特別なサポニン成分は、種々の癌細胞系に対して細胞傷害性を有することが判明した。クロナマコ由来の脱硫酸化サポニンである desulfated echinoside B（DEB）は、キンコ（*Cucumaria frondosa*）から精製された硫酸化抗癌サポニンである frondoside A（FRA）と同様に、癌細胞の増殖やブラインシュリンプの生存に対して有望な効果を示した。分子ドッキングおよび分子動力学シミュレーションを用いた実験より、FRA と比較して、DEB が発癌性キナーゼである PAK1（p21 活性化キナーゼ 1）との高い結合相互作用および安定性を有することが明らかとなった。

最後に、特別な生物資源である沖縄プロポリス（OP）について検討したところ、OP の主要成分｛ニムフェオール-A（NA）、ニムフェオール-B（NB）、ニムフェオール-C（NC）、イソニムフェオール-B（INB）、そして 3’-ゲラニル-ナリンゲニン（GN）｝が LPS 誘発 RAW 264.7 細胞における *in vitro* アルブミン変性、NO の蓄積、COX-2 酵素活性を抑制することで顕著な抗炎症効果を示すことがわかった。また、2 型糖尿病およびアルツハイマー病にそれぞれ関与するα-グルコシダーゼおよびアセチルコリンエステラーゼの阻害活性を有することが判明した。

以上のように、ゲットウ、モクタチバナ、ナマコおよび沖縄プロポリスから取得した生物活性物質が、抗炎症、メラニン産生抑制、抗癌、抗糖尿病、抗アルツハイマーなどの化学的予防機能を有することが明らかとなった。本研究結果から、これらの沖縄産生物資源は、将来的にサプリメントまたは機能性食品を開発するために、様々な化学的予防剤の供給源として商業的に利用できることが期待される。

CHAPTER-I

General Introduction

1.1. Natural resource: A novel reservoir of wonder drugs

Nature represents the oldest example of pharmacy with a lot of wonder drugs and has been a source of medicinal products for millennia. Throughout the ages, humans have relied on nature to cater not only for their foods and basic needs but also for medicines of a wide spectrum of diseases. Particularly, plants have formed the basis of this sophisticated traditional medicine systems. With the passage of time, different types of medicinal systems have been developed worldwide, for example Mesopotamian, Egyptian, Chinese, and Ayurveda (Indian-based) medicine system. However, the Greeks and Romans are thought to contribute substantially to the rational development of using herbal drugs in the ancient Western world.

An analysis of new drug sources from 1981 to 2007 reveals that almost half of the drugs approved since 1994 were based on natural products (NPs) (Katiyar et al. 2012), which clarify that natural resources are the potential source of novel drugs or drug leads. A huge number of NPs-derived drugs in various stages of recent clinical development also highlights the significance of using NPs as potential sources for new drug candidates. Although recent interests with them in drug discovery and development have slightly been declined (Mishra & Tiwari 2011), they can provide unique structural diversity with the opportunities of discovering novel low molecular weight lead compounds. Only less than 10% of the world's biodiversity has been evaluated yet for potential biological activity (Cragg & Newman 2005), hence, many more useful leads await discovery with the challenge being how to access this natural chemical diversity. Modern techniques of analytical and medicinal chemistry could pave the way to study a vast array of NPs from terrestrial and marine sources (**Figure 1.1**).

In conclusion, there is no doubt that natural resources are still among the most perfect "natural laboratories" for developing various molecules ranging from simple skeleton to highly complex chemical structures, and therefore, the untapped natural resources should be exploited gradually with the state-of-the-art techniques.

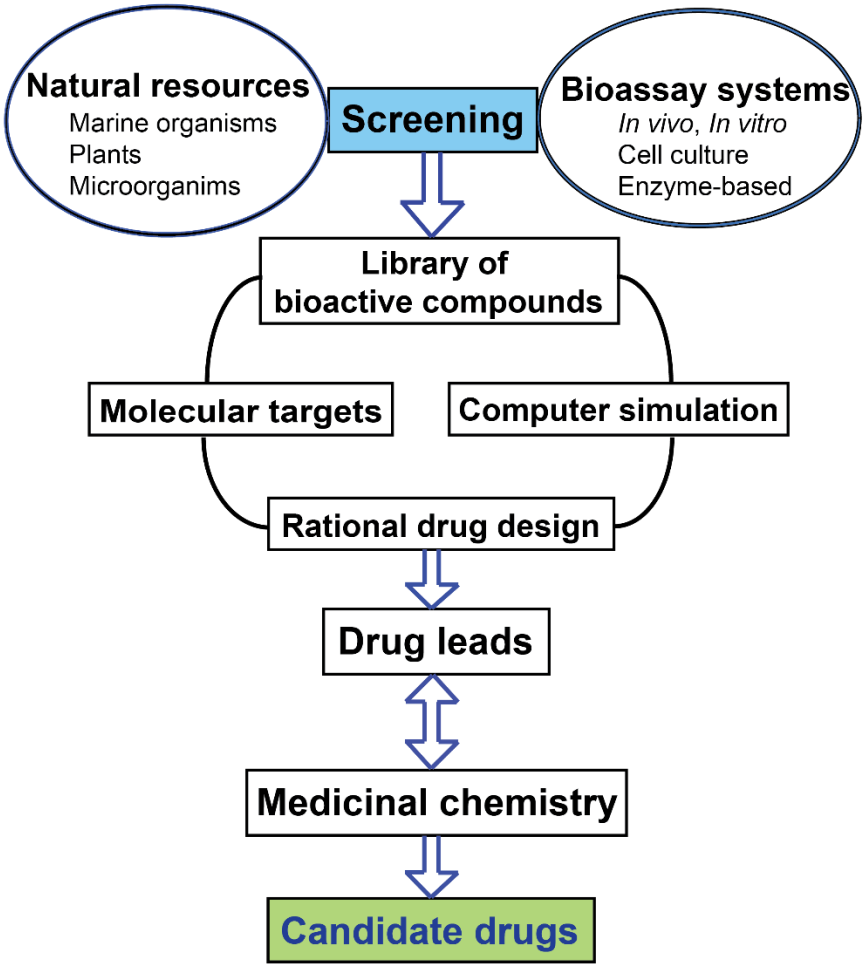

Figure 1.1. Strategy to search for promising drug leads from natural resources (adapted from Kobayashi 2016).

1.2. Therapeutic applications of natural products: A practical perspective

Since time immemorial, natural resources have been an integral part of history and culture as the backbone of traditional healing system throughout the globe. Although many medicinal plant extracts still are being used as prescription drugs in developed countries including UK, Germany, China, and France (Ji et al. 2017, Ruhsam & Hollingsworth 2017), modern drug discovery strategies discard the use of crude extracts and is driven by single compound-based medicine (Thomford et al. 2018). Bioactive compounds discovered so far have played a vital role in improving the human health and have been the drugs of choice despite facing a competition with the synthetic drugs in many ways. However, safety and efficacy of synthetic drugs are remained questionable, resulting in the dependence on NPs by more than 80% of the total population in the developing world (Veeresham 2012).

Although the use of bioactive NPs as herbal drug preparations dates back hundreds, even thousands of years ago, their application to modern drug discovery and development started only in the 19th century. A breakthrough was announced in 1804 when Sertürner purified morphine (**Figure 1.2**) as a first NPs-based drug from opium (Lockemann, 1951). However, the first semi-synthetic drug aspirin, based on a natural product salicin (**Figure 1.2**) isolated from *Salix alba*, was introduced by Bayer in 1899 (Veeresham 2012). These led others to look for active principles in medicinal plants, and throughout the century, many other bioactive pure NPs were developed as drug. For instance, cocaine from coca, codeine from opium, digitoxin from digitalis, quinine from cinchona, and pilocarpine from pilocarpus, of which some are still in use. Drug

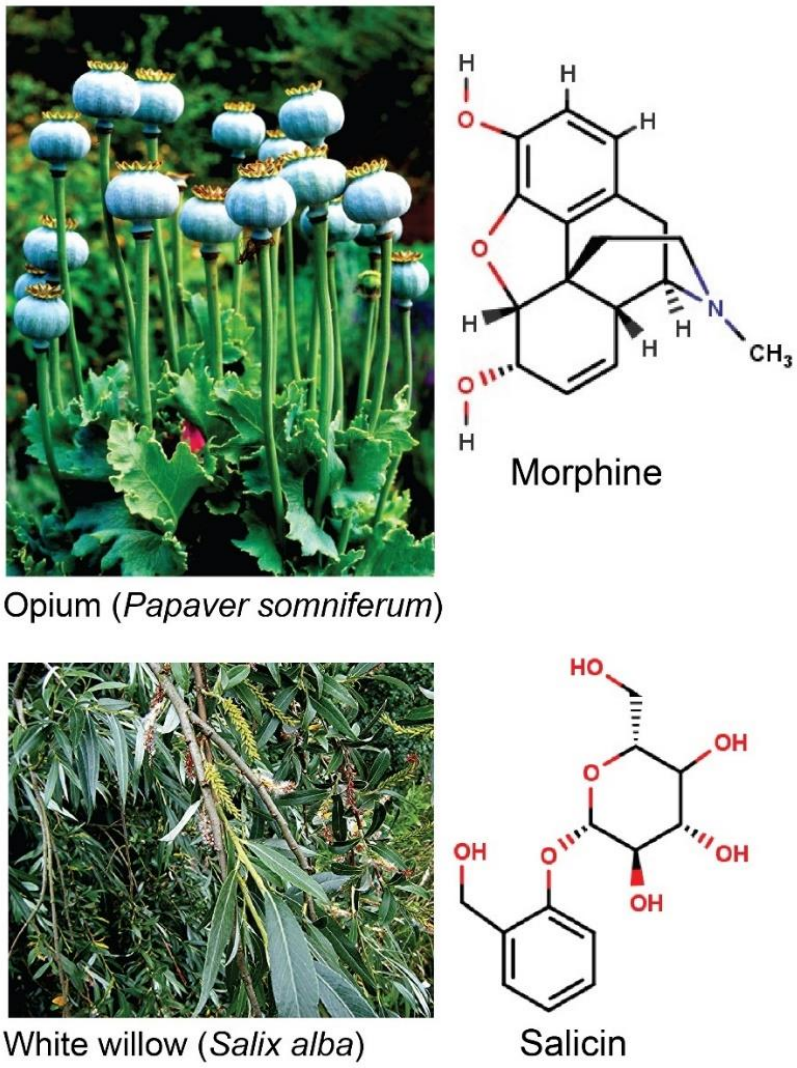

Figure 1.2. Two first purified natural product drugs. Morphine was isolated from *Papaver somniferum* (opium poppy), and salicin was purified from *Salix alba* (white willow). Salicin is involved in the origin of semi-synthetic non-steroidal anti-inflammatory drug, aspirin.

discovery research from NPs was substantially revolutionized after the discovery of penicillin by Fleming in 1928 (Kardos & Demain 2011). After significant success with penicillin, pharmaceutical industries and research groups concentrated to develop more potent antibiotics from nature and they finally developed some important antibiotics including streptomycin, chloramphenicol, chlortetracycline, cephalosporin

C, erythromycin, vancomycin, and staurosporine. All these drugs and/or derivatives thereof are commercially available.

The most recent story on NPs-based potent drug development is the discovery of artemisinin and avermectin from *Atremisia annua* and *Streptomyces avermitilis*, respectively. Artemisinin was discovered by the initiative of Chinese Government to help the North Vietnamese population combat malaria during the Vietnam War (Miller & Su 2011), whereas avermectin was purified as fermentation product showing anthelmintic activity against nematode parasites of cattle, sheep, dogs, and chickens (Burg et al. 1979). For developing artemisinin and avermectin from NPs, the Nobel prize in Physiology or Medicine for 2015 was awarded to Drs Youyou Tu, William C. Campbell, and Satoshi Ōmura (http://www.nobelprize.org).

1.3. Bioresources in Okinawa: Terrestrial and marine products

Okinawa Islands belong to the subtropical region of Japan, which have a special importance as a trove of natural resource due to the existence of a wide variety of terrestrial plants and marine organisms. This region is located at the southernmost of Japan between Kyushu Island and Taiwan, consisting of more than 100 islands known as Ryukyus (Kumazawa et al. 2007). The flora and fauna here are divided into three regions based on the three recognized biogeographic areas: the Hachisuka, Watase, and Miyake lines at south of Kyushu, Yakushima, and Okinawa Islands, respectively (White & Reimer 2012). Natural forests in Okinawa consist of unique plant diversity with relatively high endemism (Joppa et al. 2013). The area of this sub-tropical region is the only 0.6% of that of Japan, however, it includes 286 families,

1961 genera, and 5793 plant species, which is the 87% of total species recorded in Japan (Aramoto et al. 2006). Per unit area of the Ryukyu Archipelago contains 45 times as many species as the mainland Japan, that's why, this region seems to be one of the top reservoirs of natural resource in Japan (Shimabukuro 1984). The prefectural government of Okinawa published a plant red data book demonstrating 1399 vascular plants as threatened with extinction (Matsunami & Otsuka 2018). Since ancient times, more than 300 plant species have been traditionally utilized by Okinawan people as medicinal herbs (Tawata & Ota 1998). This high intake of locally grown medicinal herbs might be one of the major reasons behind the longest lifespan of Okinawan people (Hokawa 1999, Shinjo & Yamamoto 1999). Due to the above-mentioned fact, some of these plants are commercialized by different companies inside and outside of the prefecture to produce several herbal products or functional foods, subsequently contributing to the regional economy. However, many traditional plant species found in this region have not been fully explored yet for their potential pharmacological benefits and phytochemical constituents (Matsunami & Otsuka 2018).

Okinawa Islands include the islands of different geological formation, ages and sizes (Kizaki 1986). Along the west side of islands, the warm water of the Kuroshio current flows (Andres et al. 2008), which has developed the coral reefs in Okinawa (Ueda & Uemura 2008), most of them are fringing and patch reefs developed adjacent or close to the islands. However, on the southeastern coast, patch reefs have developed several kilometers offshore forming barrier like reef. These coral reefs are the biologically most diverse and the richest in the world (Ueda & Uemura 2008), hence, the islands are thought to be a region of exceptionally high species diversity and endemism (Hughes et al. 2002, Cowman et al. 2017). Due to the global demand of

protecting natural resources, these southern parts of Japan along with Taiwan rank first in global marine conservation priority, thus need rapid action for conservation of multi-taxon endemic species from over-exploitation and coastal development (Roberts et al. 2002). Since the marine resources are important sources of novel chemical classes not found in the terrestrial environment, Okinawa Islands could be exploited as a promising source of marine bioresources with a view to develop future drugs or drug leads for wide spectrum therapies.

1.4. Health-promoting benefits of Okinawan bioresources

Okinawa is rich in terrestrial and marine bioresources which are being used by indigenous people since ancient times. Of them, medicinal herbs along with different seaweeds are vigorously used as food and medicine source. However, traditional diet in Okinawa is reported to be rich in vegetables, soybean-based foods, and medicinal plants (Willcox et al. 2014). A good number of researches have been carried out with Okinawan medicinal herbs and seaweeds for their promising health benefits and therapeutic prospects. Potential health benefits of some commonly utilized Okinawan bioresources have been presented in below.

For instance, *Alpinia zerumbet* (locally called Getto) is one of the important medicinal herbs, which is routinely used for preparing traditional food items, green tea, medicinal supplements, and cosmetics. Extensive researches have been done with *A. zerumbet* and it was reported to have a wide spectrum of pharmacological effects including anti-oxidant, anti-diabetic, anti-obesity, anti-cancer, ani-HIV, anti-ageing (longevity-extending effects), anti-neuraminidase, and anti-atherogenic activities (Elzaawely et al. 2007, Chompoo et al. 2011, 2012, Upadhyay et al. 2011, 2013, Be

Tu & Tawata 2014). Major bioactive compounds of *A. zerumbet* were demonstrated to be responsible for its wide spectrum health benefits.

Another sub-tropical plant *Peucedanum japonicum*, known as Chomeiso in Japan, is frequently used as a leafy vegetable and as the main ingredient of Chomeiso-noodle in the Okinawa Islands (Nugara et al. 2014). Several coumarins purified from *P. japonicum* were found to have anti-platelet (Chen et al. 1996), anti-oxidant (Hisamoto et al. 2003), antagonistic (Takeuchi et al. 1991), anti-rheumatic (Adams et al. 2009), and anti-obesity activities (Nugara et al. 2014).

Aerial parts of *Artemisia vulgaris*, called Yomogi, are used traditionally as a folk medicince which have medicinal properties as anti-helminth, antiseptic, a tonic for vital organs and in various disorders including hepatosis (Duke et al. 2002). It was also revealed to have anti-bacterial (Chen et al. 1989) and analgesic efficacy (Yoshikawa et al. 1996).

Luffa cylindrica, called Hechima in Japanese, has been recognized as traditional medicine for the treatment of inflammatory diseases, diarrhoea, and viral infections (Abdel-Salam et al. 2019). The usual parts used include fruit, seeds, and leaves. Extracts prepared from this plant reported to have anti-cancer properties against breast cancer cells and hepatocellular carcinoma cells (Abdel-Salam et al. 2018, 2019).

Ipomoea batatus known as Imo is a widely consumed food items in Okinawa. It is a rich source of proteins, vitamins, and minerals. Along with its roots, leaves are also consumed, which are rich in polyphenols (Nagamine et al. 2014). Several reports indicated that sweet potato leaves can inhibit mutagenicity (Yoshimoto et al. 2002), growth of cancer cells (Kurata et al. 2007), increase the faecal bile acid excretion and

lower hepatic cholesterol in rats (Innami et al. 1998), and suppress the oxidation of lipoprotein in human (Nagai et al. 2011).

Momordica charantia (Goya) is the most popular cucurtbit being used as one of the typical daily food materials in the prefecture of Okinawa. In traditional medicine, it is used as an antidiabetic agent which was reported to have blood glucose lowering effects in laboratory animals (Miura et al. 2001). It is also used as a carminative and in the treatment of colic (Rahman & Lau 1996, Grover & Yadav 2004). Different parts of *M. charantia* contain many cucurbitane-type bioactive triterpenoids (Akihisa et al. 2007).

Another typical plant in Okinawa is Konnyaku (*Amorphophallus konjac*) which is used in the traditional cuisine. It is a yam-like tuber that lacks flavor, but readily absorbs the flavors of other ingredients in simmered dishes. As a key ingredient of konnyaku jelly, it is known as a component of cleaning the stomach (Salen & De Lorgeril 2011). Very low in calories, high in fiber and calcium, *A. konjac* is also an effective treatment against constipation and diabetes (Willcox et al. 2001, 2009).

Bee propolis (Okinawa propolis, OP) are traditionally exploited as an anti-microbial agent and for wound healing or dental care. Bioactive compounds of OP showed a wide range of biological activities including anti-oxidant, anti-cancer, and longevity-extending effects (Kumazawa et al. 2007, Taira et al. 2016).

The fresh or dried fruits of Okinawan pepper (*Piper retrofractum* Vahl), also known as Hihatsumodoki in Japan, are extensively used as a seasoning ingredient and for various therapeutic purposes (Takahashi et al. 2018). The major medicinal ingredients of its fruits are pungent alkaloid piperine and other phenolic compounds

(Luyen et al. 2014), which were reported to have anti-obesity (Kim et al. 2011), hepatoprotective (Matsuda et al. 2009), and antioxidative effects (Chonpathompikunlert et al. 2010).

Cladosiphon okamuranus, called Mozuku in Japanese, is a widely consumed brown seaweed naturally found in Okinawa. It is now farmed by locals, and then sold to the processing factories. Its major ingredient is the sulfated polysaccharide called Fucoidan which can function as anti-cancer (Maeda et al. 2012), anti-oxidant (Nguyen et al. 2011), and lipid lowering agent (Matanjun et al. 2010). It is also rich in minerals, dietary fibers, vitamin A, vitamin C, and several essential unsaturated fatty acids (Matanjun et al. 2009).

In conclusion, Okinawan traditional diet is low in fat and high in good quality carbohydrates and nutrients, which together contribute to reduce the risk of chronic diseases (Willcox et al. 2009) through preventing nutritional deficiency (Shroder et al. 2008) and by their potential health promoting benefits. A wide array of bioactive compounds from the consumed bioresources, however, can also function as chemopreventive herbal agents, and substantially contributes to the healthy and long lifespan of Okinawan people.

1.5. Inflammation and its role in human health and diseases

Inflammation is a critical response of our body to the danger signals, damages, harmful pathogens, and stimuli. The inflammatory process serves an important function to control and repair injuries, which can take two basic forms, acute and chronic (Pawelec et al. 2014). Acute inflammation, considered to be safe, is a part of innate immunity initiated by the immune cells that persists only for a short time, thus

it helps prevent further injury and facilitates the healing and recovery process in the body (He et al. 2015). Chronic inflammation (CI), in contrast, lasts beyond the actual injury; sometimes for months or even years through its prolonged, dysregulated, and maladaptive effects (Sun 2012). Such persistent inflammation is involved in many chronic human conditions and diseases including allergy, atherosclerosis, cancer, arthritis, autoimmune diseases, neurodegenerative disorders, and so forth (**Figure 1.3**). CI can affect any or all parts of the body, playing significant role in developing other diseases such as chronic pain, poor sleep quality, physical impairment, and overall decreased quality of life (Cortan et al. 1999). CI may also serve as a precursor to certain cancers through DNA damage (Grivennikov et al. 2010).

Recent evidences suggest that the number of people suffering from chronic diseases such as cardiovascular diseases, diabetes, respiratory diseases, autoimmune diseases, and cancers is dramatically increasing worldwide (Raghupathi & Raghupathi 2018). It has been projected that, by 2020, chronic diseases will account for almost three-quarters of all deaths worldwide (The world health report 1998). This increasing rate is thought to be associated with CI, caused by excessive and inappropriate inflammatory activity, which can be a major contributing factor in the pathology of chronic diseases (Mallbris et al. 2004, Miller et al. 2009, El-Gabalawy et al. 2010, Kolb & Mandrup-Poulsen 2010).

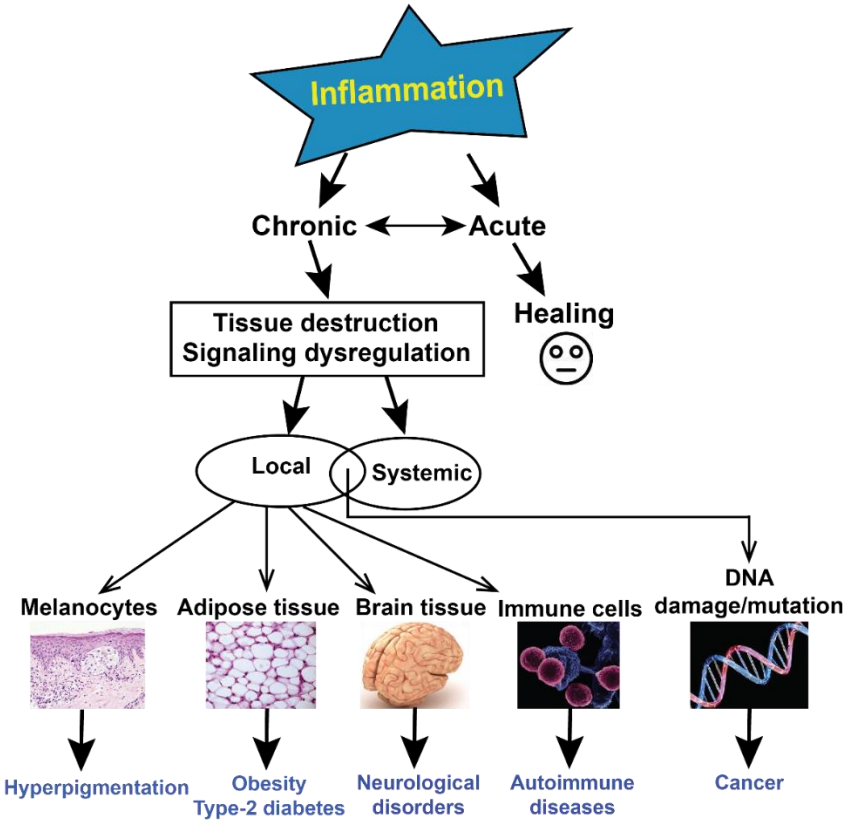

Figure 1.3. Inflammation and human diseases. Inflammation includes acute and chronic types. Acute inflammation leads to the healing process, whereas chronic inflammation is associated with various human diseases.

1.6. Inducible nitric oxide synthase (iNOS) and cyclooxygenase-2 (COX-2): Two major pro-inflammatory enzymes

Inflammatory response is a fundamental response by the body's innate immune system. Macrophages, neutrophils, and natural killer cells are the part of immune system and they use pattern recognition receptors to recognize molecular patterns associated with pathogens and other foreign particles (Medzhitov 2001). Thus, immune cells are activated by pathogens and foreign toxic substances. Activated

macrophages release a variety of effector molecules including nitric oxide (NO) to inhibit the replication of pathogens. NO is synthesized by the inducible NO synthase (iNOS) enzyme which converts L-arginine to NO and L-citrulline through the formation of intermediate *N*-hydroxy-L-arginine. iNOS can be triggered by the bacterial cell wall component lipopolysaccharide (LPS) which works through the activation of intra-cellular signaling pathways including the mitogen-activated protein kinase (MAPK) pathway and the nuclear factor kappa B (NF-κB) pathway (Lowenstein & Padalko 2004). Cytokines released from the infected host cells can also activate iNOS (Lowenstein & Padalko 2004). However, during inflammation, excessive amount of NO can interact with oxygen radicals and forms highly reactive peroxynitrite to induce cyclooxygenase-2 (COX-2) and other inflammatory cytokines (Cho et al. 2004) (**Figure 1.4**). During inflammatory diseases, NO and its derivatives target host cells and make detrimental effects to the body (Hamalainen 2008). Thus, high amounts of NO can function as a pro-inflammatory agent and plays a major role in different pathophysiological conditions such as chronic inflammation, infection, neoplastic diseases, liver cirrhosis, and diabetes etc. (Lechner et al. 2005).

COX-2 is an inducible enzyme responsible for biosynthesis of prostaglandin from arachidonic acid. It has another isoform COX-1 which produce basal levels of prostaglandin essential for gastrointestinal tract homeostasis (Cho et al. 2004). COX-1 is known as a housekeeping enzyme that is constitutively expressed in all tissues (Smith et al. 2009). It plays a role in several pathological conditions including thrombosis, atherosclerosis, and tumorigenesis. Platelet COX-1 is the target of antithrombotic agents used for the prevention of vascular occlusive event (Vitale et al. 2013). On the other hand, COX-2 is constitutively expressed only in kidney, brain,

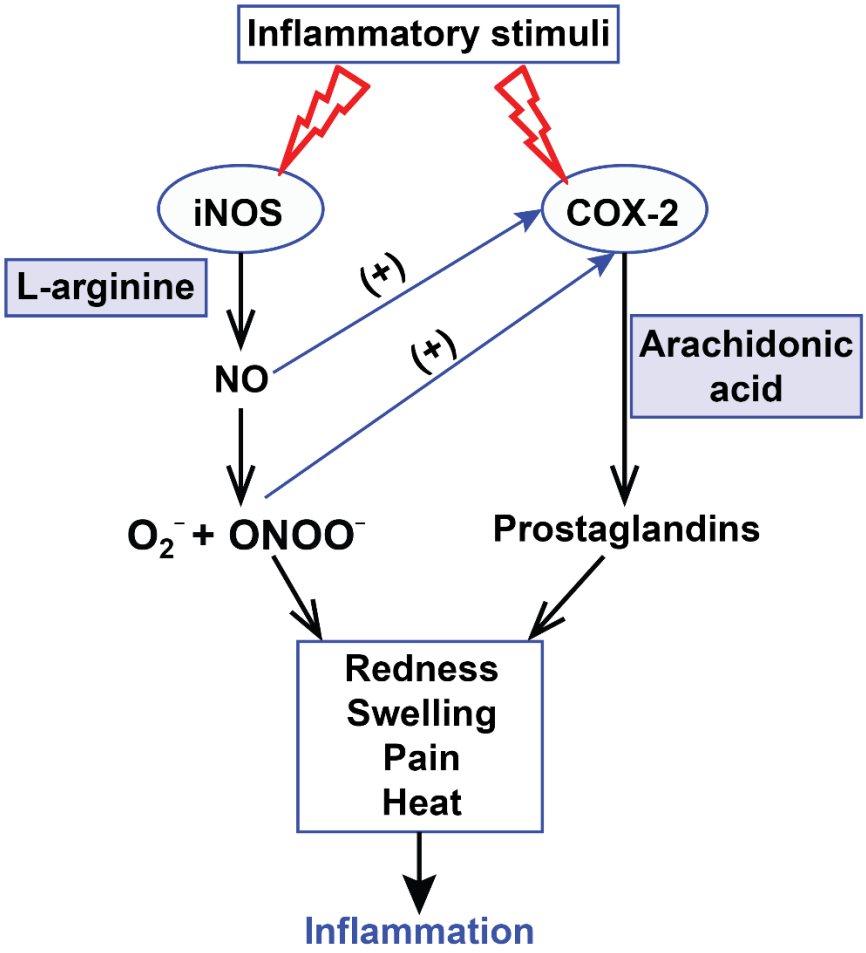

Figure 1.4. Inflammatory cascade showing the induction of iNOS (inducible nitric oxide synthase) and COX-2 (cyclooxygenase-2) by different stimuli and further development of inflammation through generating cardinal signs.

spinal cord, and ductus deferens (Fosslien 2000). It is stimulated by different agents such as oncogenes, growth factors, hormones, and mitogens etc. It is also induced by the disorders of water-electrolyte homeostasis which links it to the pathological consequences of inflammation and various cancer types (Herschman 1996, Kawamori et al. 1998, Kanaoka et al. 2007). Therefore, inhibition of COX-1 shows several undesired side effects such as gastrointestinal and renal toxicity, and the selective inhibition of COX-2 is expected for treating inflammation (Zarghi & Arfaei 2011). In conclusion, inflammation, as a multifaceted process, is governed by an array of

signaling factors, of which iNOS and COX-2 could be considered as promising therapeutic targets for resolving inflammation in a non-host disruptive manner.

1.7. Melanogenesis

Melanogenesis is the process of producing melanin pigment which plays an important photoprotective role against deleterious effects of UV radiation and in scavenging toxic drugs (Khaled et al. 2002). Melanin also plays a preponderant role in determining the color of the skin, hair, and eyes, and protecting the skin against UV radiation from the sun which accentuate the aging process and the risks of skin cancer (Riley 2003). Melanogenesis is regulated mainly by a melanocyte-specific enzyme, tyrosinase, a rate-limiting enzyme that catalyzes the hydroxylation of L-tyrosine to L-3,4-dihydroxyphenylalanine (L-DOPA) and the oxidation of L-DOPA to dopaquinone. Thus, the up-regulation of tyrosinase is proposed to be responsible for increased melanin production (Hearing & Tsukamato 1991). Three melanocyte-specific enzymes, tyrosinase, tyrosinase-related protein (TRP)-1, and TRP-2, have been reported to catalyze melanin biosynthesis (Lee et al. 2010). The expression of these three enzymes is strongly regulated by microphthalmia associated transcription factor (MITF). However, excessive production of melanin causes abnormal pigmentation such as freckles, age spots, melasma, and melanoma (Kim et al. 2012). Therefore, the search for moderating agents of pigmentation is important for treating abnormal skin pigmentation, and tyrosinase inhibitors have become increasingly important in medicinal, cosmetic and in the agro-food fields. Many tyrosinase inhibitors have been used to treat skin hyperpigmentation such as arbutin (Nakajima et al. 1998), kojic acid (Seo et al. 2003), hydroquinone (Garcia & Fulton 1996), and quercetin (Nagata et al.

2004, Kubo et al. 2007); but they confer potential mutagenicity and ochronosis (Findlay et al. 1975). Hence, there is still a need to search for new drugs, and natural products are regarded as the source of safe and potential herbal anti-melanogenic agents (Wu et al. 2019).

1.8. P21-activated kinase 1 (PAK1)

P21-activated kinase 1 (PAK1) is an oncogenic/aging kinase which belongs to a group of serine/threonine-specific intracellular protein kinase PAKs (p21-activated kinases). PAK1 has more five isoforms, and all of these PAKs are divided into two groups- I and II. PAKs coordinate signals from the cell membrane to the nucleus, and improper regulation of the PAKs is involved in multiple disorders including heart disorders, disorders of the nervous system, and infectious diseases (Lee et al. 2016, Kumar et al. 2017). Most importantly, PAK1 and PAK4 are found to be overexpressed/deregulated strongly in cancer (King et al. 2014). In oncogenic signaling, PAK1 induces cell survival and tumorigenesis through activating several downstream substrates including BAD, CRAF, caspase 7, caspase 8, merlin, estrogen receptor, beta-catenin, aurora A, histone 3, and Ras-related nuclear protein 1 (Radu et al. 2014). As a downstream effector of Ras, PAK1 can enhance the RAF/MEK/ERK signaling pathway and increase cell proliferation by phosphorylating Raf1 and MEK1 (Frost et al. 1997, Chaudhary et al. 2000). On translocation to the nucleus, it can directly affect gene transcription of several substrates such as FKHR, SHARP, C-terminal binding protein 1 (CTBP1) and snail homologue 1 (SNAI1) (Molli et al. 2009). PAK1 activates NF-κB during inflammatory signaling and thus, regulates the expression of iNOS, COX-2, and cytokines (Foryst-Ludwig & Naumann 2000, Tak &

Firestein 2001, Kawai & Akira 2007). It also contributes to the melanogenic signaling cascade through activating beta-catenin/MITF (Microphthalmia-associated transcription factor) pathway (Be Tu et al. 2016). Since PAK1 functions as a node of multiple signaling pathways and facilitates cross-talk among several important signaling factors (**Figure 1.5**), it has been implicated in generating a variety of human diseases/disorders such as neurofibromatosis, Alzheimer's disease, diabetes (type 2), hypertension, infectious and inflammatory diseases, epilepsy, schizophrenia, depression, autism, obesity, cancers, and short lifespan (Maruta 2014). Thus, PAK1 is nowadays thought to be a major therapeutic target for treating several human diseases/disorders, and the selective small molecule PAK1-blockers are thought to have a huge market value for the purpose of treating PAK1 signaling-dependent diseases.

1.9. Type 2 diabetes

Diabetes mellitus (DM) is a chronic metabolic disorder resulting from a defect in insulin secretion, insulin action, or both. As a result, there is a disturbance of carbohydrate, fat, and protein metabolism, and hence, it is commonly characterized by high blood glucose levels. Its long-term complications include retinopathy, nephropathy, neuropathy, and increased risk of cardiovascular diseases. It has two types- type 1 and type 2. Type 2 DM is the most common form of DM characterized by hyperglycemia, insulin resistance, and relative insulin deficiency. People with type 2 DM are more vulnerable to various forms of both short and long-term complications often leading to premature death. It has been estimated that approximately 415 million people were diagnosed with diabetes globally in 2015, which was predicted to rise to

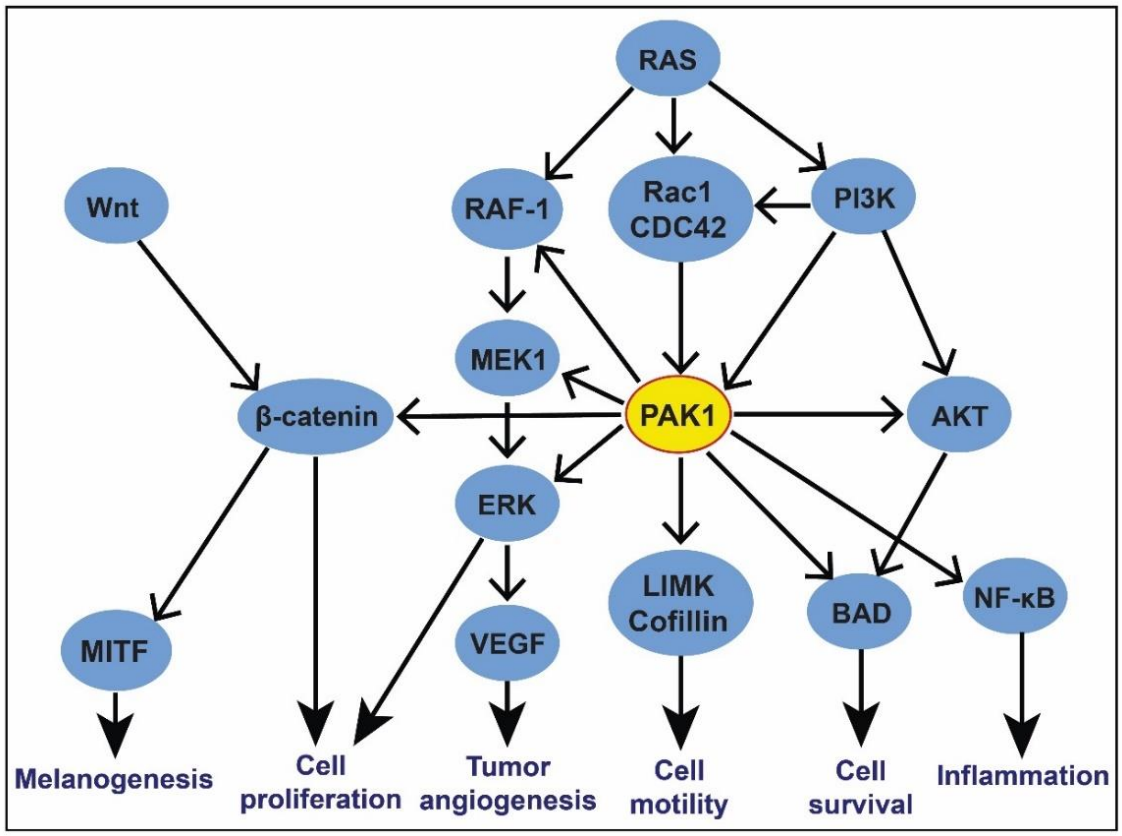

Figure 1.5. PAK1, as a central node, facilitates cross-talk among different important signaling pathways (adapted from Kumar et al. 2006, Kichina et al. 2010, Ye & Field 2012, Radu et al. 2014, Huynh & He 2015, Be Tu et al. 2016, and Ahn et al. 2017). MITF: Microphthalmia-associated transcription factor; LIMK: LIM kinase; PI3K: Phosphatidylinositol 3 kinase; VEGF: Vascular endothelial growth factor.

642 million until to 2040 (Herman 2017). Type 2 DM is due primarily to lifestyle factors and genetics, and a number of lifestyle factors known to be involved in its development are physical inactivity, sedentary lifestyle, cigarette smoking, and generous consumption of alcohol. However, obesity has been found to contribute to approximately 55% of cases. One of the effective managements of DM, in particular, type 2 DM, is to retard the absorption of glucose by inhibition of carbohydrate

hydrolyzing enzymes, such as α-glucosidase and α-amylase in the digestive organs (Kumar et al. 2011). α-Glucosidase is an exo-type carbohydrase which is the key enzyme for catalyzing the final step in the digestive process of carbohydrates (Kimura et al. 2004). Hence, α-glucosidase inhibitors (AGIs) can retard the liberation of d-glucose from dietary complex carbohydrates and delay glucose absorption, resulting in reduced postprandial plasma glucose levels and suppression of postprandial hyperglycemia. Inhibition of this enzyme can slow the elevation of blood sugar following a carbohydrate meal (Lebovitz 1997). Through inhibition of α-glucosidase in the intestine, the rate of hydrolytic cleavage of oligosaccharide is decreased and the process of carbohydrate digestion spreads to the lower part of small intestine. This spreading of digestion process delays the overall absorption rate of glucose into the blood. It has proved to be one of the best strategies to decrease the postprandial rise in blood glucose and in turn help avoiding the onset of late diabetic complications (Kumar et al. 2011). Currently, AGIs from herbal resources have received increasing interest because of its low toxicity and efficiency. For instance, acarbose and voglibose, purified from microorganisms, are being widely used as herbal AGIs, of these, acarbose is the most commonly prescribed drug (Lee et al. 2014).

1.10. Alzheimer’s disease

Alzheimer's disease (AD) is a progressive neurodegenerative disorder which is the leading cause of dementia in the elderly. It is estimated to affect as many as 24 million people worldwide and is expected to double every 20 year (Reitz et al. 2011), and, by 2030, approximately 65 million people could suffer from this illness (Masoumi et al. 2018). Although there is limited understanding of the etiologic mechanisms

behind AD, toxic amyloid beta (Aβ) plaques and neurofibrillary tangles in the brain are thought to progress the disease (Hardy & Allspo 1991). The Aβ proteins are produced from the amyloid precursor protein through amyloidogenic pathway under the action of β and γ-secretases, whereas, the neurofibrillary tangles are hyperphosphorylated Tau protein originated from different Tau pathologies (He et al. 2018). The accumulation of protein plaques in the brain of AD patients is associated with several events such as mitochondrial dysfunction, impaired cell stress response, abnormal accumulation of transition metals, altered lipid metabolism, enzymatic dysregulation, neuroinflammation, and oxidative stress (Mancuso & Santangelo 2018). Aβ deposition activates the astrocytes and microglia in the brain, which are responsible for the production of inflammatory mediators, and consequently, the plaques become amyloid fibrils (Akiyama et al. 2000, Sadleir et al. 2016, Cattaneo et al. 2017). Pharmacological therapy attempting to cure AD is, until now, to use partial inhibitors rather than curative, and cholinesterase inhibitors have been the mainstay of drugs available to treat AD. Cholinesterase inhibitors can inhibit the activities of the enzyme acetylcholinesterase (AChE) which is linked to AD pathogenesis either by increasing cholinergic deficit or exacerbating Aβ fibril formation and toxicity (Nalivaeva & Turner 2016). Besides of using medications, several nutritional and behavioral approaches are suggested for managing the cognitive dysfunction in the brain of AD patients. Inappropriate dietary patterns can facilitate AD development, whereas, a healthier and ketogenic diet having anti-oxidant or anti-inflammatory nutrients might function as chemopreventive agents in attenuating its development (Fernández & Ribeiro 2018, Broom et al. 2019).

1.11. Computational approaches in modern drug discovery

The rapid progress of parallel and combinatorial chemistry expanded compound databases and subsequently expedited the drug discovery process (Jhoti et al. 2013, Lavecchia & Di Giovanni 2013). However, the typical process of drug discovery with high-throughput screening technologies is a time-consuming, risky and costly process which takes approximately 14 years to accomplish (Myers & Baker 2001) and costs 0.8 to 1.0 billion USD (Moses et al. 2005). For this reason, the output from drug discovery programs in the past decades is not positively proportional to the investment, although the investment was increased yearly (Shekhar 2008). Modern drug discovery is, therefore, aimed to examine the huge libraries of compounds in short period of time, and the top pharmaceutical companies have started to use various modern tools for shortening the research cycle and for reducing the expense and risk of failure. Computer-aided drug design (CADD) is one of the most prominent approaches of using sophisticated computational tools, which accelerate the drug development process in a more cost-efficient way, minimizing failures in the final stage (Macalino et al. 2015). Thus, it is gaining rapid popularity, implementation, and appreciation for modern drug discovery.

CADD covers many other aspects of drug discovery program, including computer programs/software for designing compounds, tools for systematically assessing potential lead candidates, developing digital repositories for studying chemical interactions, and designing libraries with the potential to generate molecular variants (Song et al. 2009). It has already been applied to different successful drugs, some of which are available in the market as commercial drugs such as imatinib and nilotinib (Druker & Lydon 2000, Weisberg et al. 2005). In the modern era, CADD

could be applied to the most aspects of drug discovery and the developmental process starting from target identification to lead discovery and optimization; it can even be helpful for preclinical studies with novel drugs (Jorgensen 2004, Shekhar 2008, Zhang 2011, Xiang et al. 2012). It has been estimated that CADD approaches could reduce the cost for drug discovery by up to 50% (Tan et al. 2010). It is, therefore, now a widely recognized alternative and complement to high-throughput screening technologies for drug discovery (Song et al. 2009).

CADD is mainly categorized into two methods (**Figure 1.6**), structure-based drug design (SBDD) and ligand-based drug design (LBDD) (Ou-Yang et al. 2012, Sliwoski et al. 2014, Arodola et al. 2017). SBDD relies on the availability of the three-dimensional structure of target macromolecules, which is developed through X-ray crystallography, NMR (nuclear magnetic resonance) spectroscopy, and homology modeling (Chen et al. 2012). It uses several tools such as molecular docking, *de novo* drug design, and molecular dynamics (MD), and finally selects a set of molecules which can form favorable interactions with the binding sites of target proteins (Sliwoski et al. 2014). On the other hand, LBDD is an indirect approach which uses a group of known ligands to infer the prospective structure of active ligands for target proteins (Sliwoski et al. 2014, Hung & Chen 2014). It has two fundamental approaches: (1) selection of compounds based on the chemical similarities to the known ligands and (2) the construction of a QSAR (quantitative structure-activity relationship) model for predicting bioactivity using chemical structures (Sliwoski et al. 2014). The first one is termed pharmacophore modeling. LBDD approaches are strictly applied whenever the structure of the biological target is unknown, however, sometimes it shows high potency in identifying active compounds compared to the

SBDD-based methods (Stumpfe et al. 2012). Nowadays, wide varieties of computational tools are being used in drug discovery, suggesting that there are no fundamentally superior techniques. Each technique shows varied performance based on the target protein, available data, and resources. However, recent advances in computer sciences, molecular and structural biology, combinatorial chemistry, quantum chemistry, medicinal chemistry, and molecular dynamics have paved the way of using CADD widely and cost-effectively for modern drug discovery researches.

1.12. Molecular docking: A powerful tool for structure-based drug design

The number of therapeutic targets for drug discovery has been tremendously increased after the completion of human genome project. At the same time, high-throughput protein purification, X-ray crystallography, and NMR techniques have been developed, which resulted in the development of structural information of proteins and protein-ligand complexes (Meng et al. 2011). These developments together compelled pharmaceutical companies to use fast and reliable computational tools for virtual screening of millions of drugs within a short period. Molecular docking is one of the most important computational tools, that is widely used in the structure-based drug designing. It was developed on the basis of different algorithm programs which have made the docking an increasingly important tool in pharmaceutical research since its first inception in the 1980s (Kuntz et al. 1982, López-Vallejo et al. 2011). It can predict the conformation of small-molecule ligands within the appropriate target binding site with a substantial degree of accuracy (Meng et al. 2011). It also predicts the binding affinity of ligand to form a stable complex with

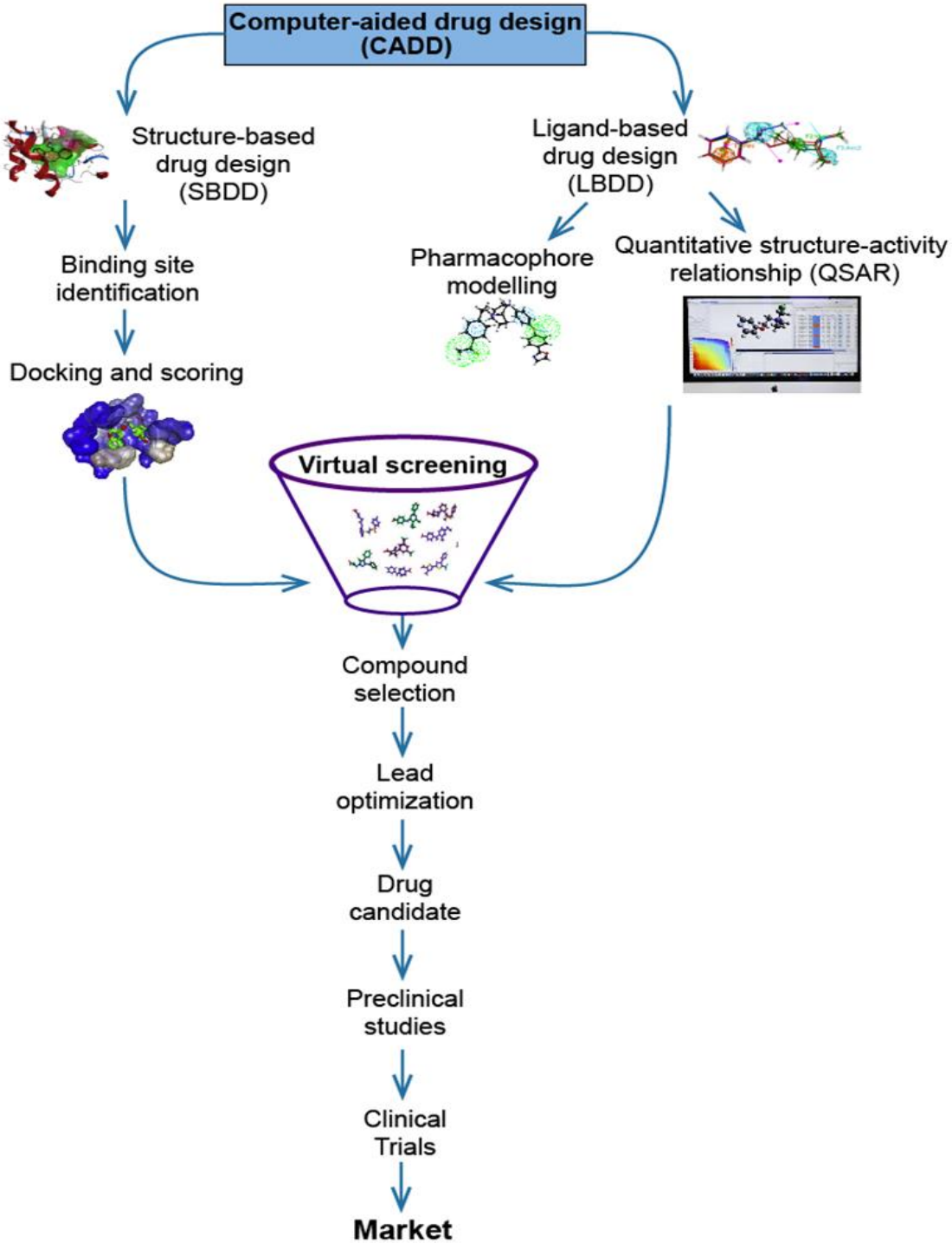

Figure 1.6. Schematic representation of drug discovery and development process through using computational approaches.

target protein by finding preferred orientation of minimum free binding energy (Ferreira et al. 2015), allowing to characterize the behavior of small molecules in the binding sites as well as to elucidate fundamental biochemical processes (McConkey et al. 2002). The docking process mainly consists of two basic steps: prediction of the ligand conformation and assessment of the binding affinity. Multiple steps of molecular docking are presented in **Figure 1.7**.

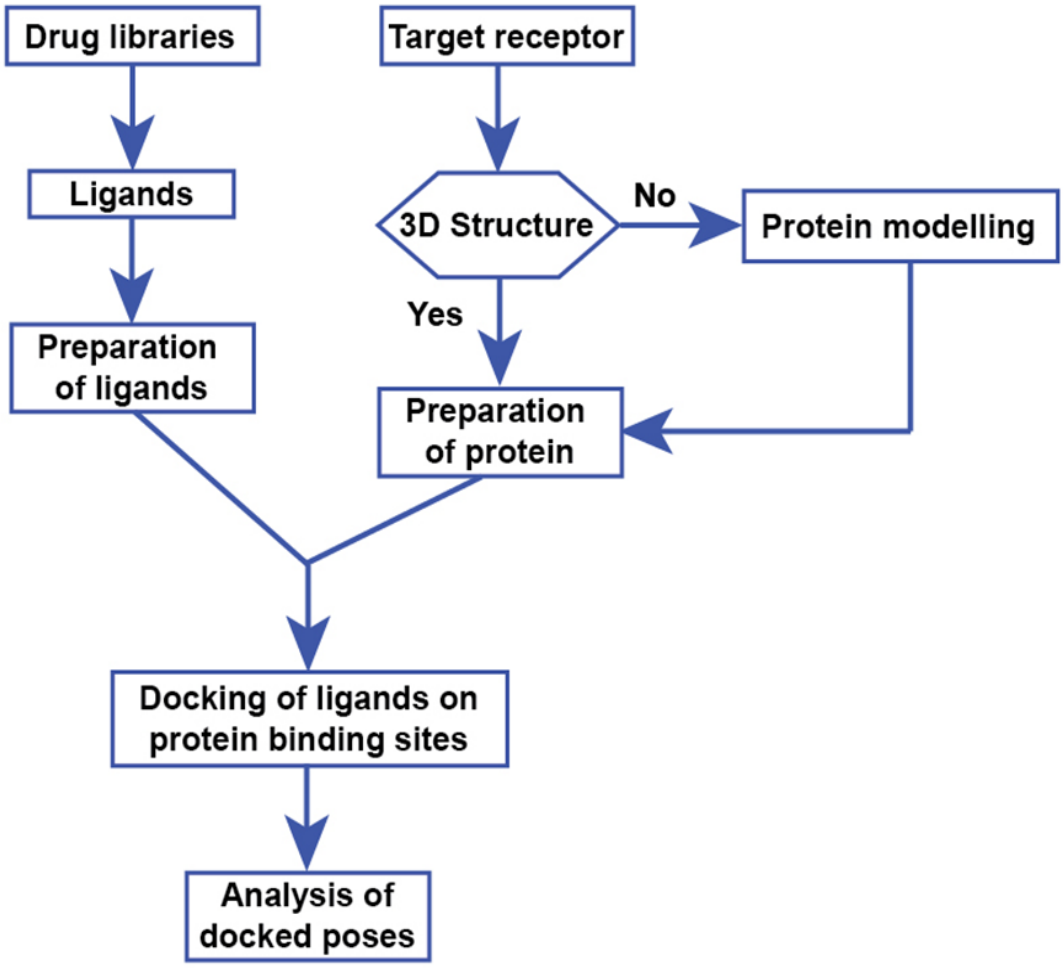

Figure 1.7. Basic steps of molecular docking simulation.

For docking simulation, it is necessary to know the location of ligand binding sites of the target proteins. In most of the cases, binding site information is available, however, in some cases that information is not found. One can obtain information

about the binding sites from similar protein types sharing similar functions. Moreover, binding site information can also be simulated using different bioinformatics tools such as GRID (Kastenholz et al. 2000), CASTp (Dundas et al. 2006), POCKET (Levitt & Banaszak 1992), PASS (Brady & Stouten 2000), and MMC (Mezei 2003). When docking runs without any prior knowledge on the binding sites of protein, it is termed blind docking which involves several runs and energy calculations before a favorable protein-ligand complex pose is found (Hassan et al. 2017).

Nowadays, many docking programs are available such as DOCK (Ewing et al. 2001), AutoDock (Morris et al. 1998), AutoDock Vina (Trott & Olson 2010), GOLD (Jones et al. 1997), FlexX (Rarey et al. 1996), Glide (Friesner et al. 2004), ICM (Abagyan et al. 1994), and Surflex (Jain et al. 2003) etc. It is, therefore, necessary to find a suitable program for users' purposes from the available programs. Thus, evaluation of docking programs is important for the selection of the best one, and many comparative analyses for docking pose prediction have been reported so far (Cole et al. 2005). However, a reliable and successful program should be: 1) a method to explore the ligand-receptor conformation space for plausible poses [the search algorithm] and 2) a method to relatively order those plausible poses [the scoring function] (Hassan et al. 2017). Recently, Wang et al. carried out a comprehensive evaluation of ten famous docking programs including five commercial and five academic programs and found that AutoDock Vina ranked first among all the programs, showing the highest-scoring power (Wang et al. 2016).

1.13. Motivation and objective of this study

Traditional herbal medicines were based on concoctions and concentrated extracts without isolation of active compounds, however, modern medicines are mainly characterized by the identification and purification of active principles. Development of combinatorial chemistry and high throughput screening in three decades ago, and the current knowledge on CADD together dramatically accelerated medicinal chemistry and drug discovery concepts, and hence, NPs are now experiencing a renaissance in recent decades not only for developing future therapeutics but also for improving their drug properties such as therapeutic potency, bioavailability, or metabolism by carefully modifying a molecule's structure (Guo 2017). The present study was encouraged by the resurgence of interest in NPs-based drug development and strongly motivated by the following motivation:

Motivation: The Okinawa Islands in Japan are famous for their high numbers of centenarians compared to anywhere else in the world, and the keys to the longevity of Okinawan people mainly lie in their traditional lifestyle as well as genetic factors (Teschke & Xuan 2018). The lifestyle linked to their healthy and long lifespan is their local cuisine – "Okinawan diet" (Hokama & Binns 2008) which is low in calories but nutritionally rich due to the presence of vegetables and fruits in abundant (Willcox et al. 2007, 2009). This traditional cuisine, developed based on the idea of "food and medicine from the same source", consists of a wide range of medicinal herbs and vegetables including Getto (*Alpinia zerumbet*), Goya (*Momordica charantia*), Shikwasa (*Citrus depressa*), Ucchin (*Curcuma longa*), Yomogi (*Artemisia vulgaris*), Hechima (*Luffa cylindrica*), Chomeiso (*Peucedanum japonicum*), Imo (*Ipomoea batatus*), Kudzu (*Pueraria lobata*), Konnyaku (*Amorphophallus konjac*), and

Hihatsumodoki (*Piper retrofractum*) etc. (Willcox et al. 2013). Okinawan people also traditionally use marine resources as their foods which mainly include several seaweeds and fishes. They routinely use soybean products mostly Natto, Tofu, and Miso, which have been claimed as one of the important factors for their longevity. Moreover, the local people utilize a wide range of biological resources ranging terrestrial to marine organisms to prepare herbal medicines such as decoctions as topical or oral medications for their primary healthcare and healing of different diseases. It is, therefore, assumed that biological resources found in Okinawan Islands might have novel chemopreventive constituents which contribute to the good health and long lifespan of its inhabitants.

Finally, this study was designed with terrestrial medicinal plants, sea cucumbers, and bee propolis and carried out with the following specific objectives:

I) To investigate terrestrial and marine natural resources for their chemopreventive properties against inflammation, hyperpigmentation, diabetes, cancer, and Alzheimer's disease etc.
II) To identify and purify the major bioactive components responsible for chemopreventive and therapeutic potentialities.
III) To incorporate computational tools such as molecular docking and molecular dynamics for simulating the binding interactions of bioactive compounds with the target macromolecules.

CHAPTER-II

Anti-inflammatory and Anti-melanogenic Effects of *Alpinia zerumbet* Leaf-derived Major Components

2.1. Summary

The leaves of *Alpinia zerumbet* var. *excelsa* (*Alpinia*) are used to prepare traditional food items and folk medicines. This study was carried out with *Alpinia* leaves to explore its major components for anti-inflammatory and anti-melanogenic properties. Five compounds, 5,6-dehydrokawain (DK), dihydro-5,6-dehydrokawain (DDK), (*E*)-5-methoxy-8-(4-methoxy-2-oxo-2*H*-pyran-6-yl)-7-phenyl-1-styryl-2-oxabicyclo[4.2.0]oct-4-en-3-one (AS-2), kaempferol 3-*O*-*β*-D-glucuronide (KOG), and quercetin 3-*O*-*β*-D-glucuronide (QOG) were purified from the leaves. Of them, AS-2 and QOG were purified for the first time. Their anti-inflammatory effects were primarily assessed with protein denaturation and proteinase assay. Their inhibitory effects on nitrite accumulation and prostaglandin E2 (PGE_2) production in lipopolysaccharide (LPS)-induced RAW 264.7 cells were also evaluated. For anti-melanogenic assays, all compounds were tested on α-MSH (α-melanocyte stimulating hormone)-stimulated B16F10 cells and on mushroom tyrosinase *in vitro*. Cytotoxicity was evaluated using fibroblast cell line 3T3L-1 and brine shrimps. All compounds significantly inhibited albumin denaturation and proteinase activity. AS-2, KOG, and QOG remarkably inhibited nitric oxide formation with IC_{50} values of 8.2, 13.3, and 12.6 µM, respectively in RAW 264.7 cells. They also inhibited PGE_2 production with IC_{50} values 19.8–23.7 µM. They showed anti-melanogenic effects reducing tyrosinase activity (IC_{50} values 29.6–112.5 µM) and melanin formation (IC_{50} values 30.8–164.4 µM) in B16F10 cells, and inhibiting mushroom tyrosinase (IC_{50} values 61.5–456.4 µg/ml). Taken together, major components of *Alpinia* leaf could be utilized as a potent herbal drug and food supplement with therapeutic prospects against inflammatory disorders and hyperpigmentation.

2.2. Introduction

Inflammation is nowadays implicated as one of the important pathophysiological mechanisms underlying several diseases or disorders including diabetes, cardiovascular diseases, cancer, arthritis, neurodegenerative diseases, and autoimmune diseases. Chronic inflammation is thought to be one of the major triggering factors for several pigmentary disorders (Lee & Choi 1999, Briganti et al. 2003). In post-inflammatory sites on the skin, hyperpigmentation occurs mainly due to high accumulation of histamine and arachidonic acid metabolites (Tomita et al. 1989). Prostaglandin E2 (PGE_2) is also found to be increased in inflamed skin regions (Tomita et al. 1989). These all are termed as inflammatory mediators which accelerate melanin production in melanocytes and transfer the melanin pigments to the neighboring keratinocytes (Tomita et al. 1989). Moreover, UV radiation, a major factor for skin hyperpigmentation, causes inflammation through releasing inflammatory mediators (Tomita et al. 1989, Briganti et al. 2033) and thus, it causes photoaging, hyperpigmentation, wrinkles, and loss of skin firmness and flexibility (Brenner & Hearing 2008). Recently, an oncogenic/aging kinase PAK1 (RAC/CDC42-activated kinase 1) has been reported to be a key factor for inflammation and melanogenic signaling pathways (Song et al. 2002, Nguyen et al. 2017a). As a downstream effector, PAK1 activates COX-2 (cyclooxygenase-2) and iNOS (inducible nitric oxide synthase) and regulates the pathways involved in pain and inflammation (Song et al. 2002, Nguyen et al. 2017a). In melanogenic pathway, it is activated by the major growth hormone PDGF (platelet derived growth factor), which subsequently activates beta-catenin and MITF (microphthalmia-associated transcription factor) (Maruta et al. 2017). They induce the expression of tyrosinase and

tyrosinase related protein (TRP) genes essential for melanin formation (Maruta et al. 2017). Therefore, PAK1 blocking components might be effective for inhibiting inflammation and melanogenesis, and they could be a good therapeutic choice for treating inflammation, skin hyperpigmentation and other inflammatory disorders as well.

Alpinia zerumbet is a perennial zingiberous plant which is widely distributed in subtropical and tropical regions worldwide. Two varieties of this plant, Tairin (*A. zerumbet* (Pers.) B. L. Burtt and R. M. Sm. var. *excelsa* Funak and T. Y. Ito) and Shima (*A. zerumbet* (Pers.) B. L. Burtt and R. M. Sm.), are found in Okinawa, Japan, and they differ from each other with their morphological features and biological activities (Be Tu & Tawata 2015). Tairin variety is found to be grown there in abundant. However, leaves from both varieties are traditionally used there to prepare rice cakes, herbal teas and to flavor the noodles. Japanese people also prepare leaf decoctions from *A. zerumbet* for treating fever and common cold (Tawata et al. 2008, Chan et al. 2009). This plant was investigated for its pharmacological benefits against obesity, diabetic, hypertension, and atherosclerosis (Chompoo et al. 2011, 2012, da Cunha et al. 2013, Be Tu & Tawata 2014), but no studies have examined yet on its anti-inflammatory effects. Moreover, the phytochemicals isolated from this plant were reported to have PAK1 blocking activities (Nguyen et al. 2014, 2016, Taira et al. 2017). Hence, it was predicted that *Alpinia* compounds might have inhibitory effects on inflammatory disorders, and this study was undertaken to investigate the anti-inflammatory and anti-melanogenic effects of major leaf components of *A. zerumbet* var. *excelsa* (*Alpinia*).

2.3. Materials and methods

2.3.1. Cell culture and reagents

Murine macrophage cell line (RAW 264.7) and melanoma cell line (B16F10) (American Type Culture Collection [ATCC], Manassas, Virginia, USA) were cultured in Dulbecco's Modified Eagle Medium (DMEM, Sigma-Aldrich, Saint Louis, Missouri, USA) supplemented with 10% fetal bovine serum (FBS, HyClone, Victoria, Australia) and 1% penicillin/streptomycin (10,000 U/ml and 100 μg/ml) at 37°C in a humidified atmosphere containing 5% CO_2. The mouse embryonic fibroblast cell line 3T3-L1 (ATCC) was cultured in the same conditions using 10% newborn calf serum (CS, HyClone, Victoria, Australia) instead of FBS. DMEM without phenol red was purchased from Thermo Fisher Scientific (Massachusetts, USA). Casein, griess reagents, 70% perchloric acid, and 3-(4,5-dimethylthiazol-2-yl)-2,5-diphenyl-tetrazolium bromide (MTT) were purchased from Sigma-Aldrich. Chicken egg albumin and trypsin were purchased from Funakoshi Co. Ltd. (Tokyo, Japan). All other chemicals and reagents used in this study were of analytical grade and obtained from either Wako Pure Chemical Industries Ltd. (Osaka, Japan) or Kanto Chemical Co., Inc. (Tokyo, Japan).

2.3.2. Plant material

Alpinia leaves were collected from the field of Subtropical Field Science Center, University of the Ryukyus, Okinawa, Japan. The plant material was identified by Prof. Shinkichi Tawata, and the voucher specimens (PRC-2016-01) are stored at PAK Research Center, University of the Ryukyus. The materials were collected in a plastic bag and used in the extraction process soon after the collection.

2.3.3. Extraction and purification of DK, DDK, and AS-2

Fresh leaves were cut into small pieces and washed with tap water. The leaves were then kept at room temperature for 24 h and placed into an oven at 45°C for 48 h. The dried leaves were used to make powder using a kitchen blender. Approximately 30 g of leaf powder was soaked in 400 ml acetone for 48 h, and then the extracts were collected through filtration. Extraction was performed twice and following that, the solvent was evaporated with reduced pressure at 4°C using a rotary evaporator. Dried extracts were dissolved in water (200 ml), then partitioned with ethyl acetate, and the final 940.1 mg (3.13%) of ethyl acetate extract was collected. The ethyl acetate extract was subjected to high performance liquid chromatography (HPLC, Shimadzu, Kyoto, Japan) using a semipreparative C18 column (Inertrsil ODS-3, 250 × 10 mm, GL Sciences Inc., Tokyo, Japan), and three compounds: 5,6-dehydrokawain (DK), dihydro-5,6-dehydrokawain (DDK), and (*E*)-5-methoxy-8-(4-methoxy-2-oxo-2*H*-pyran-6-yl)-7-phenyl-1-styryl-2-oxabicyclo[4.2.0]oct-4-en-3-one (AS-2) (**Figure 2.1**) were purified. Water (solvent A) and methanol (solvent B) were used as mobile phases with a flow rate of 2.5 ml/min. HPLC conditions were as follows: 0–44 min, 60% solvent B; 0–30 min, 75% solvent B; 30.01–37 min, 100% solvent B; 37.01–44 min, 60% solvent B.

2.3.4. Extraction and purification of KOG and QOG

Fresh leaves (250 g) were directly placed into 500 ml boiling water, extracted for 15 min, and then the extract was cooled at room temperature. The extract was then filtered and partitioned with *n*-hexane, dichloromethane, and chloroform. Afterwards, the extract was fractioned continuously with ethyl acetate and butanol to produce a crude extract (ALEB). The ALEB extract was chromatographed with Sephadex LH-

20 (GE Healthcare Life Sciences) with ethanol/acetone gradient elution to yield two fractions. Fraction 1 was subjected to preparative TLC (thin-layer chromatography) with butanol/acetic acid/water solvent (6:1:2). Kaempferol 3-*O*-*β*-D-glucuronide (KOG) and quercetin 3-*O*-*β*-D-glucuronide (QOG) (**Figure 2.1**) were purified through HPLC using a mobile phase of 0.1% acetic acid in distilled water (solvent A) and 0.1% acetic acid in methanol (solvent B). The gradient elution was performed as follows: 0–27 min, 10% solvent B; 27–30 min, 90% solvent B.

2.3.5. Spectral details and structure determination of the compounds

The chemical structures of the purified compounds were identified using nuclear magnetic resonance (NMR) and mass spectrometry data. The ^{1}H NMR and ^{13}C NMR spectra were recorded on a Bruker Biospin GmbH (Rheinstetten, Germany) in $CDCl_3$. Chemical shifts are expressed in parts per million (δ) relative to tetramethylsilane. DK and DDK were confirmed by comparing their physical data (mass spectra, ^{1}H and ^{13}C NMR spectra) with the values reported in literature (Upadhyay et al. 2011). Similarly, KOG was identified by comparing its mass spectra as well as ^{1}H and ^{13}C NMR spectra to the published data (Taira et al. 2017). Spectral details for AS-2 and QOG are as follows: AS-2: ESI-MS: *m/z* 457.1 $[M + H]^+$ (calculated for $C_{28}H_{25}O_6$, 457.49). ^{1}H NMR (500 MHz, $CDCl_3$): *δ* 7.45-7.27 (10H, aromatic), 6.98 (1H, d, *J* = 15.9 Hz), 6.62 (1H, d, *J* = 15.9 Hz), 5.94 (1H, d, *J* = 2.2 Hz), 5.37 (1H, d, *J* = 2.2 Hz), 5.32 (1H, s), 4.39 (1H, dd, *J* = 11.0, 9.8 Hz), 4.19 (1H, d, *J* = 11.0 Hz), 3.75 (3H, s), 3.62 (1H, d, *J* = 9.8 Hz), 3.30 (3H, s). ^{13}C NMR (500 MHz, $CDCl_3$): *δ* 170.5 (C-4), 169.9 (C-4′), 164.56 (C-2), 163.85 (C-2′), 158.64 (C-6), 135.89 (C-9′), 135.62 (C-9), 131.52 (C-8′), 128.75, 128.47, 128.3, 127.84 (C-11,12,13,11′,12′,13′), 127.54 (C-10/14), 126.89 (C-10′/14′), 124.41 (C-7′), 102.67 (C-

5), 91.8 (C-3′), 88.73 (C-3), 79.43 (C-6′), 55.88 (C-15), 55.4 (C-15′), 54.5 (C-7), 45.73 (C-5′), 39.22 (C-8); QOG: ESI-MS: *m/z* 479.0 $[M + H]^+$ (calculated for $C_{21}H_{19}O_{13}$, 479.36). ^{1}H-NMR (400 MHz, MeOD-d_4): δ 3.27–3.51 (H2″, H3″, H4″, H5″, m, 4H), 5.32 (H1″, d, J = 7.2, 1H), 6.22 (H8, d, J = 2.0 Hz, 1H), 6.42 (H6, d, J = 2.0 Hz, 1H), 6.82 (H5′, d, J = 8.4 Hz, 1H), 7.41 (H6′, dd, J = 8.4, 2.0 Hz, 1H), 7.43 (H2′, d, J = 2.0 Hz, 1H); ^{13}C NMR (400 MHz, MeOD-d_4): δ 177.6 (C-4), 170.2 (C-6′), 164.6 (C-7), 161.6 (C-5), 157.1 (C-2), 156.7 (C-9), 149.1 (C-4′), 145.4 (C-3′), 133.7 (C-3), 121.3 (C-1′), 122.1 (C-6′), 116.4 (C-2′), 115.6 (C-5′), 104.3 (C-10), 101.5 (C-1″), 99.1 (C-6), 94.0 (C-8), 76.5 (C-3″), 76.2 (C-5″), 74.2 (C-2″), 71.8 (C-4″). Spectral data of AS-2 and QOG agreed with the values reported in the literature (Fujita et al. 1994, Kim et al. 2014).

2.3.6. Cell growth/viability assay

Cell viability for B16F10, RAW 264.7, and 3T3-L1 cells was evaluated through MTT assay (Ha et al. 2007). Briefly, all the cells were seeded in 48-well plates for 24 h. B16F10 cells were seeded with a density of 1×10^4 cells/well, whereas RAW 264.7 and 3T3-L1 cells were seeded with a density of 1×10^5 cells/well. The culture medium was then replaced with fresh medium containing various sample concentrations. Indomethacin was used as control in Raw 264.7 cells, whereas kojic acid was used as control in B16F10 cells. Both indomethacin and kojic acid were used as negative control in 3T3-L1 cell culture. After adding the samples with desired concentrations, RAW 264.7 cells were incubated for 24 h, while B16F10 and 3T3-L1 cells were incubated for 48 h. The supernatant was then removed and aliquots of 100 µl MTT solution (0.5 mg/ml in phosphate buffer saline [PBS]) were added to each well, and the plate was incubated again at 37°C for 3 h in humidified conditions

supplemented with 5% CO_2. After 3 h, 500 µl of DMSO (dimethyl sulfoxide) was added to each well, and the plate was shaken for 30 min to dissolve the formazan crystals. Finally, the absorbance was measured at 570 nm wavelength and cell viability was calculated from the absorbance of treated versus untreated cells.

2.3.7. Protein denaturation inhibition assay

Protein denaturation inhibition assay was carried out using egg albumin according to the previously described method (Osman et al. 2016) with slight modifications. Briefly, the reaction mixture contains 0.1 ml egg albumin, 0.7 ml PBS and 0.5 ml of varying concentrations of different compounds. Negative control contains similar amount of distilled water instead of the compounds. The mixtures were then incubated at 37°C for 15 min and heated at 70°C for 5 min. After cooling, the absorbance was measured at 660 nm using microplate reader. Diclofenac sodium was used as positive control. The inhibition percentage of protein denaturation was calculated according to the following formula:

Percentage of inhibition = [{1 − (A / B)} × 100]

Where, A = absorbance of the test sample, and B = absorbance of the negative control

2.3.8. Proteinase inhibitory activity

It was done according to the method described previously (Govindappa et al. 2011). The reaction mixture (2 ml) was consisting of 0.08 mg trypsin, 1 ml of 20 mM Tris HCl buffer (pH 7.4) and 1 ml of test compounds at desired concentrations. The mixture was then incubated at 37°C for 5 min. After that, 0.8% (w/v) casein (1 ml) was added and the mixture was incubated for additional 20 min. 1 ml of 70% perchloric acid was added to terminate the reaction. Finally, the reaction mixture was centrifuged,

and the absorbance of supernatant was measured at 210 nm. The experiment was performed twice in triplicate. The percentage inhibition of proteinase inhibitory activity was calculated by using the following formula.

Percentage of inhibition = [(Absorbance of control − Absorbance of sample) / Absorbance of control] × 100

2.3.9. Nitrite accumulation in RAW 264.7 cells

RAW 264.7 cells were seeded in 24-well plates with a density of 2×10^5 cells/well for 24 h. After aspirating the medium, 400 µl DMEM (without phenol red) containing 10% FBS and 1% penicillin/streptomycin was added to each well. Cells were incubated for 24 h with LPS (500 ng/ml final concentration) and various concentrations of the test compounds. Indomethacin at 100 µM concentration was used as a positive control. Nitrite accumulation in each well was determined using the Griess reagents (Sigma-Aldrich, Saint Louis, MO, USA). The culture supernatant (100 µl) was mixed with equal volumes of Griess reagents and incubated for 10 min at room temperature. The absorbance was recorded at a wavelength of 550 nm and compared to the standard curve prepared using a series of known concentrations of sodium nitrite.

2.3.10. Measurement of prostaglandin E2 in RAW 264.7 cells

PGE_2 is one of the major inflammatory mediators produced following COX-2 activation. RAW 264.7 cells (2×10^5 cells/well) were seeded in 24-well plates for 24 h. Cells were then treated with LPS (500 ng/ml) and different concentrations of the test compounds for 24 h. Indomethacin at 10 µM concentration was used here as a positive control. The PGE_2 levels were determined in the culture supernatant using a PGE_2 ELISA kit (Cayman Chemical Co., Ann Arbor, Michigan, USA) according to

the manufacturer's instructions. Absorbance was measured at 450 nm with a microplate reader.

2.3.11. Determination of melanin content in B16F10 cells

In vitro melanin content was measured according to a method described previously (Be Tu & Tawata 2015). In brief, the B16F10 melanoma cells were seeded with a density of 2×10^4 cells/well in 24-well plates and incubated overnight. The cells were then exposed to various sample concentrations for 48 h in the presence of 100 nM α-MSH. Then, the cells were washed twice with PBS and lyzed with 400 µl of 1 N NaOH containing 10% DMSO and incubated for 1 h at 80°C. The optical density of the mixed homogenate was measured at a wavelength of 405 nm using a microplate reader. The rates of melanin inhibition in the treatment groups were calculated in comparison to the control group.

2.3.12. Intracellular tyrosinase inhibition in B16F10 cells

Intracellular tyrosinase activity in B16F10 cells was measured with a modified way of a previous method (Be Tu & Tawata 2015). Cells were seeded at a density of 2×10^4 cells/well in 24-well plates for 24 h and exposed to different sample concentrations for 48 h in the presence of 100 nM α-MSH. The cells were then washed with ice-cold PBS and lyzed with 500 µl of phosphate buffer containing 1% TritonX and then frozen at −80°C for 30 min. After thawing and mixing, 100 µl of 0.5% L-DOPA was added to each well. Following incubation at 37°C for 2 h, the absorbance was measured at 492 nm wavelength. Intracellular tyrosinase activity was calculated in comparison to the α-MSH treated control group.

2.3.13. Mushroom tyrosinase assay

The effects of different compounds on cell free mushroom tyrosinase activity were determined spectrophotometrically with a modified method (Be Tu & Tawata 2015). Tyrosinase activity was measured using tyrosine as a substrate. In brief, 120 µl of phosphate buffer (20 mM, pH 6.8), 20 µl of sample and 20 µl of mushroom tyrosinase (500 units/ml in 20 mM phosphate buffer) were added to each well of a 96-well plate. The reaction mixture was pre-incubated at room temperature for 10 min, and then reaction was initiated by adding 20 µl of 0.85 mM L-tyrosine solution to each well, and incubation was continued for next 20 min at room temperature. Kojic acid was used as a standard tyrosinase inhibitor. The amount of dopachrome formed due to the action of tyrosinase enzyme was determined at 470 nm in a microplate reader. The percentage of tyrosinase inhibition was calculated as follows:

$$\text{Tyrosinase inhibition (\%)} = [(A - B) - (C - D)]/ (A - B) \times 100$$

Where, A is the absorbance of the control with the enzyme, B is the absorbance of the control without the enzyme, C is the absorbance of the test sample with the enzyme, and D is the absorbance of the test sample without the enzyme.

2.3.14. Brine shrimp toxicity assay

Toxicity of different compounds was evaluated with brine shrimp (*Artemia salina*) toxicity assay (Solis et al. 1993). Briefly, 200 mg of dried brine shrimp eggs (Tetra Brine Shrimp Eggs, Spectrum Brands Holdings, Inc., Kanagawa, Japan) was hatched in artificial seawater supplemented with dried yeast with suitable aeration at 28°C in room conditions for 48 h. Then, active nauplii were transferred to a glass Petri dish containing artificial seawater. Samples were primarily dissolved in DMSO and then diluted with artificial seawater. Samples were added to each well (12–15 larvae

per well in 100 µl artificial seawater), and then the well plate was kept at 20°C. The final concentration of DMSO was 1% (v/v), and DMSO at 1% was used in the control wells. After 48 h of incubation, the number of dead larvae in each well was counted using magnifying lenses (5× or 10×). Methanol (50 µl) was then added to each well, and the total number of larvae in each well was counted after 1 h. The percentage of viability for each well was then calculated.

2.3.15. Statistical Analysis

Data are expressed as the mean ± standard error (SE). Data were analyzed by paired Student's *t* test with $p < 0.05$ and $p < 0.01$ indicating significance. However, Duncan's multiple range test (DMRT) was carried out using IBM SPSS Statistics 24 (IBM Corporation, Armonk, NY, USA) at 5% probability level.

2.4. Results and discussion

2.4.1. Inhibitory effects on protein denaturation and proteinase activity

External stimuli such as strong acid or base, inorganic salt, organic solvent or thermal treatment denature the proteins structurally, and in turn proteins are failed to explore their biological potency (Chatterjee et al. 2012, Rauf et al. 2015). Denatured proteins are one of the major causes of inflammation, rheumatic disorders, cataract, and Alzheimer's disease (Saso et al. 2001, Chatterjee et al. 2012). Moreover, proteinases secreted from the neutrophils and leucocytes at inflammatory site may cause tissue damage and further inflammation, and proteinase inhibitors are thought to be effective for significant level of tissue protection (Das & Chatterjee 1995, Govindappa et al. 2011). Herein, *Alpinia* leaf-derived compounds were investigated against protein denaturation and proteinase activity *in vitro*. All compounds were

found to exhibit potential inhibitory effects on both protein denaturation and proteinase activity in a dose-dependent manner (**Figure 2.2**). DDK showed significant inhibition on egg albumin denaturation with IC_{50} value of 14.5 µM, whereas the IC_{50} values for DK, AS-2, KOG, and QOG were 14.9, 25.5, 25.4, and 20.4 µM, respectively. On the other hand, DK showed stronger proteinase inhibitory activity with IC_{50} value 39.9 µM followed by DDK, AS-2, QOG, and KOG (IC_{50} values are 43.8, 44.5, 56.6, and 63.2 µM, respectively). All compounds were found to be more effective in both protein inhibition assay and proteinase assay compared to the positive control, diclofenac sodium (IC_{50} values are 94.6 and 113.3 µg/ml, respectively). These findings, therefore, reveal the prospect of *Alpinia* leaf components to be further studied against inflammation using another model and developed into effective pharmaceutical agents as well.

2.4.2. Anti-inflammatory effects in LPS-stimulated RAW 264.7 cells

Inflammatory mediators such as nitric oxide (NO), cytokines, chemokines and eicosanoids are produced during inflammation for generating a series of protective responses. NO is considered to be a major pro-inflammatory agent (Coleman 2001) which is involved in other diseases including asthma, rheumatoid arthritis, and atherosclerosis (Lee et al. 2013). Likewise, PGE_2 is another well-studied pro-inflammatory mediator which contributes to the development of the cardinal signs of acute inflammation through redness, swelling, and pain (Ricciotti et al. 2011). Nowadays, NO and PGE_2 inhibitions have been demonstrated as an effective treatment option for inflammation and related disorders (Tamir & Tannenbaum 1996, Surh et al. 2001). In this study, the effects of purified compounds on formation of NO and PGE_2 in RAW 264.7 cells following LPS-induced inflammation were evaluated. Firstly, all

the compounds were evaluated for their effects on RAW 264.7 cell viability through MTT assay. It was revealed that the compounds didn't show cytotoxicity on RAW 264.7 cells, whereas they showed a degree of cell proliferation at specific concentrations (**Figure 2.3**), suggesting pro-proliferative activity in RAW 264.7 cells. Therefore, the non-toxic concentrations of the five compounds were used in the subsequent experiments to determine their effects on NO and PGE_2 formation. The amount of NO in culture supernatants of LPS-induced RAW 264.7 cells was measured, in the presence or absence of each compound. All the compounds inhibited NO production in a concentration-dependent manner (**Figure 2.4**). DK and DDK showed moderate inhibitory effects (IC_{50} values- 27.6 and 28.1 µM, respectively), whereas KOG and QOG showed stronger inhibition (IC_{50} values- 13.2 and 12.5 µM, respectively) on NO formation. However, AS-2 showed superior performance to all other compounds with IC_{50} value 8.2 µM against NO production. Next, the amount of PGE_2 was measured after treating the cells with different compounds at the indicated concentrations. PGE_2 production was found to be gradually decreased with the increasing concentrations of the compounds compared to the LPS-stimulated control cells (**Figure 2.4**). AS-2, KOG, and QOG showed significant effects, whereas DK and DDK were found to be less potent with regards to PGE_2 inhibition. The IC_{50} concentrations for PGE_2 inhibition by DK, DDK, AS-2, KOG, and QOG were 69.6, 92.4, 19.8, 22.7, and 23.7 µM, respectively. AS-2 showed the highest anti-inflammatory effects compared to all other tested compounds, inhibiting both NO and PGE_2 significantly. In LPS-treated macrophages, NO and PGE_2 are produced from L-arginine and arachidonic acid, respectively, and these reactions are catalyzed by transcriptional activation of iNOS and COX-2 gene, respectively (Zhou et al. 2008,

Kacem et al. 2015). Therefore, inhibition of NO and PGE_2 production by *Alpinia* leaf compounds might be attributed to their downregulatory effects on iNOS and COX-2 activity, respectively. This notion warrants further research to explore the molecular mechanisms associated with the anti-inflammatory activities of *Alpinia* leaf derived compounds.

2.4.3. Anti-melanogenic effects

Overproduction and subsequent accumulation of melanin (hyperpigmentation) cause several aesthetic problems such as freckles, age spots, melanoderma and senile lentigo. Melanin biosynthesis (melanogenesis) is mostly regulated by the rate limiting enzyme tyrosinase. During melanogenesis, reactive oxidants including hydrogen peroxide (H_2O_2) and reactive oxygen species (ROS) are produced, causing oxidative stress in melanocytes (Kim et al. 2015). This oxidative stress subsequently leads to chronic inflammation (Reuter 2010), which in turn could mediate skin hyperpigmentation and cancer. As the compounds exhibited anti-inflammatory actions, it was hypothesized that they would also exhibit anti-melanogenic potential through inhibition of tyrosinase activity and decreasing melanin content in B16F10 cells. They were found to be non-toxic to B16F10 cells (**Table 2.1**) and therefore, used at 10, 20, 50, and 100 μM concentrations to assess their anti-melanogenic effects. As shown in **Table 2.1**, all the compounds reduced melanin content dose-dependently. Of the five compounds tested, AS-2, KOG, and QOG were found to be more potent in inhibiting cellular melanin content with IC_{50} values of 30.8, 72.6, and 63.1 μM, respectively. In contrast, the apparent IC_{50} values for DK and DDK were calculated 164.4 and 139.4 μM, respectively.

Furthermore, all the compounds downregulated intracellular tyrosinase activity (**Table 2.1)**. AS-2, KOG, and QOG demonstrated superior inhibitory action on the tyrosinase enzyme with IC_{50} values of 29.6, 63.6, and 54.0 µM, respectively. DK and DDK also inhibited cellular tyrosinase with IC_{50} values of 106.9 and 112.5 µM, respectively. In this study, AS-2, KOG, and QOG showed the highest anti-melanogenic effects without interfering with the viability of B16F10 cells. They also inhibited mushroom tyrosinase activity *in vitro* (**Figure 2.5**). Of these, DK showed stronger effects on mushroom tyrosinase with IC_{50} value of 61.5 µg/ml, whereas the IC_{50} values for DDK, KOG, QOG, and AS-2 are 243.9, 422.2, 456.4, and 123.1 µg/ml, respectively. All compounds showed weak inhibitory effects on mushroom tyrosinase compared to their inhibition on cellular tyrosinase. For the screening of potential skin-whitening agents, tyrosinase activity evaluation is thought to be important, and the cellular tyrosinase assay is a more reliable assay than the cell-free mushroom tyrosinase assay in this regard (Campos et al. 2013). However, mushroom tyrosinase is found in the cytosol while tyrosinase in melanocytes is membrane bound, that's why anti-tyrosinase effects of compounds on these tyrosinases may not be the same (Chan et al. 2011).

2.4.4. Toxic effects of the compounds

Since toxicity is the major concern to use natural compounds for medicinal/food purposes, toxic effects of *Alpinia* leaf components on 3T3-L1 fibroblast cells and on brine shrimps were tested. The brine shrimp is a small animal that is widely used as a model to determine the toxicity of heavy metals, pesticides and plant extracts/compounds (Wu 2014). The effects of different compounds on brine shrimps and on 3T3-L1 cells after 48 h of incubation were shown in **Figure 2.3**. DK

at ≥ 100 μM concentration showed toxic effects on brine shrimps, whereas all other compounds at tested concentrations were found to be non-toxic. They also didn't show cytotoxic effects on 3T3-L1 cells compared to the control. However, DK and DDK showed pro-proliferative effects on 3T3-L1 cells increasing the cell proliferation significantly. On the other hand, kojic acid and indomethacin at 100 μM concentration showed significant cytotoxicity on both 3T3-L1 cells and on brine shrimps. These results indicate that *Alpinia* leaf compounds could be used as a safe natural therapeutic source compared to the commercial synthetic drugs.

From this study, it was found that *Alpinia* leaf components inhibit tyrosinase enzyme and eventually reduce melanin content in B16F10 cell culture. They also inhibit tyrosinase enzyme activity *in vitro*. Additionally, these compounds inhibit PGE_2 production and NO formation in RAW 264.7 cells, which might be due to their down-regulating effects on COX-2 and iNOS gene expression, respectively. It was reported that *Alpinia* compounds such as DK, DDK, labdadiene (12-labdadiene-15,16-dial), MTD ((1*E*,3*E*,5*E*)-6-methoxyhexa-1,3,5-trien-1-yl)-2,5-dihydrofuran), TMOQ ((*E*)-2,2,3,3-tetramethyl-8-methylene-7-(oct-6-en-1-yl)octahydro-1*H*-quinolizine), and KOG can directly inhibit PAK1 *in vitro* with the IC_{50} values of 17, 10.3, 52.1, 58.6, 49.3, and 39.3 μM, respectively (Nguyen et al. 2014, 2016, Taira et al. 2017). Out of all compounds, DK and DDK showed the highest PAK1 blocking activities, which are due to the presence of α-pyrone ring and methoxy group in their structure (Nguyen et al. 2016). However, AS-2 contains more α-pyrone ring and methoxy group in their structure than that of DK and DDK. On the other hand, chemical structure of QOG and KOG are quite similar. Therefore, it can be assumed that AS-2 and QOG may also inhibit PAK1 directly, although their PAK1 blocking effects have not been tested yet.

Taking the present study and the previous report of PAK1 blocking effects of *Alpinia* compounds into account, possible pathways on their anti-melanogenic and anti-inflammatory actions have been proposed here based on Song et al. (2002), Nguyen et al. (2017a), and Maruta et al. (2017) (**Figure 2.6**). Their anti-melanogenic effects might be induced in two different ways- direct inhibition of tyrosinase enzyme activity or down-regulation of tyrosinase enzyme through blocking its downstream effector PAK1. Similarly, their inhibition on PGE_2 and NO formation could be due to their PAK1 blocking effects and eventual down-regulation of COX-2 and iNOS activity. These proposed actions of *Alpinia* leaf compounds could be further confirmed using molecular biology study in combination with molecular modelling techniques.

2.5. Conclusion

The major compounds of *Alpinia* leaves have considerable inhibitory effects on both inflammatory and melanogenic pathways. Importantly, this dual inhibitory action is reported here for the first time. All the compounds exhibited anti-inflammatory activities through inhibiting protein denaturation, proteinase activity, and the formation of inflammatory mediators- NO and PGE_2. They also inhibited cellular tyrosinase activity and melanin formation in cultured B16F10 cells, and mushroom tyrosinase activity *in vitro* demonstrating their anti-melanogenic potentials. These compounds can inhibit PAK1, a downstream effector of inflammatory and melanogenic signaling cascades, and hence, their anti-inflammatory and anti-melanogenic effects are thought to be attributed to their PAK1 blocking activities. Additionally, all the compounds were found to be non-toxic to the brine shrimps, 3T3-L1 cells, B16F10 cells, and RAW 264.7 cells. In conclusion, *Alpinia* leaf components

can function as a source for potent and safe natural therapies to treat inflammation and hyperpigmentation, and the leaves could be commercially utilized to develop herbal supplements as well as value-added foodstuffs.

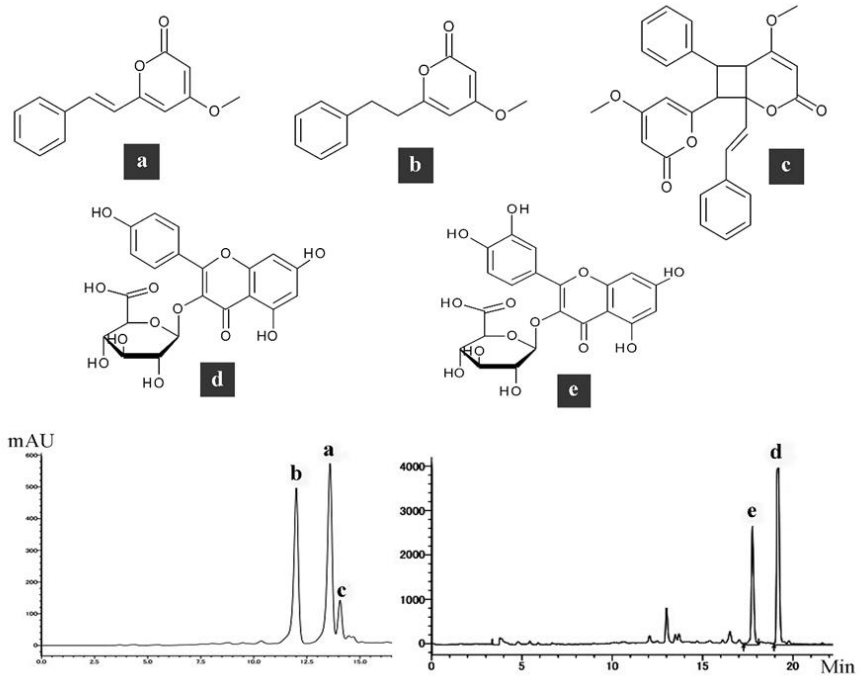

Figure 2.1. HPLC chromatograms and the chemical structures of 5,6-dehydrokawain (DK) (**a**), dihydro-5,6-dehydrokawain (DDK) (**b**), (*E*)-5-methoxy-8-(4-methoxy-2-oxo-2*H*-pyran-6-yl)-7-phenyl-1-styryl-2-oxabicyclo[4.2.0]oct-4-en-3-one (AS-2) (**c**), kaempferol 3-*O*-*β*-D-glucuronide (KOG) (**d**), and quercetin 3-*O*-*β*-D-glucuronide (QOG) (**e**).

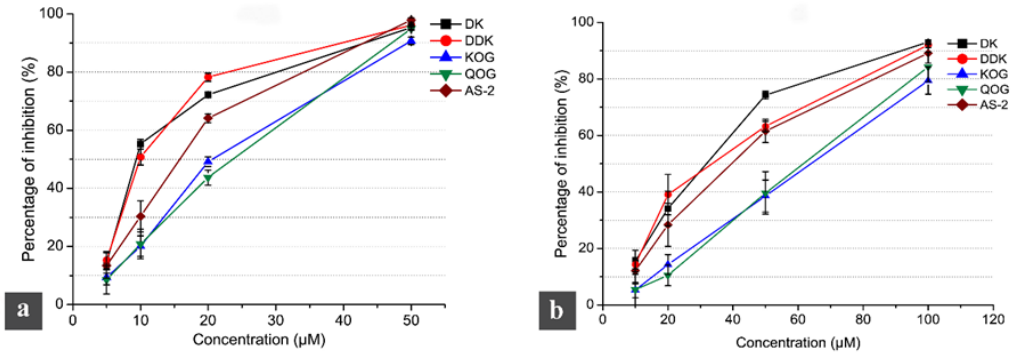

Figure 2.2. Protein denaturation inhibition effects (**a**) and proteinase inhibitory activities (**b**) of the compounds. Each data point represents mean ± SE (n = 6).

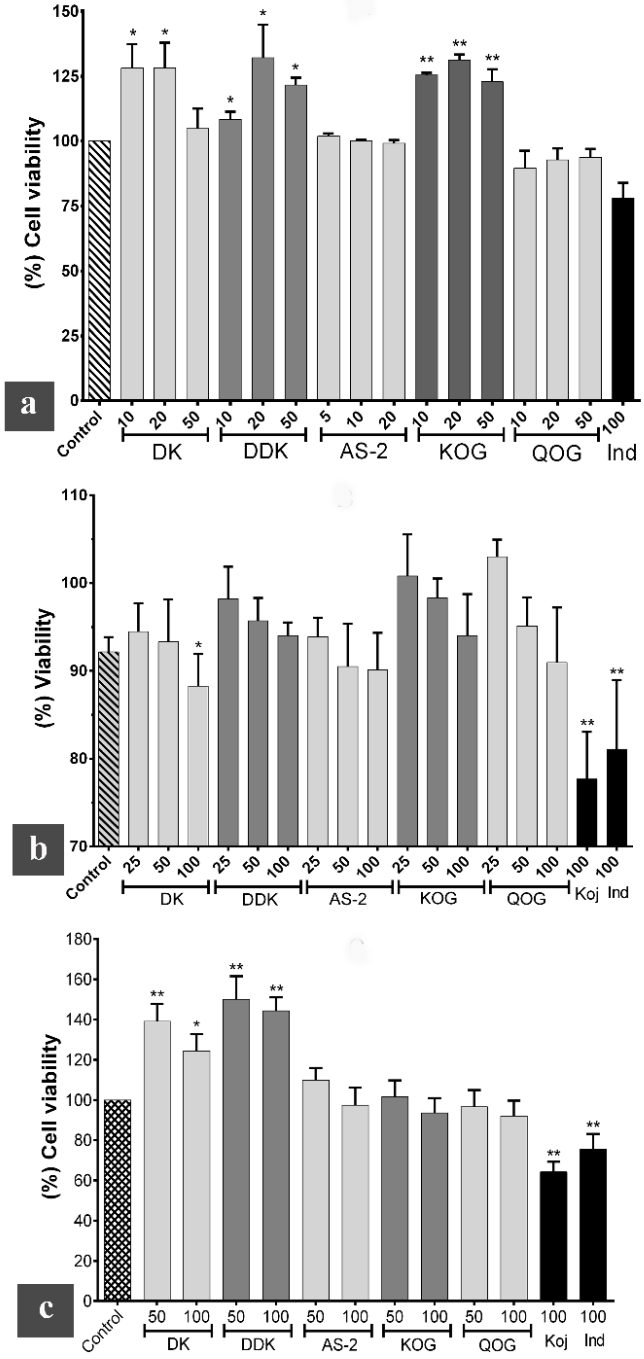

Figure 2.3. Cytotoxic effects of *Alpinia zerumbet* leaf compounds on RAW 264.7 cells (**a**), brine shrimps (**b**), and on 3T3-L1 fibroblast cells (**c**). The results are mean ± SE, and the asterisks denote significant differences compared to the control group (* $p < 0.05$; ** $p < 0.01$).

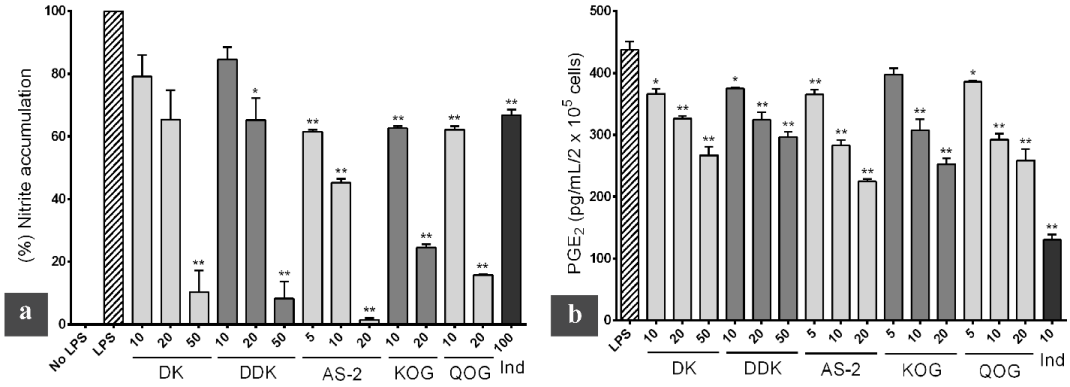

Figure 2.4. Inhibitory effects of the compounds on nitrite accumulation (**a**) and PGE_2 production (**b**) in lipopolysaccharide (LPS)-induced RAW 264.7 cells. After seeding, the cells were incubated with LPS (500 ng/ml) and varying concentrations (μM) of the tested compounds for 24 h. Data are shown as mean ± SE of two experiments. Asterisks indicate significant differences compared to the LPS-treated control group (* $p < 0.05$; ** $p < 0.01$).

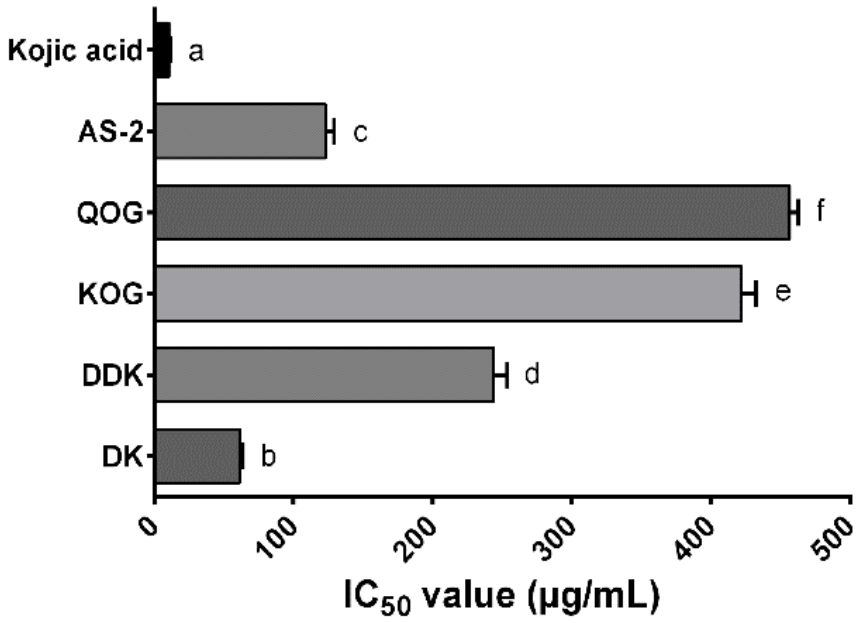

Figure 2.5. Effects of the compounds on mushroom tyrosinase activity *in vitro*. Each bar represents mean ± SE of three experiments. The different letters indicate significant differences among compounds by DMRT at 5% probability level.

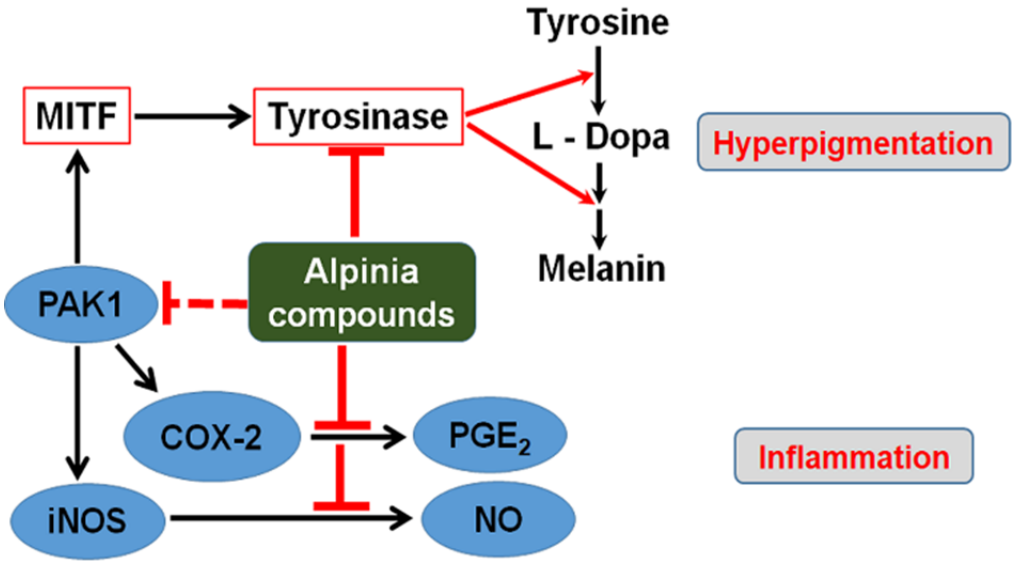

Figure 2.6. Role of PAK1 in melanogenic and inflammatory signaling pathways, and the probable inhibitory actions of *Alpinia zerumbet* components on inflammation and melanogenesis.

Table 2.1. Effects of different compounds on cell proliferation, melanin content, tyrosinase activity in B16F10 cells.

Compounds (μM)	Melanin content (% of control)	Tyrosinase activity (% of control)	Cell proliferation (% of control)
KOG			
10	82.6 ± 1.5^{ab}	79.3 ± 0.9^{b}	$106.2 \pm 0.9^{*}$
20	79.0 ± 1.3^{c}	65.0 ± 1.5^{c}	104.5 ± 1.6
50	47.8 ± 0.8^{k}	45.8 ± 1.1^{gh}	104.2 ± 0.8
100	42.4 ± 1.8^{l}	39.9 ± 1.0^{i}	99.3 ± 1.2
QOG			
10	79.9 ± 0.8^{bc}	81.7 ± 2.3^{ab}	104.0 ± 2.1
20	70.1 ± 1.1^{fg}	67.4 ± 2.9^{c}	102.3 ± 1.7
50	43.1 ± 1.1^{l}	42.5 ± 1.3^{hi}	100.6 ± 0.8
100	39.1 ± 0.6^{m}	28.7 ± 1.1^{j}	101.1 ± 1.4
DK			
10	74.0 ± 0.9^{de}	85.5 ± 2.0^{a}	104.0 ± 2.0
20	76.9 ± 1.1^{cd}	78.5 ± 2.2^{b}	100.5 ± 2.0
50	71.7 ± 1.2^{ef}	64.3 ± 2.7^{cd}	$94.2 \pm 2.8^{*}$
100	60.1 ± 0.8^{h}	54.5 ± 1.0^{ef}	$92.8 \pm 1.7^{*}$
DDK			
10	74.8 ± 1.3^{de}	86.9 ± 2.5^{a}	$106.1 \pm 1.0^{*}$
20	74.0 ± 0.8^{de}	79.1 ± 2.7^{b}	102.5 ± 2.1
50	72.6 ± 1.2^{ef}	66.8 ± 1.8^{c}	96.5 ± 2.0
100	56.3 ± 1.0^{i}	55.9 ± 1.0^{ef}	$91.2 \pm 1.5^{*}$
AS-2			
10	68.4 ± 0.3^{g}	59.2 ± 0.7^{de}	105.0 ± 0.7
20	50.9 ± 0.6^{j}	53.6 ± 0.3^{ef}	103.1 ± 0.9
50	33.8 ± 0.6^{n}	40.7 ± 0.4^{hi}	104.2 ± 1.3
100	17.3 ± 0.7^{o}	20.0 ± 0.8^{k}	100.1 ± 2.7
Kojic acid			
500	84.0 ± 0.7^{a}	51.0 ± 4.1^{fg}	98.5 ± 1.3

Values are expressed as mean ± SE (n = 6). The different letters within column 3 and 4 show significant differences among the different group means by DMRT at 5% probability level. Asterisks indicate a significant difference compared to the control group (* $p < 0.05$).

CHAPTER-III

Cytotoxic and Anti-inflammatory Bioactive Compounds from the Leaves of *Ardisia sieboldii*

3.1. Summary

Medicinal plants belonging to the genus *Ardisia* are traditionally used to cure various human diseases such as pain, swelling, rheumatism, cough, fever, diarrhea, dysmenorrhea, respiratory tract infections, inflammation, and cancer. This study was aimed to purify and characterize cytotoxic and anti-inflammatory compounds from the leaves of *A. sieboldii*. Bioassay-guided chromatographic analyses yielded three compounds, 2-methyl-5-(8*Z*-heptadecenyl) resorcinol (**1**), 5-(8*Z*-heptadecenyl) resorcinol (**2**), and ardisiaquinone A (**3**), and LC-ESI-MS (liquid chromatography-electrospray ionization-mass spectrometry) chemical profiling also revealed the presence of diverse resorcinol and alkylbenzoquinone derivatives in cytotoxic 70% methanol extracts. Chemical structures of the purified compounds (**1**–**3**) were confirmed by spectroscopic methods including ^{1}H NMR, ^{13}C NMR, and LC-ESI-MS. This study reports of purifying compounds **1** and **2** from *A. sieboldii* for the first time. Compounds **1**–**3** showed cytotoxicity against a panel of cancer cell lines and brine shrimps in a dose-response manner. Among them, compound **2** exhibited the highest cytotoxicity on cancer cells (IC_{50} values of 8.8–25.7 µM) as well as on brine shrimps (IC_{50} values of 5.1 µM). All three compounds (**1**–**3**) exhibited anti-inflammatory effects through inhibiting protein denaturation (IC_{50} values of 5.8–9.6 µM), cyclooxygenase-2 (COX-2) activity (IC_{50} values of 34.5–60.1 µM), and nitrite formation in RAW 264.7 cells. Molecular docking studies demonstrated that all compounds can strongly bind to the COX-2 protein with favorable binding free energies. The cytotoxic and anti-inflammatory activities of compounds **1**–**3** demonstrated in this study deserve further investigation for considering their

suitability as candidates or lead compounds for anti-cancer and anti-inflammatory drug development.

3.2. Introduction

Natural products discovered from the traditional medicinal plants are important sources of commercial drug development for treating of many human diseases including inflammation and cancer (Balandrin et al. 1985, Briskin 2000, Kinghorn 2008). For over 40 years, they have been playing a promising role in developing cancer chemotherapeutic agents either in their unmodified or synthetically modified forms (Kinghorn 2008). Anticancer effects of natural products are characterized by regulating immune function, inducing apoptosis or autophagy, or inhibiting cell proliferation (Rayan et al. 2017). In contrast, chemically synthesized anticancer drugs cause considerable harm to patients, mainly in the form of immune system suppression. Hence, natural products-based drugs have gained immense interest nowadays in chemotherapeutic drug discovery and development programs (Wright 2017, Yao et al. 2017). Various classes of plant derived compounds, namely the bisindole (vinca) alkaloids, the camptothecins, the epipodophyllotoxins, and the taxanes are widely used as antitumor agents (Kinghorn 2008, Molla et al. 2016). As only a small proportion of the medicinal plants have been investigated for bioactive compounds, these natural resources are still considered as important sources for the discovery of new drug candidates or lead compounds (Balandrin et al. 1985, Briskin 2000).

The genus *Ardisia* belongs to the family Myrsinaceae. Approximately 500 species of this genus are widely distributed throughout tropical and subtropical regions

of the world (Chen & Pipoly 1996). The members of this genus are known to have wide pharmacological benefits. Some novel bioactive phytochemicals such as embelin, bergenin, and resorcinol have been discovered from the species of *Ardisia*. However, a large number of species of this genus are not explored precisely for phytochemical constituents and their biological activities (Kobayashi & de Mejía 2005, de Mejía & Ramírez-Mares 2011). An evergreen shrub, *A. sieboldii* Miquel. is one of the less investigated members of *Ardisia.* Ardisiquinones A, B, C, D, E, and F were purified from the root bark and leaves of *A. sieboldii*, which exhibited inhibitory effects on 5-lipoxygenase (Ogawa et al. 1968, Fukuyama et al. 1994, 1995). No other studies have so far been conducted on isolation of cytotoxic and anti-inflammatory compounds from this medicinal plant. The leaves of *A. sieboldii* were, therefore, investigated to explore its bioactive components for cytotoxic and anti-inflammatory properties. This report describes isolation, structure elucidation, biological activities (cytotoxic and anti-inflammatory), and *in silico* studies of the isolated compounds from the leaves of *A. sieboldii*.

3.3. Materials and methods

3.3.1. Plant materials

Fresh leaves of *A. sieboldii* were collected in plastic bags from the plants grown in the premises of University of the Ryukyus, Okinawa, Japan. The plant materials were authenticated by Dr. Takahiro Ishii, Associate Professor, Department of Bioscience and Biotechnology, University of the Ryukyus, and a voucher specimen (PRC-2017-01) was deposited in PAK Research Center, University of the Ryukyus. After washing with running tap water, the leaves were dried at 45°C for 48 h and then

grounded into fine powder with a kitchen blender. The powder was stored at –80°C until using for extraction.

3.3.2. Chemicals and reagents

All the chemicals and reagents used in this study were of analytical grade. Dulbecco's Modified Eagle Medium (DMEM), casein, Griess reagents (0.1% *N*-(1-naphtyl)-ethylenediamine and 1% sulfanilamide in 5% orthophosphoric acid), 70% perchloric acid, and MTT (3-(4,5-dimethylthiazol-2-yl)-2,5-diphenyl-tetrazolium bromide) were purchased from Sigma-Aldrich (Saint Louis, Missouri, USA). The DMEM without phenol red was obtained from Thermo Fisher Scientific (Waltham, Massachusetts, USA). Fetal bovine serum (FBS) was purchased from HyClone, Victoria, Australia. Chicken egg albumin, trypsin, and penicillin or streptomycin were purchased from Funakoshi Co. Ltd. (Tokyo, Japan). All other chemicals mentioned hereafter were obtained from either Wako Pure Chemical Industries (Osaka, Japan) or Kanto Chemical Co., Inc. (Tokyo, Japan).

3.3.3. Cell culture

Murine macrophage cell (RAW 264.7), melanoma cell (B16F10), human lung cancer cell (A549), hepatocellular carcinoma cell (HuH-7), and liver cancer cell (HepG2) were cultured in DMEM supplemented with 10% FBS and 1% penicillin or streptomycin (10,000 U/ml and 100 μg/ml). Human ovarian carcinoma cell line OVCAR-3 was cultured in Roswell Park Memorial Institute (RPMI) 1640 media (Thermo Fisher Scientific, Waltham, Massachusetts, USA) supplemented with 20% FBS, 1% penicillin or streptomycin (10,000 U/ml and 100 μg/ml) and 1% insulin. All the cells were incubated at 37°C in a humidified atmosphere containing 5% CO_2.

3.3.4. Extraction, fractionation, and purification of compounds

Powdered leaf sample (40 g) was extracted repeatedly with 800 ml acetone for 6 days. Filtered extracts were evaporated with a rotary evaporator and then partitioned between ethyl acetate (EtOAc) and water (200 ml each). Collected organic layer was dried over anhydrous sodium sulfate and evaporated to get the crude extract. Crude extract was dissolved in 70% methanol (MeOH) and filtered to remove the chlorophyll and to collect the 70% MeOH extract. Similarly, 70% ethanol (EtOH) extract was also prepared from the powdered leaves. After evaporating under reduced pressure, the final yield of 70% MeOH and 70% EtOH extract was 695 and 413 mg, respectively. A portion of 70% MeOH extract (220 mg) was then fractionated by silica gel column chromatography with a step gradient of *n*-hexane/EtOAc to give six different fractions (Fraction 1–6). Fraction 2 (86 mg) was further analyzed by the preparative TLC (Thin-layer chromatography) with *n*-hexane/EtOAc (3:1) to yield compounds **1** (2-methyl-5-(8*Z*-heptadecenyl) resorcinol, 21 mg) and **2** (5-(8*Z*-heptadecenyl) resorcinol, 15 mg). Fraction 4 (80 mg) was also analyzed by the preparative TLC using *n*-hexane/EtOAc (2:3) to yield compound **3** (ardisiquinone A, 10 mg). Schematic representation of extraction and purification of *A. sieboldii* leaves is shown in **Figure 3.1**. Spectral details of the purified compounds are as follows:

Compound **1** (**Figure 3.2**): ESI-MS: *m/z* 361.4 $[M + H]^+$ (calculated for $C_{24}H_{40}O_2$, 360.57). ^{1}H NMR ($CDCl_3$, 400 MHz): δ 6.26 (2H, s), 5.37 (2H, m), 4.74 (2H, s, 1,3-OH), 2.47 (2H, t, J = 8.0 Hz), 2.12 (3H, s), 2.03 (4H, m), 1.59 (2H, m), 1.28-1.32 (20H, m), 0.91 (3H, t, J = 7.0 Hz); ^{13}C NMR ($CDCl_3$, 500 MHz): δ 154.5 (C-1 and C-3), 142.0 (C-5), 129.9 (C-8′ and C-9′), 108.0 (C-4 and 6), 107.3 (C-2), 35.5

(C-1′), 31.8 (C-15′), 31.2 (C-2′), 29.8-27.2 (C-3′-6′ and 11′-14′), 27.2 (C-7′ and 10′), 22.6 (C-16′), 14.1 (C-17′), 7.7 (2-CH_3).

Compound **2** (**Figure 3.2**): ESI-MS: *m/z* 347.3 $[M + H]^+$ (calculated for $C_{23}H_{38}O_2$, 346.54). ^{1}H-NMR ($CDCl_3$, 400 MHz): δ 6.26 (2H, d, *J* = 2.1 Hz, H-4 and H-6) 6.19 (1H, t, *J* = 2.1 Hz, H-2), 5.37 (2H, m, H-8′ and H-9′), 5.14 (2H, s, OH), 2.50 (2H, t, *J* = 7.4 Hz, H-1′), 2.01-2.06 (4H, m, H-7′ and H-10′), 1.58 (2H, m, H-2′), 1.28-1.32 (20H, m, 3′-6′, 11′-14′, 15′ and 16′), 0.90 (3H, t, *J* = 7.0 Hz, H-17′); ^{13}C NMR ($CDCl_3$, 500 MHz): δ 156.6 (C-1 and C-3), 146.1 (C-5), 129.9 (C-8′), 129.9 (C-9′), 108.0 (C-4 and C-6), 100.2 (C-2), 35.8 (C-1′), 31.8 (C-15′), 31.0 (C-2′), 29.8, 29.7, 29.5 29.5, 29.3, 29.0 (C-3′- C-6′ and C-11′-C14′), 27.2 (C-7′ and C-10′), 22.6 (C-16′), 14.1 (C-17′).

Compound **3** (**Figure 3.2**): ESI-MS: *m/z* 529.4 $[M + H]^+$ (calculated for $C_{30}H_{40}O_2$, 528.64). ^{1}H-NMR ($CDCl_3$, 400 MHz): δ 7.26 (2H, s, 2,2′-OH), 5.86 (2H, s, H-6 and H-6′), 5.36 (2H, brs, H-14 and H-14′), 3.88 (6H, s, C_5-OMe and $C_{5'}$-OMe), 2.46 (4H, brt, *J* = 6.1 Hz, H-7 and H-7′), 2.02 (4H, m, H-13 and H-13′), 1.48 (4H, m, H-8 and H-8′), 1.28-1.37 (16H, m, H-9-12 and H-9′-12′); ^{13}C NMR ($CDCl_3$, 500 MHz): δ 182.8 (C-1 and 1′), 181.7 (C-4 and 4′), 161.1 (C-5 and 5′), 151.5 (C-2 and 2′), 130.0 (C-14 and 14′), 119.2 (C-3 and 3′), 102.2 (C-6 and 6′), 56.8 (C_5-OMe and $C_{5'}$-OMe), 29.7-29.2 (C-9-12 and 9′-12′), 28.0 (C-8 and 8′), 27.1 (C-13 and 13′), 22.6 (C-7 and 7′).

3.3.5. LC-ESI-MS analysis

Phytochemical analysis of fraction 3 and fraction 6 was carried out with LC-ESI-MS (liquid chromatography-electrospray ionization-mass spectrometry) method.

Samples were analyzed on a UFLC XR (Shimadzu, Kyoto, Japan) liquid chromatography system coupled to a Waters Quattro micro API Mass Spectrometer (Waters Corporation, 34 Maple Street, Milford, MA, USA). Separations were performed using a 150 × 2.0 mm (i.d., 5 μM, Nacalai tesque) COSMOSIL C18 column. The mobile phase consisted of water containing 0.1% formic acid (A) and acetonitrile (B). The program for gradient elution started at 10% solvent B and increased linearly to 100% solvent B in 20 min. The flow rate was 0.2 ml/min, and the injection volume was 5 μl. In all experiments, the column was kept at room temperature. The UV absorbance detection wavelength was set at 254 nm. The mass spectra were obtained at a mass-to-charge ratio (*m/z*) scan range from 100 to 500. Sample was analyzed in positive ESI mode. The following MS parameters were used for the analysis: capillary voltage, 4.0 kV; source temperature, 150°C; desolvation temperature, 350°C; cone gas flow (L/h), 100; desolvation gas flow (L/h), 800. The relative collision energy was 2–3%.

3.3.6. Cytotoxicity assay

Cytotoxic effects of extracts, fractions, and purified compounds from *A. sieboldii* on cancer cell lines were evaluated through MTT assay (Shahinozzaman et al. 2018b). All the cells were seeded overnight in 48-well plates with different density. Cell density for A549, B16F10, HuH-7, HepG2, and OVCAR-3 cells were 4×10^4, 1×10^4, 2×10^4, 1×10^4, and 4×10^4 cells/well, respectively. After seeding, the cells were incubated with extracts, fractions and with the purified compounds at desired concentrations. After 48 h of incubation, the supernatant was removed, and aliquots of 100 μl MTT solution (0.5 mg/ml in phosphate buffer saline [PBS]) were added to each well. The plate was incubated again at 37°C for 3 h. After 3 h, 400 μl of DMSO

(dimethyl sulfoxide) was added to each well, and the plate was shaken for 30 min to dissolve the formazan crystals. Finally, the absorbance was measured at 570 nm wavelength with a microplate reader, and the cytotoxicity was calculated compared to the control. Similarly, the cytotoxicity was determined with the purified compounds on RAW 264.7 cells. However, in this case, the cells were seeded at a density of 2×10^5 cells/well for 24 h and then treated with the compounds at different concentrations for next 24 h.

3.3.7. *In vivo* cytotoxicity assay with brine shrimp

In vivo cytotoxicity of the compounds was tested using brine shrimp nauplii (*Artemia salina*) (Shahinozzaman et al. 2018b). The eggs of brine shrimp were hatched in a tank filled with artificially prepared sea water supplemented with dried yeast with suitable aeration at 28°C in room conditions for 48 h. No food supplement was given during experimental periods. Compounds were dissolved in DMSO (15 mg/ml) and diluted with artificial seawater. Then, the compounds were added to each well containing 10–15 nauplii/well in 100 µl artificial seawater, and the well plate was incubated at 20°C for 48 h. DMSO concentration in each well was kept below 0.5%. The negative control was prepared in the same manner without the samples. After incubation period, the well plate was observed using a magnifying glass, and the number of survivors in each well were counted and noted. The IC_{50} values were calculated using the plot of percentage of mortality and concentrations of the compounds tested. All tests were performed in triplicate.

3.3.8. Albumin denaturation assay

Albumin denaturation inhibition assay was carried out using the egg albumin (Shahinozzaman et al. 2018c). The reaction mixture consisted of egg albumin (0.1 ml),

PBS (0.7 ml), and varying concentrations of different compounds (0.5 ml). Similar amount of distilled water instead of the compounds was used in the negative control. Afterwards, the reaction mixtures were incubated at 37°C for 15 min and heated at 70°C for 5 min. The absorbance was measured at 660 nm after cooling at room conditions. Diclofenac sodium was used as a positive control. Albumin denaturation inhibition percentage was calculated according to the following formula:

Percentage of inhibition = [{1 – (A / B)} × 100]

Where, A = absorbance of the test sample, and B = absorbance of the negative control

3.3.9. Nitrite assay

Nitrate assay was carried out using RAW 264.7 cells (Shahinozzaman et al. 2018c). Cells were plated on a 24-well plate with a density of 2×10^5 cells/well and treated with lipopolysaccharide (LPS, 500 ng/ml final concentration) and the test compounds for 24 h. Each 100 µl of culture supernatant was mixed with an equal volume of Griess reagents and incubated at room temperature for 10 min. The formation of an azo compound was measured spectrophotometrically at 550 nm with a microplate reader. Nitrite concentration was determined from a standard curve prepared with sodium nitrite. Nitrite produced by the untreated control cells was considered as 100% and based on it, the inhibition percentages were calculated. Indomethacin was used as a reference drug.

3.3.10. *In vitro* cyclooxygenase-2 (COX-2) inhibition assay

Inhibitory effects of the compounds on cyclooxygenase-2 (COX-2) enzyme activity were determined through a previously reported method (Nguyen et al. 2017a). Briefly, the recombinant human COX-2 was treated with the samples at the indicated

concentrations (10–100 µM) for 5 min at room temperature in the presence of arachidonic acid. Then, the absorbance was measured at 590 nm. The COX-2 activity in the wells without containing the test samples were used as negative control, whereas the wells which didn't have COX-2 were used as blank for calculating their inhibitory effects on COX-2.

3.3.11. Molecular docking

Three-dimensional structures of the compounds **1**, **2**, and **3** were drawn and fully optimized by B3LYP/6-31G (d,p) level of theory using Gaussian 09 program suit (Frisch et al. 2009). Subsequent vibrational frequencies of these compounds were computed at same level of theory to confirm that the stationary points correspond to the minima on the potential energy surface. The optimized structures of these compounds were then saved as pdb (protein data bank) format. The crystal structures of COX-2 protein (PDB ID: 5F19) was retrieved from the RCSB Protein Data Bank (https://www.rcsb.org/). Prior to docking, all heteroatoms (such as water, ions etc.) were removed from the crystal structure using Accelrys Discovery Studio 4.5 (Accelrys, San Diego, CA, USA). Molecular docking studies were carried out with AutoDock Vina software (The Scripps Research Institute, La Jolla, CA). During docking simulation, grid box was determined based on the active site residues of COX-2 (Labib et al. 2018, Omar et al. 2018, Kaur et al. 2018). Center of the grid box size was 8.98, 49.02, 59.34 in x, y, z axis, and the dimensions were 31.74, 23.66, and 25.0 Å in x, y, and z axis, respectively. The docked poses with the highest negative values was selected to be the best pose which was finally visualized and analyzed by PyMOL Molecular Graphics System 2.0 (DeLano Scientific LLC, San Carlos, CA, USA) and Accelrys Discovery Studio 4.5.

3.3.12. Data analysis

Results are expressed as the mean ± SE (standard error) of three independent experiments in triplicate. Multiple comparisons were performed using one-way analysis of variance followed by Duncan's multiple range tests using IBM SPSS Statistics 24 (IBM Corporation, Armonk, NY, USA) at 5% probability level.

3.4. Results and discussion

3.4.1. Bioactivity-guided isolation of chemical constituents

Acetone extract prepared from the powdered leaves of *A. sieboldii* was dark green color, hence, it was speculated that acetone extract contains high amount of chlorophyll contents. To remove the insoluble chlorophyll pigments, 70% MeOH and 70% EtOH extract was prepared stepwise from acetone crude extract (Kitai et al. 2015). Both 70% MeOH and 70% EtOH extracts were tested on four cancer cell lines including A549, B16F10, HuH7, and HepG2. They showed varied toxicity on cancer cells, however, 70% MeOH extract was found to have the highest toxicity on all cancer cells. IC_{50} values for 70% MeOH extract were 24.8–42.7 µg/ml, whereas for 70% EtOH extract, IC_{50} values were 38.4–61.8 µg/ml (**Figure 3.3**). These results demonstrated that 70% MeOH extract contains bioactive compounds responsible for notable cytotoxic effects on cancer cells. To identify the active principles in 70% MeOH extract, it was further fractionated through silica gel column chromatography that yielded six fractions (fractions 1–6). All fractions were evaluated against cancer cells, and fractions 2, 3, 4, and 6 showed notable toxicity on cancer cells (**Table 3.1**). Fractions 2 and 3 significantly inhibited cell proliferation with IC_{50} values 14.1–32.6 and 23.6–36.7 µg/ml, respectively. Effects of fractions 2 and 3 were followed by fractions 6 and 4. IC_{50} values for fraction 6 were 33.7–66.9 µg/ml and for fraction 4

were 37.3–80.3 µg/ml. In contrast, fraction 5 showed moderate cytotoxic effects with IC_{50} values more than 100 µg/ml for all the cell types tested, whereas, fraction 1 didn't show cytotoxicity. Then, fractions 2 and 4 were subjected to preparative TLC, and fractions 3 and 6 were analyzed by LC-ESI-MS in the next step to determine their active constituents. TLC analysis leads to purification of two resorcinol derivatives, **1** and **2**, from fraction 2 and an alkylbenzoquinone derivative, **3**, from fraction 4. Compounds **1** and **2** were purified from *A. sieboldii* plant for the first time. Chemical structures of the purified compounds (**1**–**3**) were determined by comparing their spectral data to those reported in the literature (Fukuyama et al. 1995, Zheng & Wu 2007, Liu et al. 2009).

3.4.2. Phytochemical profile of fractions 3 and 6 by LC-ESI-MS analysis

Chemical profiling of fractions 3 and 6 was done with LC-ESI-MS analysis (Souli et al. 2018, Zihad et al. 2018). The sample solution was injected in LC-MS system according to the previously-mentioned chromatographic conditions with positive-ion MS scanning and was analyzed by mass spectrum. Recorded total ion chromatograms (TIC) offered help to detect the desired ion peaks which were matched with the previously reported chemical constituents of *A. sieboldii* (Ogawa et al. 1968, Fukuyama et al. 1995, Horgen et al. 1997, Yang et al. 2001, Ndontsa et al. 2012). Based on the molecular weights and recorded mass of molecular ions ($[M + H]^+$), nine compounds were tentatively identified in fraction 3 and 6. The LC-ESI-MS analysis indicated that the peaks appearing at 8.49, 18.18, 18.69, 20.08, 20.59, and 21.02 min (**Figure 3.4**) in fraction 3 are ardisiquinone H, ardisenone, ardisiquinone F, ardisiquinone B, ardisiquinone C, and ardisiquinone D, respectively (**Table 3.2**). On the other hand, the peaks appearing at 15.68, 18.10, and 19.12 min (**Figure 3.4**) in

fraction 6 are ardisiquinone I, ardisiquinone P, and ardisiquinone N, respectively (**Table 3.2**). All of these identified compounds were reported to have a wide array of biological activities. Of them, ardisenone showed cytotoxic effects against a panel of human cancer cell lines (Horgen et al. 1997). However, ardisiquinone N was recommended as a promising antimicrobial agent (Ndontsa et al. 2012, Paul et al. 2014). It was also reported to have significant cytotoxicity on brine shrimps with 72% mortality (Ndontsa et al. 2012). Ardisiquinones D and E were demonstrated as 5-lipoxygenase enzyme inhibitors (Fukuyama et al. 1995). Chromatographic separation and LC-ESI-MS studies revealed that *A. sieboldii* leaf contains diverse bioactive components which warrant of further study.

3.4.3. Cytotoxic effects of the purified compounds

Compounds **1**, **2**, and **3** were tested against five cancer cell lines to assess their effects on cancer cell proliferation through MTT assay technique. In this assay, only viable cells convert MTT to purple formazan dye that was measured spectrophotometrically after solubilizing with DMSO. All three compounds showed notable but varying levels of cytotoxicity on cancer cell lines with a dose-response manner. Compound **2** showed the highest cytotoxicity (IC_{50} values of 8.8–25.7 µM) followed by compound **1** (IC_{50} values of 18.2–32.7 µM) and compound **3** (IC_{50} values of 27.8–41.3 µM) (**Table 3.1**). Of the five cell lines tested, B16F10 cell proliferation was greatly affected by all compounds, indicating that the tested compounds could effectively be used to treat melanoma skin cancer compared to treating other cancer types. These observations are consistent with several previous studies where resorcinol and alkylbenzoquinone derivatives from *Ardisia* spp. were reported to have cytotoxic

effects on different cancer cells like PANC-1, A549, SGC7901, MCF-7, PC-3, and EMT6 etc. (Liu et al. 2009, Bao et al. 2010, Chen et al. 2011).

To reinforce the *in vitro* findings, *in vivo* cytotoxic effects of the isolated compounds (**1**–**3**) were evaluated using brine shrimp nauplii which is an excellent model for testing *in vivo* cytotoxicity of natural compounds/drugs (Meyer et al. 1982). All compounds dose-dependently affected the viability of brine shrimps (**Figure 3.5**). Similar to the *in vitro* observations, compound **2** showed stronger effects with IC_{50} value of 5.1 µM, followed by compounds **1** and **3** with IC_{50} values of 21.8 and 7.3 µM, respectively. Importantly, compound **3** was found to be less toxic on cancer cells, however, it showed the second highest inhibitory effects on brine shrimps. These results conform with a previous observation by Ndontsa et al. (2012) who purified six alkylbenzoquinone derivatives from the leaves and stems of *A. kivuensis* and found them as cytotoxic against brine shrimps. These data, therefore, together demonstrate the potentiality of purified compounds from *A. sieboldii* as cytotoxic agents and their future prospect of utilizing as promising chemotherapeutic drugs.

3.4.4. Anti-inflammatory effects of *A. sieboldii* metabolites

Epidemiological evidences reveal a connection between inflammation and cancer progression, and approximately 25% of cancers are associated with inflammation. Inflammatory mediators exert pleiotropic effects during cancer development (Multhoff et al. 2012). Hence, inflammation is nowadays considered to be a hallmark of cancer (Colotta et al. 2009). In this study, the purified compounds were primarily tested *in vitro* to assess their inhibitory effects on protein denaturation. Cellular proteins are denatured during inflammation, and subsequently failed to explore their biological potency (Rauf et al. 2015). All the compounds showed stronger

inhibition on albumin denaturation concentration-dependently (**Figure 3.6**) with IC_{50} values of 9.6, 7.7, and 5.8 µM for compounds **1**, **2**, and **3**, respectively, clarifying their prospective role as anti-inflammatory agents. Their nitrite inhibitory potential in LPS-stimulated RAW 264.7 cells was also tested. Firstly, all compounds were tested on RAW 264.7 cells to explore their cytotoxicity. They didn't show toxicity to the RAW 264.7 cells as they showed on cancer cells. Compounds **1** and **3** were not found to be toxic up to 50 µM concentration, whereas, compound **2** showed significant toxicity at 20 µM concentration. Then, the compounds only at their non-toxic concentrations were treated on LPS-stimulated RAW 264.7 cells and they showed nitrite inhibitory properties in a concentration-dependent manner (**Table 3.3**). Compound **2** showed the strongest effect on nitrite formation. At 20 µM concentration, compound **2** inhibited 21.3% nitrite production in cell supernatants. On the other hand, compounds **1** and **3** inhibited 37.3% and 40.6% nitrite formation at 50 µM. Nitrite is used as an index of iNOS (inducible nitric oxide synthase) activity in LPS-stimulated cell cultures and it is one of the major pro-inflammatory mediators involved in various inflammation-related diseases (Sharma et al. 2007). Hence, nitrite inhibition activities of the compounds observed in this study might be attributed to their downregulatory effects on iNOS protein expression. All the compounds were then evaluated for their inhibitory actions on COX-2 enzyme which is responsible for producing inflammatory mediator PGE_2. They also dose-dependently suppressed *in vitro* COX-2 enzyme activity (**Figure 3.6**). The IC_{50} values for COX-2 inhibition by compounds **1**, **2**, and **3** were 60.1, 34.5, and 41.7 µM, respectively. Drugs showing inhibitory effects on both nitrite formation and COX-2 enzyme could be potent for treating inflammation and related disorders (Shahinozzaman et al. 2018a). Moreover, natural product-derived

drugs are implicated to be safe, effective, and even better as anti-inflammatory agents than synthetic drugs (Yatoo et al. 2018). Thus, *A. sieboldii* leaf-derived compounds **1**–**3** can be used as safe herbal drugs for treating inflammation successfully.

3.4.5. Docking study

Molecular docking is the most common method being widely used in drug development and pharmaceutical researches (Pripp 2007, Meng et al. 2011). In this study, molecular docking was performed using the resolved crystal structure of COX-2 protein (PDB ID: 5F19) to investigate the possible binding interactions of compounds **1**–**3** with the COX-2 and to predict their mechanisms of action as anti-inflammatory agents. Probable binding orientations of the compounds **1**–**3** inside the COX-2 are shown in **Figure 3.7**. Docking study revealed that compounds **1** and **3** can bind to the active site of COX-2, whereas compound **2** can bind to allosteric site very close to the catalytic cleft. However, all compounds showed good binding energy ranging −7.5 to −9.0 kcal/mol. Compound **3** showed higher affinity with the lowest binding free energy (−9.0 kcal/mol), which can form hydrogen bond to the active site residue Tyr355 (**Table 3.4**). It can also form more three hydrogen bonds with the backbone residues Ser119, Pro86, and Phe529. Compound **2** can form one hydrogen bond only with the allosteric site residue, Met522 close to the active site. But, compound **1** can interact only with hydrophobic bonds, which can form one hydrophobic bond with the active site residue Tyr355. In short, docking studies reported here validate the prospect of using compounds **1**–**3** for developing anti-inflammatory drugs as COX-2 inhibitors.

3.5. Conclusion

In this study, three cytotoxic and anti-inflammatory compounds (**1**–**3**) were purified from 70% methanol extract of *A. sieboldii* leaves through bioassay-guided fractionation. In addition, phytochemical profiling with LC-ESI-MS analysis demonstrated this plant to be a rich source of bioactive compounds. However, the purified compounds **1**–**3** exhibited considerable cytotoxic activities against four cancer cell lines and anti-inflammatory effects through inhibiting protein denaturation, nitrite formation, and COX-2 activity *in vitro*. Since these compounds didn't show notable toxicity to the non-cancerous murine macrophage RAW 264.7 cells, their cytotoxicity could be more specific towards cancer cells. Molecular docking studies revealed that compounds **1**–**3** have favorable binding affinities with COX-2 protein, where compounds **1** and **3** can bind to the active sites and compound **2** can bind to the allosteric sites. Taken together, bioactive components from *A. sieboldii* leaves merit further investigation to evaluate their usefulness as safe natural drug candidates for treating cancer and inflammatory disorders in human.

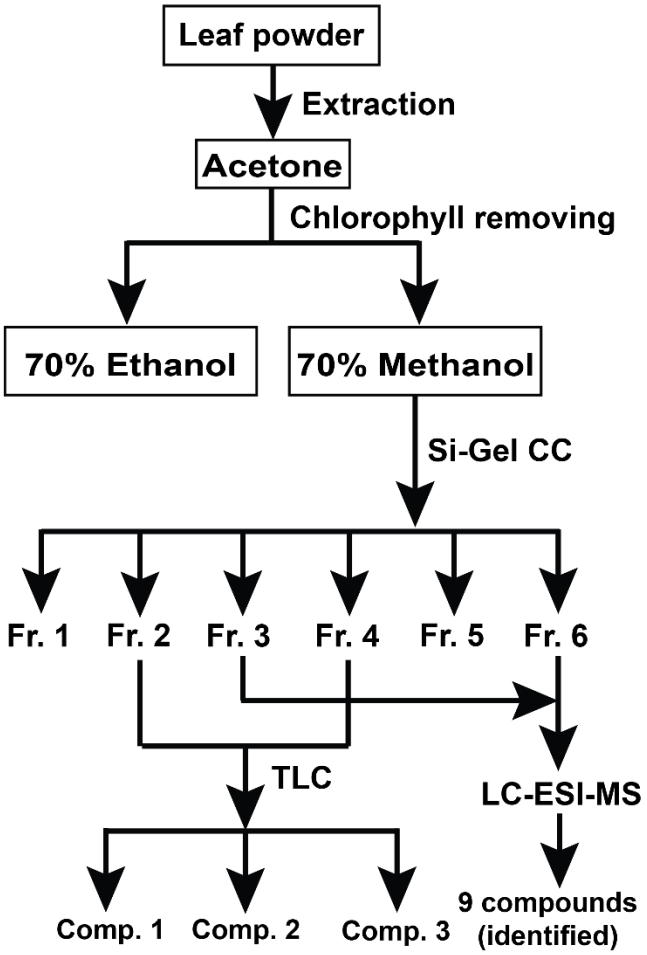

Figure 3.1. Schematic representation of the extraction method of *Ardisia sieboldii* leaves. Si-Gel CC: Silica gel column chromatography; Fr: Fraction; TLC: Thin-layer chromatography; LC-ESI-MS: Liquid chromatography-electrospray ionization-mass spectrometry; Comp: Compound.

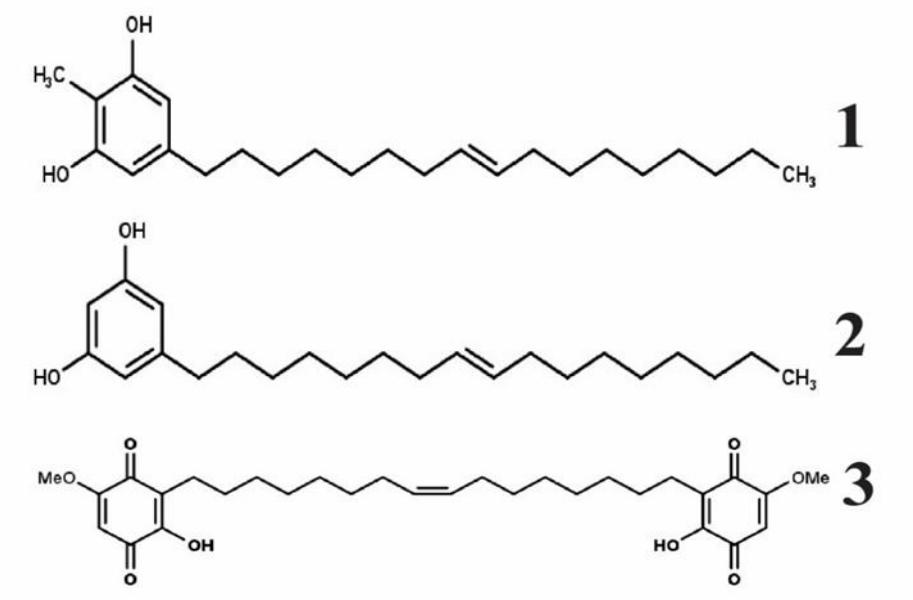

Figure 3.2. Structures of the compounds **1** {2-methyl-5-(8*Z*-heptadecenyl) resorcinol}, **2** {5-(8*Z*-heptadecenyl) resorcinol}, and **3** (ardisiaquinone A).

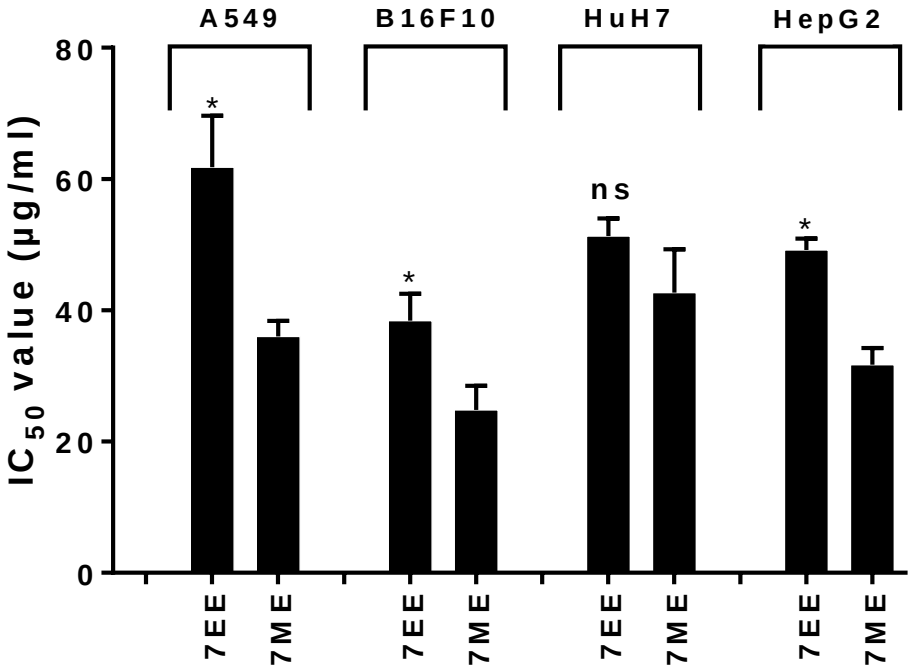

Figure 3.3. Cytotoxic effects of two extracts on different cancer cells. Each bar represents mean ± SE of three independent experiments in triplicate. * $p < 0.05$ *vs*. others in the same group; ns = non-significant; 7EE = 70% ethanol extract; 7ME = 70% methanol extract.

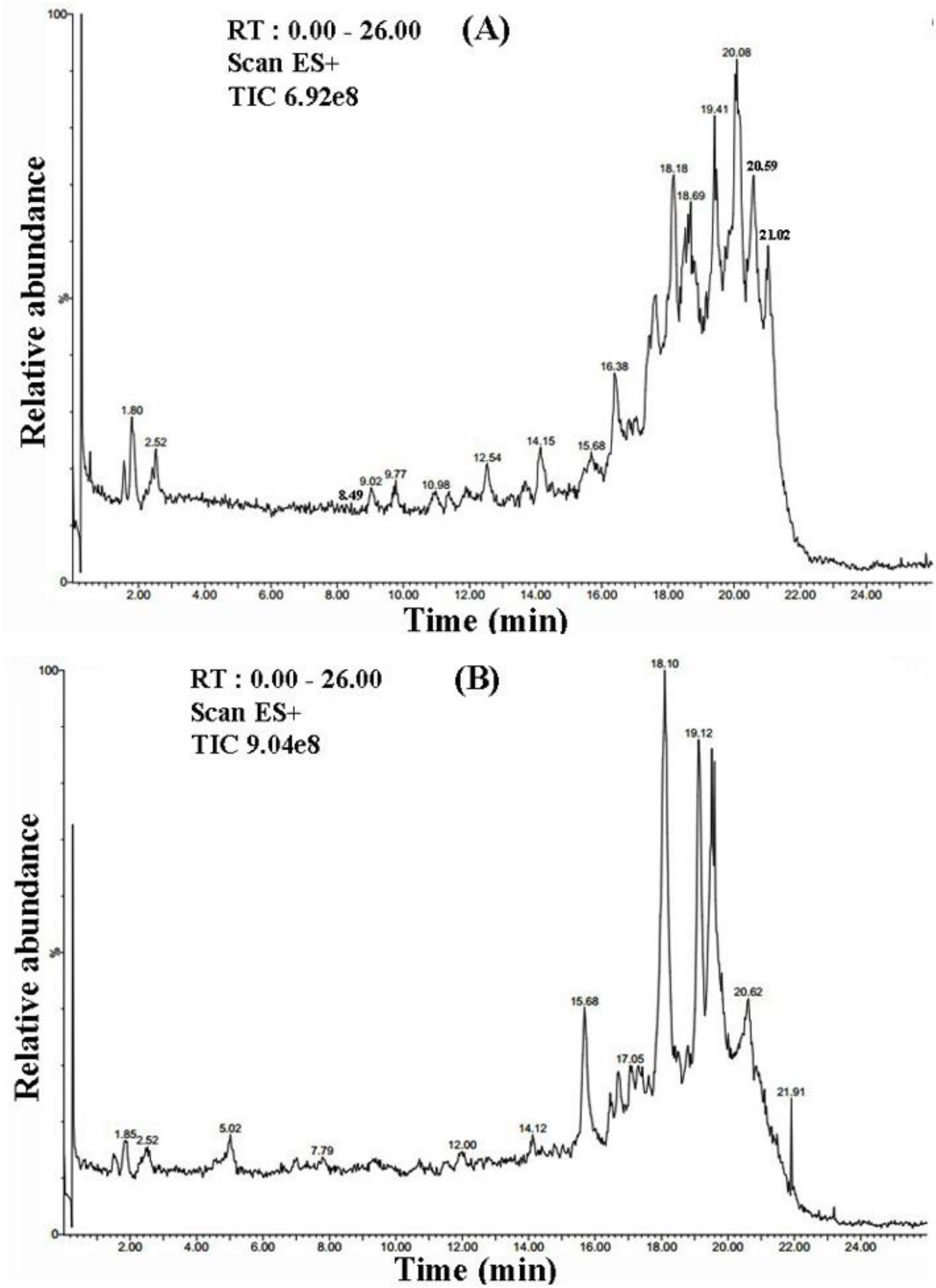

Figure 3.4. Total ion chromatograms of fraction 3 (**A**) and fraction 6 (**B**) prepared from the 70% methanol extract of *Ardisia sieboldii* leaves.

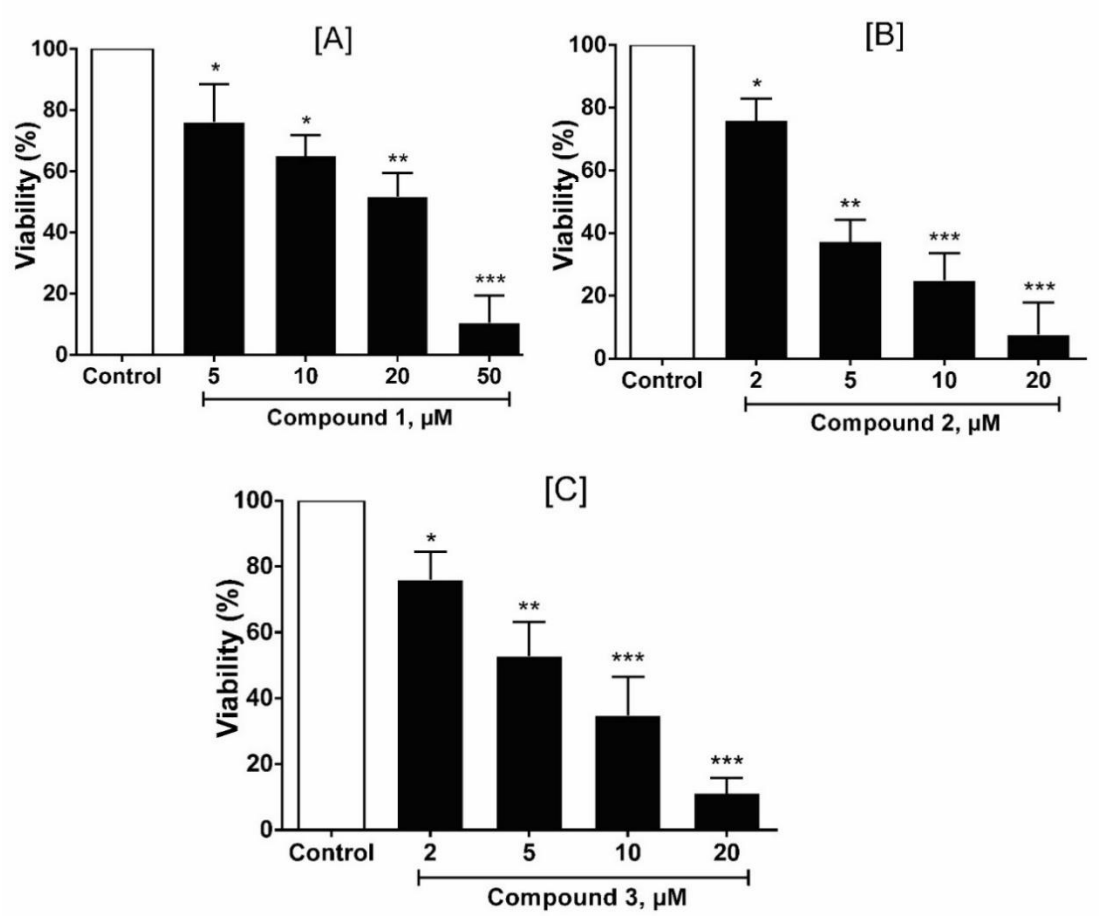

Figure 3.5. Effects of compounds **1** (A), **2** (B), and **3** (C) on the viability of brine shrimps. The results are mean ± SE of three independent experiments. Asterisks indicate statistically significant differences between the control and treatment. * $p < 0.05$, ** $p < 0.01$, *** $p < 0.001$.

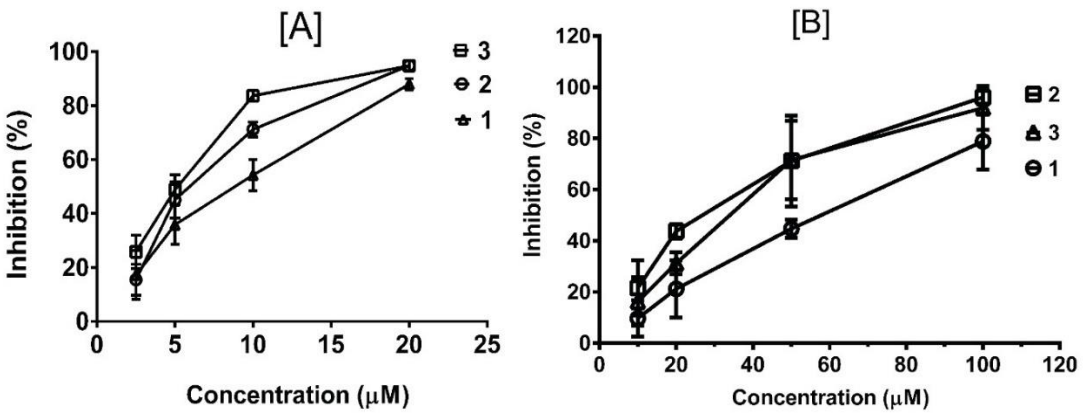

Figure 3.6. Inhibitory effects of the compounds on albumin denaturation (**A**), and COX-2 (cyclooxygenase) activity (**B**). Each data point represents mean ± SE of three independent experiments.

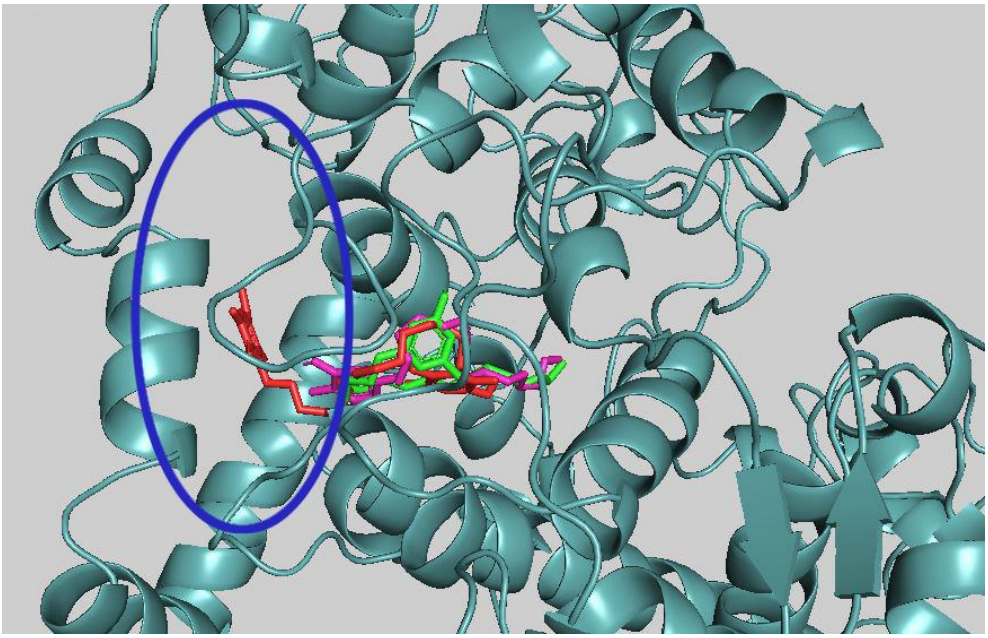

Figure 3.7. Binding orientations of the compounds inside the cyclooxygenase-2 (COX-2) protein. Compounds **1**, **2**, and **3** were demonstrated in magenta, green, and red color, respectively. Blue circle represents the position of the active site of COX-2.

Table 3.1. Cytotoxic effects of different fractions and purified compounds of *Ardisia sieboldii*.

Fractions	IC_{50} value[a]			
	A549	**B16F10**	**HuH7**	**HepG2**
Fr 1	nc	nc	nc	nc
Fr 2	26.1 ± 4.5^{cd}	14.1 ± 3.7^{d}	32.6 ± 4.7^{cd}	24.6 ± 1.8^{cd}
Fr 3	36.7 ± 6.7^{c}	23.6 ± 5.4^{c}	36.6 ± 5.4^{bc}	29.0 ± 2.9^{c}
Fr 4	80.3 ± 2.1^{a}	47.8 ± 1.7^{a}	55.3 ± 6.7^{a}	37.3 ± 1.7^{ab}
Fr 5	>100	>100	>100	>100
Fr 6	66.9 ± 1.9^{b}	33.7 ± 4.8^{ab}	48.9 ± 3.9^{b}	39.6 ± 2.7^{a}
Compounds	IC_{50} value[b]				
	A549	**B16F10**	**OVCAR-3**	**HUH-7**	**HepG2**
1	27.7 ± 5.2^{b}	18.2 ± 4.7^{b}	32.7 ± 3.4^{a}	22.7 ± 6.1^{b}	20.7 ± 7.4^{b}
2	15.2 ± 4.8^{c}	8.8 ± 9.7^{c}	25.7 ± 5.2^{b}	17.9 ± 9.1^{bc}	14.0 ± 6.9^{bc}
3	41.3 ± 2.9^{a}	27.8 ± 4.8^{a}	nd	31.7 ± 4.3^{a}	29.2 ± 2.7^{a}

Data represents mean ± SEM of three experiments. [a] Values are expressed in μg/ml. [b] Values are expressed in μM. nd = not determined; nc = no cytotoxicity observed. Different superscript letters indicate significant differences by Duncan's multiple range tests at 5% probability.

Table 3.2. LC-ESI-MS identification of the major compounds in fraction 3 and fraction 6 prepared from *Ardisia sieboldii* leaves.

Si. No.	Suggested compounds	RT (min)	Chemical formula	Molecular mass (Calculated)	$[M + H]^+$ (Experimental)	References
1	Ardisenone	18.18	$C_{30}H_{40}O_6$	496.63	497.4	Horgen et al. (1997)
2	Ardisiquinone B	20.08	$C_{30}H_{40}O_8$	528.63	529.4	Ogawa et al. (1968)
3	Ardisiquinone C	20.59	$C_{32}H_{42}O_9$	570.67	571.4	Ogawa et al. (1968)
4	Ardisiquinone D	21.02	$C_{31}H_{42}O_8$	542.66	543.5	Fukuyama et al. (1995)
5	Ardisiquinone F	18.69	$C_{30}H_{42}O_6$	498.65	499.5	Fukuyama et al. (1995)
6	Ardisiquinone H	8.49	$C_{32}H_{43}O_{10}$	587.68	588.5	Yang et al. (2001)
7	Ardisiquinone I	15.68	$C_{33}H_{45}O_{10}$	601.70	602.4	Yang et al. (2001)
8	Ardisiquinone N	19.12	$C_{28}H_{38}O_8$	502.60	503.4	Ndontsa et al. (2001)
9	Ardisiquinone P	18.10	$C_{30}H_{44}O_8$	532.66	533.4	Ndontsa et al. (2001)

RT: Retention time

Table 3.3. Effects of different compounds on cell viability and nitrite inhibition in lipopolysaccharide-induced RAW 264.7 cells.

Compounds (μM)		Cell viability (%)	Nitrite inhibition (%)
1	10	106.1 ± 6.4	9.4 ± 1.6^{f}
	20	$119.2 \pm 1.4^{**}$	16.6 ± 3.8^{ef}
	50	99.0 ± 2.4	37.3 ± 3.8^{ab}
2	5	104.9 ± 5.2	11.1 ± 2.5^{f}
	10	102.9 ± 1.4	21.3 ± 1.6^{de}
	20	$63.9 \pm 3.2^{**}$	nd
3	10	101.5 ± 4.2	15.7 ± 1.4^{ef}
	20	100.4 ± 6.5	26.9 ± 1.6^{cd}
	50	97.9 ± 2.7	40.6 ± 0.3^{a}
Indomethacin	100	$78.0 \pm 5.9^{**}$	33.1 ± 1.9^{bc}

Data represents mean ± SEM of three experiments. 'nd'= not determined due to high toxicity. ** $p < 0.01$ *vs*. untreated control. Different superscript letters indicate significant differences by Duncan's multiple range tests at 5% probability.

Table 3.4. Binding free energy, type of interactions of compounds **1**–**3** with the cyclooxygenase-2 protein.

Compounds	Binding energy (kcal/mol)	Hydrogen bonds residue	Distance (Å)	Hydrophobic interactions residue
1	−7.5	-	-	Ala527, Val116, Ile377, Phe209, Tyr355, Val349, Leu351
2	−8.5	Met522	2.71	Val228, Ile377, Phe209, Leu352, Val523
3	−9.0	Ser119 Ser119 Tyr355 Pro86 Phe529	2.57 2.94 2.87 3.76 3.09	Val349, Ala527, Leu531,Val 89

CHAPTER-IV

Cytotoxic Desulfated Saponin from *Holothuria atra* Predicted to Have Inhibitory Effects on PAK1

4.1. Summary

Sea cucumbers have long been utilized in foods and Asiatic folk medicines for their nutritive and health benefits. In this study, three sea cucumber species were investigated, of which *Holothuria atra* showed the highest cytotoxicity on different cancer cells. Next, a desulfated saponin, desulfated echinoside B (DEB), was purified from *H. atra* through bioassay-guided fractionation. LC-ESI-MS analysis also showed *H. atra* to be a rich source of saponins. DEB showed cytotoxicity on cancer cells with IC_{50} values of 0.5–2.5 µM, and on brine shrimps with an IC_{50} value of 9.2 µM. In molecular docking studies, DEB was found to bind strongly with the catalytic domain of PAK1 (p21-activated kinase 1) and it showed binding energy of −8.2 kcal/mol compared to binding energy of −7.7 kcal/mol for frondoside A (FRA). Both of them bind to the novel allosteric site close to the ATP-binding cleft. Molecular dynamics (MD) simulation demonstrated that DEB can form a more stable complex with PAK1, remaining inside the allosteric binding pocket and forming the maximum number of hydrogen bonds with the surrounding residues. Moreover, important ligand binding residues were found to be less fluctuating in the DEB-PAK1 complex than in the FRA-PAK1 complex throughout MD simulation. Experimental and computational studies showed that both DEB and FRA can act as natural allosteric PAK1 inhibitors and DEB appeared to be more promising than FRA. Furthermore, *H. atra* could be a suitable marine source for exploring more potent saponins against cancer cell proliferation.

4.2. Introduction

Marine resources represent novel reservoirs of biologically active components, and thus are valued as nutritious foods and traditional medicines worldwide (Blunden

2001, Guerard et al. 2011). In recent decades, many significant bioactive substances have been extracted from marine organisms (Sarfaraj et al. 2012). Sea cucumbers are an important marine organism, which are widely consumed in China and other Asian countries, due to having numerous health benefits (Kiew & Don 2012). In addition to their good flavor, they are traditionally used to treat many diseases including wounds, eczema, arthritis, hypertension, and impotence (Sugawara et al. 2006, Ridzwan 2007). Saponins (triterpene glycosides) are thought to be the major ingredient of sea cucumbers, which have been used in drug discovery due to their diverse biological activities. Recent studies have demonstrated that sea cucumber saponins can cause growth arrest of cancerous cells (Janakiram et al. 2015), along with their antioxidant, anti-inflammatory, anti-fungal, anti-angiogenesis, anti-tumor, and immunomodulatory effects (Zou et al. 2003, Tian et al. 2005). In a recent report, it has been demonstrated that frondoside A (FRA), a sulfated saponin extracted from *Cucumaria frondosa*, can selectively inhibit the major oncogenic kinase PAK1 (p21-activated kinase 1), thereby showing significant anti-cancer effects (Nguyen et al. 2017b). PAK1 is essential for the development of RAS cancers which represent over 90% of pancreatic cancer, 50% of colon cancer and 30% of lung cancer (Nguyen et al. 2018). It is also involved in generating many other diseases such as viral/bacterial infections, inflammatory diseases (asthma and arthritis), type 2 diabetes, neurofibromatosis, tuberous sclerosis, epilepsy, depression, schizophrenia, autism etc. (Maruta 2014). Recently, developing PAK1 inhibitors has gained immense interest among researchers and pharmaceutical industries, particularly those involved in cancer drug development (Maruta & Ahn 2017). To date, several synthetic PAK1-blockers have been developed; however, none has received FDA approval as a commercial drug due to non-selectivity and toxicity

(Maruta 2014). Hence, sea cucumbers, as a promising marine product, were considered for this study with a view to exploring their anti-cancer properties and developing a series of potent PAK1 blocking saponins. In this study, three sea cucumber species were investigated *in vitro* for cytotoxicity, and further *in silico* evaluation of the binding interactions of purified saponin with PAK1 through molecular docking and molecular dynamics (MD) simulation (Mangiaterra et al. 2017, Razzaghi-Asl et al. 2018, Niazi et al. 2018) was carried out. This combined approach, therefore, would be a benchmark for developing better PAK1-blocking cancer chemotherapeutics.

4.3. Materials and methods

4.3.1. Cell culture and reagents

Human lung cancer cell line A549, hepatocarcinoma cell line HuH-7, liver cancer cell line HepG2, and murine melanoma cell line B16F10 were maintained in DMEM (Dulbecco's Modified Eagle Medium, Thermo Fisher Scientific, Waltham, MA, USA) supplemented with 10% FBS (Fetal bovine serum, HyClone, Victoria, Australia) and 1% penicillin/streptomycin (10,000 U/ml and 100 μg/ml) at 37°C in a humidified atmosphere containing 5% CO_2. 3-(4,5-Dimethylthiazol-2-yl)-2,5-diphenyl-tetrazolium bromide (MTT) and FRA were purchased from Sigma-Aldrich (Saint Louis, MO, USA). All other reagents were of analytical grade and were obtained from either Wako Pure Chemical Industries (Osaka, Japan) or Kanto Chemical Co., Inc. (Tokyo, Japan).

4.3.2. Collection of sea cucumber species and their extraction

Holothuria atra and *H. leucospilota* (**Figure 4.1**) were collected by diving on the coast of the Pacific Ocean near Uruma city, Okinawa, Japan. *Parastichopus*

nigripunctatus (**Figure 4.1**) was collected from the coastal areas of Mie prefecture, Japan. They were carefully dissected to collect the body walls which were then dried at 50°C for 4 days. Dried body walls (100 g) were ground to make a powder which was soaked in 1000 ml 70% ethanol (EtOH) for 72 h. Then, the supernatant was collected through vacuum filtration, and the remaining powder was again soaked in 70% EtOH for the next 72 h. Extraction was done thrice and combined. Hot water extraction was done by soaking the powder in boiling water for 1 h. The hot water supernatant was collected through vacuum filtration. Both the extractions were dried under reduced pressure using rotavapor (Buchi, Switzerland).

4.3.3. Extraction of crude saponin and its fractionation

The 70% EtOH extract of each species was further partitioned between water and chloroform, and the aqueous layer was extracted with *n*-butanol. The organic layer was evaporated to yield *n*-butanol extract which was then concentrated and dissolved in water and chromatographed with reversed-phase C18 silica gel, using water-methanol gradient elution to yield several fractions. The fraction eluted with 100% methanol is referred as crude saponin (Hu et al. 2010, Bahara et al. 2016, Moghadam et al. 2016). Crude saponin of *H. atra* was further fractionated with high performance liquid chromatography (HPLC, Shimadzu, Kyoto, Japan). The HPLC conditions were as follows: column- semipreparative reversed phase column Luna 5u C18 (10 × 250 mm); solvent A-0.1% ammonium acetate (1 M); solvent B-acetonitrile + 0.1% ammonium acetate (1 M); flow rate-3.0 ml/min; absorbance-200 nm. The elution was performed with 60% solvent B for 45 min. Fr 4 was identified as a pure saponin, desulfated echinoside B (DEB) (**Figure 4.2**), and the retention time for DEB was 20 min. Its structure was determined based on ^{1}H, ^{13}C NMR, and ESI-MS spectral data

and by comparison with those previously reported in the literature (Kitagawa et al. 1985, Anjaneyulu & Raju 1996). In addition, GC (gas chromatography) and GCMS (gas chromatography mass spectrometry) analyses of trimethylsilyl (TMS) and 2-octyl-glycoside derivatives from DEB further confirmed that the sugar moiety consists of D-xylose and D-quinovose.

Desulfated echinoside B (DEB): white solid; $[\alpha]_D^{24}$ –15.4 (*c* 0.1, pyridine). ESI-MS: *m*/*z* 789.6 $[M + Na]^+$ (calculated for $C_{41}H_{66}O_{13}Na$, 789.4401). ^{1}H NMR (pyridine-d_5, 400 MHz): δ 5.58 (1H, d, *J* = 4.3 Hz), 5.19 (1H, d, *J* = 5.9 Hz), 4.77 (1H, d, *J* = 5.9 Hz), 1.72 (3H, s), 1.65 (3H, d, *J* = 6.6 Hz), 1.65 (3H, s), 1.37 (3H, s), 1.33 (3H, s), 1.16 (3H, s), 0.81 (6H, d, *J* = 5.3 Hz). ^{13}C NMR (pyridine-d_5, 100 MHz): δ 174.7 (C-18), 154.1 (C-9), 115.5 (C-11), 106.2 (C-1″), 105.7 (C-1′), 89.2 (C-17), 88.8 (C-3), 87.1 (C-20), 84.0 (C-2′), 78.1 (C-3′), 77.8 (C-3″), 77.1 (C-4″), 76.7 (C-2″), 73.5 (C-5″), 71.3 (C-12), 70.8 (C-4′), 66.7 (C-5′), 58.5 (C-13), 52.8 (C-5), 46.3 (C-14), 40.8 (C-8), 40.1 (C-4), 39.7 (C-10), 38.8 (C-24), 36.6 (C-22), 36.4 (C-1), 35.8 (C-16), 28.3 (C-28), 28.1 (C-25), 27.9 (C-7), 27.1 (C-15), 27.1 (C-2), 22.9 (C-30), 22.6 (C-21), 22.5 (C-27), 22.5 (C-26), 22.2 (C-23), 21.2 (C-6), 20.0 (C-19), 18.6 (C-6″), 16.7 (C-29).

4.3.4. Phytochemical characterization of crude saponin

To analyze the major ingredients in crude saponin of *H. atra*, LC/MS analysis was performed on a UFLC XR (Shimadzu, Kyoto, Japan) liquid chromatography system coupled to a Waters Quattro micro API Mass Spectrometer (Waters Corporation, 34 Maple Street, Milford, MA, USA). Samples were analyzed with a flow rate of 0.2 ml/min for 40 min and with the following gradient program: solvent A: 0.1% formic acid; solvent B: acetonitrile; gradient: 0–3 min 10% B, 3–30 min 10 to 100% B, 30–35 min 100% B, 35.01–40 min 10% B. The injection volume was 10 µl.

The mass spectra were obtained at a mass-to-charge ratio (*m/z*) scan range from 100 to 2000, and the sample was analyzed in positive ESI mode. Respective MS conditions were as follows: capillary voltage, 4.0 kV; source temperature, 120°C; desolvation temperature, 350°C; cone gas flow (L/h), 100; desolvation gas flow (L/h), 800. All data were processed using MassLynx 4.1 software (Waters Corporation, 34 Maple Street, Milford, MA, USA).

4.3.5. Cytotoxicity assay

Cells were cultured in the absence and presence of sea cucumber components in variable concentrations, and cytotoxic effects were evaluated through MTT assay (Ha et al. 2007). Briefly, seeded cells were incubated with the desired samples for 72 h. Then the supernatant was removed and aliquots of 100 µl MTT solution (0.5 mg/ml in phosphate buffer saline) were added to each well, and the plate was incubated again at 37°C for 3 h. Afterwards, 500 µl DMSO (dimethyl sulfoxide) was added to each well, and the plate was shaken for 20 min to dissolve the formazan crystals. The absorbance was measured spectrophotometrically at 570 nm wavelength, and the cell viability was calculated from the absorbance of treated versus untreated cells.

4.3.6. *In vivo* cytotoxicity assay

The *in vivo* cytotoxicity of pure saponin was determined using brine shrimps (*Artemia salina*) (Solis et al. 1993). In brief, the desired sample solution (100 µl) was added into each well of a 96-well plate, containing 5–10 larvae in artificial seawater (100 µl). The plate was incubated at 20°C for 24 h. The number of dead larvae in each well was counted using a magnifying lens (5× or 10×). Larvae were considered dead if they did not exhibit any movement. Methanol (50 µl) was added to each well and

after 1 h the total number of larvae was counted, and then the toxicity was calculated for each sample.

4.3.7. Molecular docking simulation

The three-dimensional (3D) structure of the catalytic domain of PAK1 (PDB ID: 3FXZ) was downloaded from the protein data bank (https://www.rcsb.org/). Then this protein was prepared for docking through removing the heteroatoms with Discovery Studio 4.5 (Accelrys, San Diego, CA, USA). Two dimensional (2D) structures of the ligands were drawn and converted to 3D structures using ChemBio3D Ultra 12.0 (CambridgeSoft, Cambridge, MA, USA). Full optimization of the ligands was carried out via Gaussian 09 (Gaussian, Inc., Wallingford, CT, USA) using the PM6 semi-empirical method. The ligands were saved in pdb format and further used as the input file for molecular docking simulation. AutoDock Vina (The Scripps Research Institute, La Jolla, CA, USA) was used for molecular docking simulation. It is an open source program widely used for molecular docking simulation, which significantly improves the accuracy of the binding mode predictions compared to AutoDock 4 (Trott & Olson 2010). The grid box size was set to maximum to include all the PAK1 catalytic domain, and the dimensions of the grid box were 52.06, 59.09, and 44.73 Å for the x, y, and z axes, respectively. The binding pose with the lowest binding affinity was selected as the best pose for the corresponding ligand, and the best poses were further compared with previous studies. The ligand-protein interactions were then visualized and analyzed using PyMol (Schrödinger, Inc., New York, NY, USA) and Discovery Studio 4.5 (Accelrys, San Diego, CA, USA).

4.3.8. Molecular dynamics (MD) simulation

MD simulation was conducted on the docked DEB and FRA complex employing the AMBER14 force field (Maier et al. 2015) in YASARA dynamics suite (Krieger et al. 2003, 2004). The MD system was neutralized by adding NaCl (0.9%) with a pH of 7.4. Unless otherwise noted, the temperature of the simulation was set to 298 K. The transferable intermolecular potential3 points (TIP3P) water model was employed and the total water molecules were 4729 with a density of 1.012 g/cm^3. The periodic boundary condition (PBC) was adopted for performing the simulation, where the box size was 80.5 × 80.5 × 80.5 Å^3. The initial energy minimization process of each simulation system was performed by the simulated annealing method, using the steepest gradient approach (5000 cycles). For measuring the long-range electrostatic interactions, the particle-mesh Ewald approach (Darden et al. 1993) was used. In addition, for short-range van der Waals and Coulomb interactions, a cut-off radius of 8.0 Å was applied. A multiple time step algorithm together with a simulation time step interval of 2.50 fs was used. At a constant pressure of 1 bar and a temperature of 298 K using the Berendsen thermostat, the production run was performed for 20 ns where trajectories were saved at every 100 ps. The MD trajectories were analyzed by a macro program written in YANACONDA language. In this analysis, time, energy, bond distance, bond angle, dihedral angles, columbic and van der Waals interactions, and root mean square deviation (RMSD) values for backbone, alpha carbon, and heavy atoms were collected. To detect the binding affinities after 20 ns MD simulation, ligands were extracted from the simulated complexes and redocked to the corresponding receptor using AutoDock Vina (The Scripps Research Institute, La Jolla, CA, USA) with the same protocol as stated before.

4.3.9. Data analysis

MTT assays were carried out with 5–6 different treatments having at least 5 replications. Data are represented as IC_{50} values which were calculated through linear regression analysis.

4.4. Results and discussion

4.4.1. Cytotoxic effects of sea cucumber components

Since ancient times, sea cucumbers have been used as a dietary ingredient and traditional medicine, especially in Asian countries. Many recent studies suggest that sea cucumber-derived saponins have significant cytotoxicity on cancer cells through multiple mechanisms including cell cycle progression interference, inducing apoptosis, microtubule stabilization, and generation of ceramide (Kim & Himaya 2012, Yun et al. 2012, Tian et al. 2013). This study was, therefore, aimed to identify and purify the cytotoxic saponin from sea cucumber. Three different species were collected and extracted with hot water and 70% EtOH separately. Both extracts were investigated for their cytotoxic effects on A549 and B16F10 cells. Irrespective of the extraction methods, *H. atra* showed the highest cytotoxicity, followed by *H. leucospilota* and *P. nigiripunctatus* (**Table 4.1**). Compared to hot water extractions, hydro-alcoholic extractions were found to be more cytotoxic. 70% EtOH extract of *H. atra* strongly inhibited both A549 and B16F10 cells with IC_{50} values of 10.5 and 7.9 µg/ml, respectively, indicating that this extract could be utilized for further fractionation to purify the active components. These results were found to be promising compared to a previous study by Dhinakaran and Lipton (2014) who reported methanol extract of *H. atra* to be cytotoxic to the Hela and MCF-7 cells with IC_{50} values 468.0 and 352.0 µg/ml, respectively. Next, crude saponin was prepared from hydro-alcoholic extracts

of the three species and investigated on cancer cell proliferation. Compared to *H. leucospilota* and *P. nigiripunctatus*, *H. atra* crude saponin induced the highest toxicity on A549 and B16F10 cells with IC_{50} values of 1.8 and 0.5 µg/ml, respectively (**Table 4.1**). These findings demonstrated that cytotoxic effects of sea cucumbers might be due to their saponin contents, and hence, an attempt was taken to purify individual saponin from *H. atra* crude saponin.

Through HPLC, five fractions (Fr 1–Fr 5) were prepared from *H. atra* crude saponin and tested on A549 and B16F10 cells (**Table 4.2**). Fr 2 showed the maximum cytotoxicity (IC_{50} values 0.72 and 0.24 µg/ml, respectively) followed by Fr 4 (IC_{50} values 1.34 and 0.50 µg/ml, respectively). Fr 4 was identified as a pure saponin DEB via spectroscopic evidence, and this is the first report of purifying DEB from natural source. DEB was tested for cytotoxicity on cancer cells, and its effects were compared to another active saponin FRA (**Figure 4.2**). DEB showed cytotoxic effects on different cancer cell lines similar to those of FRA. In the case of A549 and B16F10 cells, however, DEB induced more cytotoxicity than FRA with IC_{50} values of 1.5 and 0.5 µM, respectively (**Table 4.3**). The cytotoxicity of DEB was also confirmed through *in vivo* assay with brine shrimps (Parveen et al. 2016). It was also found to be more toxic to the brine shrimps than FRA, and the IC_{50} value was 9.2 µM. These findings together confirm the anti-cancer potential of *H. atra* and the future prospect of DEB in chemotherapeutic drug development research.

4.4.2. Phytochemical profile of *H. atra* saponin

LC-ESI-MS analysis was carried out to reveal the phytochemical profile of *H. atra* crude saponin. The sample solution dissolved in methanol was injected into the LC-MS system and analyzed with positive-ion MS scanning. Total ion chromatogram

(TIC) was recorded and the corresponding *m/z* value of the base peak was collected from the source fragmentation (**Figure 4.3**). One aglycone and two saponins were tentatively identified comparing their *m/z* values to those reported in the literature. The peaks appearing at 15.86, 16.81, and 20.68 min are holothurinogenin B, holothurinoside K_1, and philinopgenin B, respectively (Van Dyck et al. 2010, Hidalgo 2013, Van Thanh et al. 2017). During this investigation, molecular ions with *m/z* values ranging from 200–800 $[M + H]^+$ were observed in abundance, indicating the presence of aglycones or saponins with low molecular weight. This analysis only allowed to identify the known saponins; however, it is necessary to purify individual saponins and then check them using sophisticated spectroscopic techniques for more clarification.

4.4.3. Molecular docking studies

Herein, molecular docking techniques were used to explore the binding orientation, affinities, and interaction type of DEB and FRA with the kinase domain of PAK1. All docked compounds were found to bind to the same binding cleft near the hinge region between the C-terminal lobe and the N-terminal lobe (**Figure 4.4**). They bind to an allosteric site close to the ATP-binding site, which has been reported to be a novel binding site for allosteric inhibitors (type III kinase inhibitors) (Karpov et al. 2015). In this study, DEB showed binding free energy of −8.2 kcal/mol compared to −7.7 kcal/mol for FRA. Both of them showed hydrogen bond interaction with the α*C* helix residue Glu315 situated in the DFG-out pocket. FRA also interacted with Asp407, a DFG-motif residue, and Thr541, Leu347, Gln278, Arg299, Gly350, Asp354, Thr406 via hydrogen bonds (**Table 4.4**). DEB showed more interaction with Arg299 and Tyr346 through hydrogen bond formation. Arg299 was reported to interact with

bound ATP in PAK1-KD^{K299R} and with bound FRAX597 in the PAK1 kinase domain (Wang et al. 2011, Licciulli et al. 2013). DEB and FRA formed one hydrogen bond to the hinge residue Tyr346 and Leu347, respectively, but they did not show hydrogen bond interactions to Glu345 and Leu347 together (**Table 4.4**). Glu345 and Leu347 are found in the activation loop and are responsible for the binding of ATP-competitive inhibitors to PAK1 (Balupuri et al. 2016). However, none of the ligands interacted with the gatekeeper residue Met344. These types of interactions are also observed in some other PAK1 crystal structures co-crystallized with different native ligands (4ZLO, 4ZJJ, 4ZJI). In conclusion, both DEB and FRA could be utilized as promising allosteric PAK1 inhibitors and they might also exhibit selective features to the PAK1. Allosteric inhibitors are preferred nowadays due to their selectivity to the kinase, whereas ATP-competitive inhibitors bind to the highly conserved ATP site of all kinases (Karpov et al. 2015).

4.4.4. Molecular dynamics

The molecular docking simulation of DEB and FRA against PAK1 protein is further confirmed by 20 ns molecular dynamics. The RMSD of backbone atoms in DEB-PAK1 complex revealed that the system becomes stable at around 800 ps and remained within 1.5 Å compared to the docked pose (**Figure 4.5**). However, the FRA-PAK1 complex becomes stable after 6 ns and continued to be stable up to 20 ns at around 2.0 Å. Overall, MD simulation further confirmed that both ligands remained within the allosteric binding pocket of PAK1 similar to the docking results (**Figure 4.6**). RMSF (root mean square fluctuation) was also analyzed to observe per residue fluctuations throughout the simulation. A large fluctuation was observed in both cases with more than 3.0 Å, but most of the residues were found to be stable within 2.0 Å

(**Figure 4.5**). Importantly, residues (Arg299, Glu315 and so forth) responsible for ligand binding in the allosteric site were found to be slightly less fluctuating (dynamic) in the DEB-PAK1 complex (RMSF: 0.03–0.178 Å) compared to those in the FRA-PAK1 complex (RMSF: 0.086–0.213 Å). Moreover, DEB and FRA were extracted from the 20 ns MD simulated complexes and redocked with the PAK1 conformer. The binding free energy of −9.3 kcal/mol was observed in the DEB-PAK1 complex, compared to −7.6 kcal/mol in the FRA-PAK1 complex (**Table 4.5**). After 20 ns MD simulation, it was found that DEB forms six hydrogen bonds; among them one bond with αC helix residue Glu315, four bonds with DFG motif residue Asp407, and one bond with Gly277. On the other hand, the number of hydrogen bonds was reduced in MD simulated FRA-PAK1 complex where only three hydrogen bond interactions with Asp354, Thr406, and Tyr346 were observed. Results indicate that DEB could form a more stable complex with PAK1 than FRA, hence DEB might be a potent natural allosteric inhibitor.

4.5. Conclusion

In short, the sea cucumber species studied here possess remarkable cytotoxic effects, and among them *H. atra* was found to be the best, irrespective of the extraction method. Their cytotoxic effects may be due to the presence of special saponin ingredients. Phytochemical investigation demonstrated that *H. atra* could be further studied as a rich source of saponins. Desulfated saponin DEB exhibited stronger cytotoxicity on cancer cells and on the brine shrimps than FRA. Molecular docking analysis predicted strong molecular interactions of DEB with the active domain of PAK1, where it binds to the allosteric ligand binding pocket. During MD simulation,

DEB showed more stable binding with PAK1 compared to FRA. This study concludes that *H. atra* could be a significant source of cytotoxic saponins, and DEB could be effectively used for chemotherapeutic drug development with more selective inhibitory effects on PAK1 than FRA.

Figure 4.1. Sea cucumber species after dissection and drying. (**A**) *Holothuria atra*; (**B**) *H. leucospilota*; (**C**) *Parastichopus nigripunctatus.*

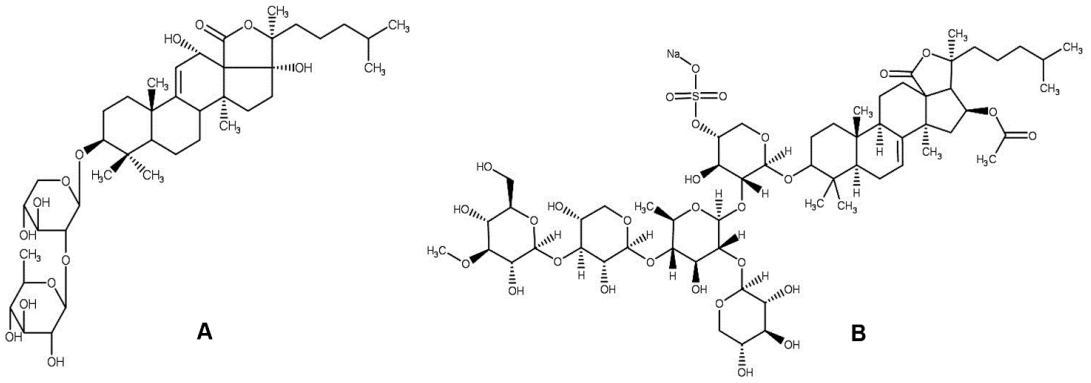

Figure 4.2. Chemical structures of desulfated echinoside B (DEB) (**A**) and frondoside A (FRA) (**B**).

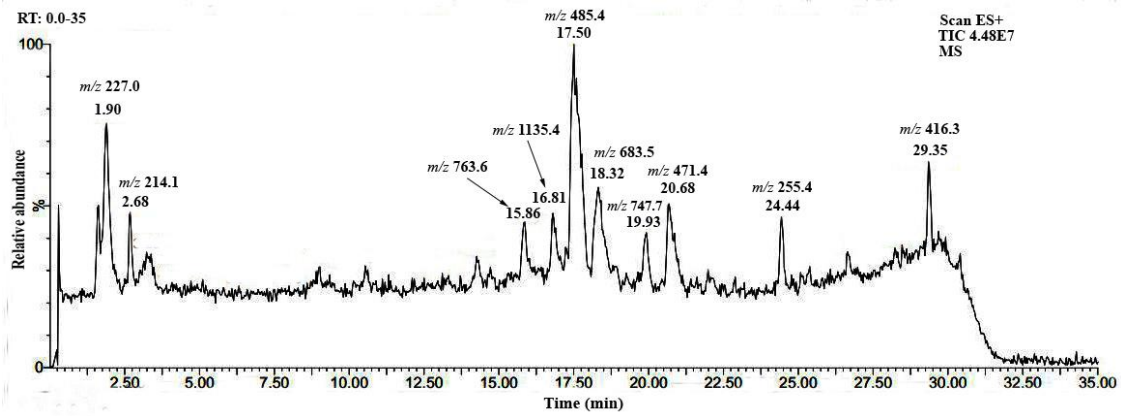

Figure 4.3. Total ion chromatogram of crude saponin of *Holothuria atra* showing the mass spectrum (MS) values of major components.

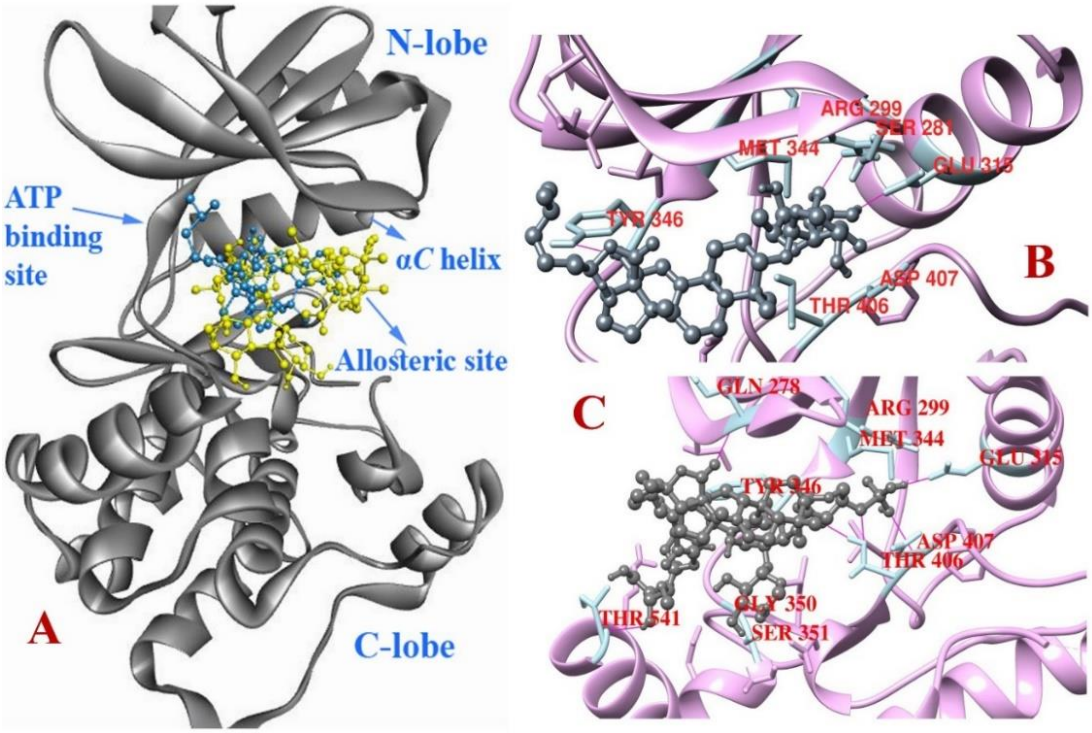

Figure 4.4. Predicted pose from the docking analysis shows binding orientation of DEB (Desulfated echinoside B) (blue) and FRA (Frondoside A) (yellow) in the allosteric site of PAK1 kinase domain (**A**). Non-bonding interactions of DEB and FRA to the allosteric site residues (**B**, **C**). Representative hydrogen bonds between ligand and receptor are shown with lines (pink).

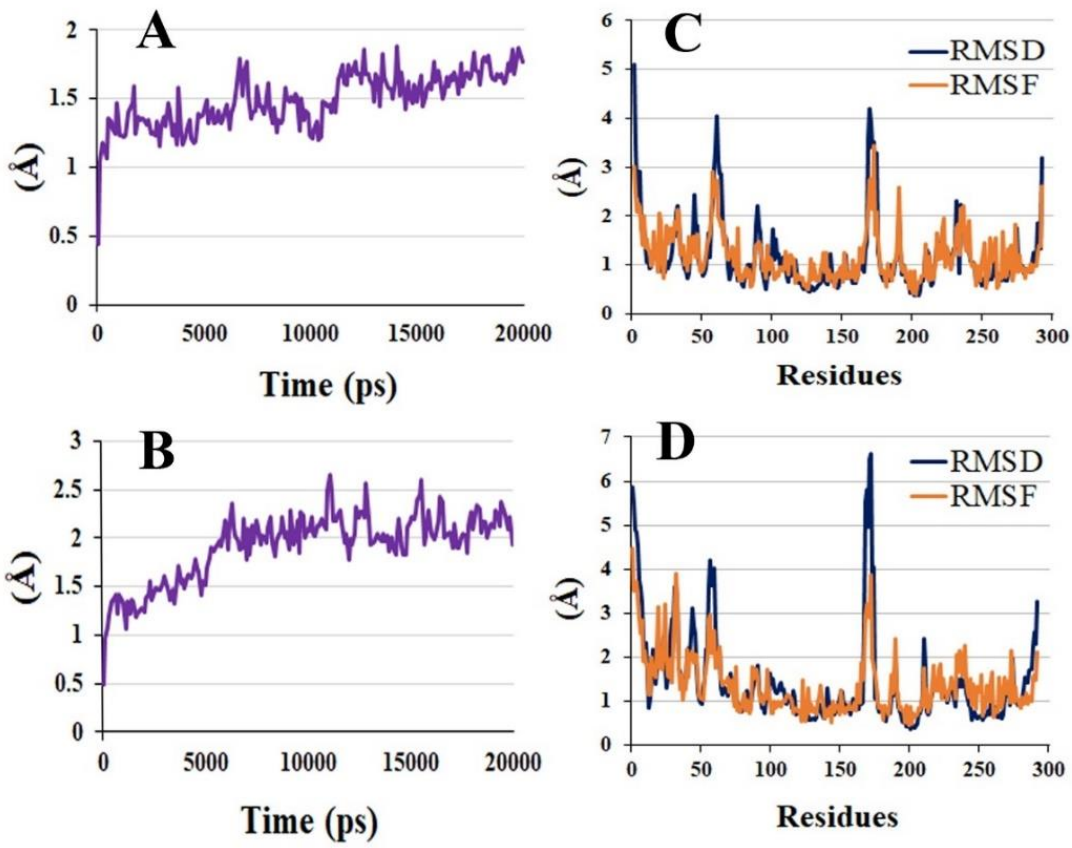

Figure 4.5. The time series of root mean square deviations of backbone atoms for DEB (Desulfated echinoside B) and FRA (Frondoside A) complex (**A**, **B**). Structural modification of protein by means of root mean square deviations (RMSD) and root mean square fluctuations (RMSF) for DEB and FRA complex (**C**, **D**).

Figure 4.6. Ligand-protein complex poses after 20 ns molecular dynamics (MD) simulation compared to that of docked complexes. Receptor after molecular docking simulation: yellow; Receptor after 20 ns MD simulation: pink; Ligand after molecular docking simulation: green; Ligand after 20 ns MD simulation: blue; (**A**) DEB (Desulfated echinoside B)-PAK1 complex; (**B**) FRA (Frondoside A)-PAK1 complex.

Table 4.1. Cytotoxic effects of different sea cucumber extracts/crude saponin.

Sea cucumber species	Extracts/Crude saponin	Cytotoxic effects (IC_{50} value, µg/ml)	
		A549	**B16F10**
H. atra	70% EtOH Extract	10.5	7.9
	Hot Water Extract	20.9	85.0
	Crude Saponin	1.8	0.5
H. leucospilota	70% EtOH Extract	15.9	9.5
	Hot Water Extract	28.5	125.3
	Crude Saponin	3.7	1.4
P. nigripunctatus	70% EtOH Extract	36.9	8.0
	Hot Water Extract	26.5	-
	Crude Saponin	11.5	3.3

"-" no cytotoxicity was observed up to 400 µg/ml concentration.

Table 4.2. Cytotoxic effects of different fractions of *Holothuria atra* crude saponin.

Fractions	Cytotoxic effects (IC_{50} value, µg/ml)	
	A549	**B16F10**
Fr 1	1.35	0.60
Fr 2	0.72	0.24
Fr 3	3.40	0.90
Fr 4	1.34	0.50
Fr 5	2.38	2.42

Table 4.3. Anti-proliferative effects of desulfated echinoside B and frondoside A.

Compounds	Cytotoxic effects (IC_{50} value, μM)				
	A549	**B16F10**	**HuH-7**	**HepG2**	**Brine Shrimp**
Desulfated echinoside B	1.5	0.5	2.5	2.1	9.2
Frondoside A	1.6	0.6	0.4	0.6	11.5

Table 4.4. Binding affinity and non-bonding interaction of saponins with the catalytic domain of PAK1 obtained using AutoDock vina.

Comp.	Binding affinity (kcal/mol)	Hydrogen bond interactions		Hydrophobic interactions	
		Residue	Distance (Å)	Residue (Bond)	Distance (Å)
DEB	−8.2	Glu315	2.17	Tyr346 (Alkyl-Pi)	5.34
		Tyr346	2.50	Leu396 (Alkyl)	5.37
		Arg299	2.52	Leu396 (Alkyl)	4.01
		Arg299	2.17	Ile276 (Alkyl)	5.31
		Thr406	2.76	Tyr346 (Alkyl)	5.10
FRA	−7.7	Lys538	2.93	Tyr346 (Alkyl-Pi)	5.04
		Thr541	2.08	Ile276 (Alkyl)	5.39
		Leu347	2.79	Ala297 (Alkyl)	4.23
		Glu315	1.97		
		Gln278	2.07		
		Thr406	2.28		
		Asp407	2.00		
		Asp354	2.21		
		Lys538	2.76		
		Asp354	2.66		
		Asp354	2.75		
		Arg299	2.57		
		Gly350	2.88		

Table 4.5. Non-bonding interactions of ligands with the catalytic domain of PAK1 obtained after 20 ns molecular dynamics simulation.

Comp.	Binding affinity (kcal/mol)	Hydrogen bond interactions		Hydrophobic interactions		Electrostatic interactions	
		Residue	Distance (Å)	Residue (Bond)	Distance (Å)	Residue	Distance (Å)
DEB	−9.3	Asp407	1.63	Tyr346 (Pi-alkyl)	5.32		
		Glu315	1.78	Leu396 (Alkyl)	5.24		
		Asp407	2.72	Met344 (Alkyl)	4.65		
		Asp407	2.40	Ile276 (Alkyl)	4.33		
		Gly277	2.81				
		Asp407	2.35				
FRA	−7.6	Asp354	1.82	Tyr346 (Pi-alkyl)	4.80	Arg299	5.48
		Thr406	1.89	Ile276 (Alkyl)	4.93		
		Tyr346	2.65	Val284 (Alkyl)	4.27		

CHAPTER-V

Anti-inflammatory, Anti-diabetic, and Anti-Alzheimer's Effects of Prenylated Flavonoids from Okinawa Propolis

5.1. Summary

Okinawa propolis (OP) and its major ingredients were reported to have anti-cancer effects and lifespan-extending effects on *Caenorhabditis elegans* through inactivation of the oncogenic kinase, p21-activated kinase 1 (PAK1). In this study, five prenylated flavonoids from OP, nymphaeol-A (NA), nymphaeol-B (NB), nymphaeol-C (NC), isonymphaeol-B (INB), and 3′-geranyl-naringenin (GN), were evaluated for their anti-inflammatory, anti-diabetic, and anti-Alzheimer's effects using *in vitro* techniques. They showed significant anti-inflammatory effects through inhibition of albumin denaturation (IC_{50} values of 0.26–1.02 µM), nitrite accumulation (IC_{50} values of 2.4–7.0 µM), and cyclooxygenase-2 (COX-2) activity (IC_{50} values of 11.74–24.03 µM). They also strongly suppressed *in vitro* α-glucosidase enzyme activity with IC_{50} values of 3.77–5.66 µM. However, only INB and NA inhibited acetylcholinesterase significantly compared to the standard drug donepezil, with IC_{50} values of 7.23 and 7.77 µM, respectively. Molecular docking results indicated that OP compounds have good binding affinity to the α-glucosidase and acetylcholinesterase proteins, making non-bonded interactions with their active residues and surrounding allosteric residues. In addition, none of the compounds violated Lipinski's rule of five and showed notable toxicity parameters. Density functional theory (DFT)-based global reactivity descriptors demonstrated their high reactive nature along with the kinetic stability. In conclusion, this combined study suggests that OP components might be beneficial in the treatment of inflammation, type 2 diabetes mellitus, and Alzheimer's disease.

5.2. Introduction

Acute inflammation is thought be a good defense strategy to remove injurious stimuli and to initiate the healing process in the body. Chronic inflammation (CI), by contrast, is considered unfavorable, as it is involved in many diseases and disorders through its prolonged, dysregulated, and maladaptive effects (Sun 2012). Inflammation and its acute responses are well defined, whereas little is known on the development and progression of CI (Medzhitov 2008). During CI, increasing numbers of macrophage cells at inflammatory sites play an important role in the defense system, but produce several toxins themselves including reactive oxygen or nitrogen species (ROS or RNS). They together stimulate CI, inducing cyclooxygenase-2 (COX-2), inflammatory cytokines (tumor necrosis factor alpha (TNFα), interleukin 1 (IL-1), and IL-6), chemokines (IL-8 and C–X–C chemokine receptor 4 (CXCR4)), and pro-inflammatory transcription factors (nuclear factor kappa B (NF-κB)) (Gupta et al. 2012). CI was demonstrated as a common feature in the natural course of diabetes, and the inflammatory mediators correlate with diabetic incidence and prevalence (Lontchi-Yimagou et al. 2013). Inflammatory responses contribute to type 2 diabetes (T2D) occurrence by causing insulin resistance, and, in turn, they are intensified in the presence of hyperglycemia and promote long-term diabetic complications (Lontchi-Yimagou et al. 2013). Both inflammation and T2D trigger the age-related neurodegenerative disorder, Alzheimer's disease (AD) which is often termed as type 3 diabetes due to its pathophysiological similarities with T2D (Akiyama et al. 2000, Moreira 2012, Alam et al. 2016). Individuals with T2D have nearly a twofold higher risk of AD than non-diabetic individuals (Kroner 2009). Importantly, AD patients also have elevated insulin levels, which play a vital role in developing neuropathological

hallmarks of AD through increasing amyloid beta (Aβ) accumulation and tau phosphorylation in the brain (Gasparini et al. 2002, Phiel et al. 2003, Stanley et al. 2016). Hence, targeting inflammatory pathways could be a significant strategy for treating diabetes (Shoelson et al. 2006, Hirabara et al. 2012), and subsequently, for diminishing AD onset and progression (Roses 2008, Reger et al. 2008, Sato et al. 2011).

Propolis is a complex resinous material collected by honeybees, which has been used as a potent herbal and dietary supplement since ancient times of human civilization. Its pharmacological properties were extensively studied in several fields including inflammation, hypertension, diabetic complications, infectious diseases, microbial contaminations, cancer, and so on. Depending on surrounding vegetation, propolis collected from different regions shows differences in its major ingredients. For example, New Zealand propolis contains caffeic acid phenethyl ester (CAPE), Brazilian propolis contains artepillin C, and Taiwan propolis contains propolin G (Taira et al. 2016). However, the major ingredients of Okinawa propolis (OP) are a variety of prenylated flavonoids which originate from *Macaranga tanarius* plant (Kumazawa et al. 2014). These components were found to have anti-oxidant, anti-bacterial, and anti-angiogenic effects (Kumazawa et al. 2007, Taira et al. 2016). In a previous report, OP was demonstrated to inhibit the major oncogenic kinase, p21-activated kinase 1 (PAK1) directly, and hence, it is suggested to be utilized as a potent herbal drug for treating cancer, hyperpigmentation, and for extending the lifespan (Taira et al. 2016). In another work, nymphaeol A (NA) and nymphaeol C (NC), two major compounds of OP, were demonstrated to have strong selectivity in their inhibitory effects on PAK1 compared to that on other oncogenic kinases (Nguyen et al. 2017b). PAK1 is responsible for a variety of human diseases/disorders and it is

currently considered to be a major therapeutic target for the treatment of cancer, diabetes, hypertension, and neurodegenerative disorders (Maruta 2014). Suppressive effects of OP and its ingredients on PAK1 activities, therefore, encouraged this study to further evaluate their anti-inflammatory, anti-diabetic, and anti-Alzheimer's effects. Herein, both *in vitro* techniques and computational approaches were used, which precisely explained the pharmacological effects of OP compounds and their drug likeness, as well as their toxicological and quantum chemical properties. This combined effort could effectively be used as a potential guideline for expanding OP as a safe natural drug for treating inflammation, diabetes, and neurodegenerative disorders.

5.3. Materials and methods

5.3.1. Chemicals and reagents

Chemicals and reagents used in this study were of analytical grade. Dulbecco's Modified Eagle Medium (DMEM), casein, Griess reagents (0.1% *N*-(1-naphtyl)-ethylenediamine and 1% sulfanilamide in 5% orthophosphoric acid), 70% perchloric acid, lipopolysaccharide (LPS), MTT (3-(4,5-dimethylthiazol-2-yl)-2,5-diphenyl-tetrazolium bromide), α-glucosidase (from yeast), and acetylcholinesterase (AChE) (from electric eel) were purchased from Sigma-Aldrich (Saint Louis, MO, USA). Fetal bovine serum (FBS) was purchased from HyClone, Victoria, Australia. DMEM without phenol red was collected from Thermo Fisher Scientific (Waltham, Massachusetts, USA). Chicken egg albumin, trypsin, and penicillin/streptomycin were purchased from Funakoshi Co. Ltd. (Tokyo, Japan). All other chemicals used were

obtained from either Wako Pure Chemical Industries Ltd. (Osaka, Japan) or Kanto Chemical Co., Inc. (Tokyo, Japan).

5.3.2. Sample collection and purification of compounds

Propolis collected from the Okinawa Yoho bee farm (Okinawa, Japan) was dried at 45°C and then grounded with a mortar and pestle to make powder. Then, 1 g of powder was extracted with 50 ml of ethanol by sonicating for 3 h and shaking for 24 h at 25°C (Bio-Shaker, BR-300LF, Taitec Corporation, Tokyo, Japan). Extraction was collected by filtering with Whatman filter paper and centrifuged several times at 4000 rpm for 5 min. Finally, the clear supernatant was dried with a rotavapor apparatus (BUCHI, Flawil, Switzerland) under reduced pressure, and a yellow-colored dried crude extract was obtained (yield: 32%). Crude extract was dissolved in ethanol at 30 mg/ml concentration and subjected to high performance liquid chromatography (HPLC, Shimadzu, Kyoto, Japan) using a semipreparative C18 column (COSMOSIL 5C18-AR-II 250 mm × 10 mm, Nacalai Tesque, Kyoto, Japan). Distilled water (solvent A) and acetonitrile (solvent B) were used as mobile phases with a flow rate of 3.0 ml/min. HPLC conditions were as follows: 0–30 min, isocratic conditions 80% solvent B; 30.01–38 min, linear gradient 80–100% solvent B; 38.01–40 min, linear gradient 100–10% solvent B; 40 min, stop. Five compounds, NA, NB (nymphaeol B), NC, INB (isonymphaeol-B), and GN (3′-geranyl-naringenin) (**Figure 5.1**), were purified and their chemical structures were confirmed based on the comparison of their physical data to that of published data (Kumazawa et al. 2014).

5.3.3. Albumin denaturation inhibition assay

Albumin denaturation inhibition effects of the compounds were confirmed through a previously described method (Osman et al. 2016). Egg albumin was used in

this experiment, and the reaction mixture contained 0.1 ml of egg albumin, 0.7 ml of phosphate buffer saline (PBS), and varying concentrations of different compounds (0.5 ml). Mili-Q water (0.5 ml) instead of the compounds was used in the negative control. The reaction mixtures were incubated at 37°C for 15 min and heated at 70°C for 5 min. The absorbance was measured at 660 nm after cooling at room temperature. Ketorolac was used as a standard drug. Percentage of albumin denaturation inhibition was calculated according to the following formula:

Percentage of inhibition = $\{1 - (A/B)\} \times 100$

Where, A = absorbance of the test sample, B = absorbance of the negative control

5.3.4. Cell viability assay

RAW 264.7 cell viability was evaluated through the MTT assay (Shahinozzaman et al. 2018b). Cells were seeded in a 24-well plate at a density of 2×10^5 cells/well and incubated with the OP compounds for 24 h. Ketorolac (200 μM) was also assessed to determine its cytotoxicity on RAW 264.7 cells. After incubation, the supernatant was removed, and the cells were washed with PBS. Aliquots of 100 μl of MTT solution (0.5 mg/ml in PBS) were added to each well, and the plate was incubated at 37°C for 3 h. Afterwards, dimethyl sulfoxide (400 μl) was added to each well, and the plate was shaken for 10 min at room temperature to dissolve the formazan crystals. The absorbance was measured at 570 nm wavelength using a microplate reader, and the cell viability was calculated from the absorbance of the treated versus untreated control cells.

5.3.5. Nitrite inhibition assay

As an indicator of NO (nitric oxide) synthesis, nitrite amount was measured in the supernatant of LPS-stimulated RAW 264.7 cells. Cells were plated on a 24-well plate with a density of 2×10^5 cells/well. After seeding, cells were treated with LPS (500 ng/ml final concentration) and varying concentrations of the test compounds for 24 h. Ketorolac (200 µM) was used as a standard drug. Then, 100 µl of culture supernatant from each well was mixed with an equal volume of Griess reagent, and incubated at room temperature for 10 min. The formation of an azo compound was measured spectrophotometrically at 550 nm wavelength. Finally, nitrite concentration was determined from a standard curve of sodium nitrite, and nitrite inhibition percentages of test compounds and the reference drug were calculated based on the amount of nitrite produced by the control cells (treated only with LPS).

5.3.6. Cell-based assay for COX-2 inhibition

This assay was carried out according to the method described by Stanikunaite et al. (2009) with some modifications. In brief, RAW 264.7 cells (2×10^5 cells/well) were cultured in a 24-well plate in DMEM supplemented with 10% FBS and incubated at 37°C for 24 h for seeding. After seeding, cells were washed with PBS (400 µl) and treated with 500 ng/ml LPS for the next 24 h to induce the production of COX-2. Then, the induced cells were washed thoroughly with PBS to remove LPS completely and treated with different concentrations of test compounds for 4 h. Arachidonic acid (300 µM) was added and the cells were further incubated for 30 min. Next, the prostaglandin E2 (PGE_2) levels were determined in the culture supernatant using a PGE_2 ELISA kit (Cayman Chemical Co., Ann Arbor, MI, USA) according to the manufacturer's instructions. COX-2 enzyme activity was determined by the conversion of exogenous

arachidonic acid to PGE_2, and was expressed as the percentage of negative control (without test compounds). Finally, IC_{50} values were calculated for all the tested compounds. Indomethacin was used as a positive control.

5.3.7. α-Glucosidase inhibition assay

The α-glucosidase assay was performed with slight modifications of a previous method (Afrapoli et al. 2012). In short, 15 µl of the test sample at various concentrations was added to 140 µl of enzyme solution (0.0073 U/ml of α-glucosidase in 0.05 M sodium phosphate buffer containing 100 mM NaCl) in a 96-well plate. Reaction mixtures were incubated at 37°C for 15 min. Then, 25 µl of 0.7 mM *p*-nitrophenyl-*α*-D-glucopyranoside (PNPG) solution in 0.05 M sodium phosphate buffer (pH = 6.8) was added to each well. The increase in absorption at 405 nm wavelength due to the hydrolysis of PNPG by α-glucosidase was monitored continuously with a microplate reader.

5.3.8. Acetylcholinesterase inhibition assay

The AChE inhibitory properties of the compounds were determined using a 96-well microplate colorimetric method (Fawole et al. 2010) as described by Ellman et al. (Ellman et al. 1961). Donepezil was used as a positive control. Each sample was tested in triplicate, and the percentage of inhibition was determined as follows:

AChE inhibition (%) = {1 − (sample reaction rate/blank reaction rate)} × 100

5.3.9. Molecular docking

5.3.9.1. Preparation of receptors

The crystal structures of target proteins were retrieved from RCSB Protein Data Bank (http://www.rcsb.org). Isomaltase from *Saccharomyces cerevisiae* co-

crystallized with maltose (PDB ID: 3A4A) was used here as the α-glucosidase protein since it shows 85% similarity to yeast α-glucosidase (MAL12) through homology modeling (Taha et al. 2018). On the other hand, acetylcholinesterase protein co-crystalized with donepezil (PDB ID: 4EY7) was used for docking calculations. Water molecules, heteroatoms, and ligands were removed from the crystal structure of proteins using Discovery Studio 4.5 (Accelrys, San Diego, CA, USA). Polar hydrogen atoms were also added with Discovery Studio 4.5. The energy minimization of receptors was then carried out with Swiss-PdbViewer 4.1 (Swiss Institute of Bioinformatics, Lausanne, Switzerland).

5.3.9.2. Preparation of ligands

Chemical structures of all compounds were drawn by Marvin Sketch (ChemAxon, Budapest, Hungary), and then, were converted to three-dimensional format using ChemBioDraw Ultra 12.0 (CambridgeSoft, Cambridge, MA 02140, USA). Geometry optimization was done with Gaussian09 software (Frisch et al. 2009) by density functional theory (DFT) at the B3LYP/6–31G (d,p) level of theory. Finally, all the compounds were saved as pdb (protein data bank) format for further docking simulations.

5.3.9.3. Docking simulation

AutoDock Vina (The Scripps Research Institute, La Jolla, CA, USA) was used here for the molecular docking simulations. As an open source program, it is widely used for molecular docking, which significantly improves the accuracy of the binding mode predictions compared to AutoDock 4 (Trott & Olson 2010). Depending on the binding mode of co-crystalized ligands, active site residues of the proteins were determined using Discovery Studio 4.5 (Accelrys, San Diego, CA, USA), and then,

the grid box size was defined accordingly. In the α-glucosidase protein, the dimensions (Å) of the grid box were 45.24, 29.91, and 25.00, and the center (x, y, z) of the grid box was 33.06, −7.65, 18.63. Similarly, in the acetylcholinesterase protein, the dimensions (Å) of the grid box were 49.96, 45.69, and 25.00, and the center (x, y, z) of the grid box was −7.34, −44.19, 30.87.

5.3.9.4. Analysis and visualization of docking results

After the docking simulation, the docked pose with the highest negative value was selected as the best for the corresponding compound and protein. The best-docked pose was visualized and analyzed to explore the non-bonded interactions using PyMOL Molecular Graphics System 2.0 (DeLano Scientific LLC, San Carlos, CA, USA), UCSF Chimera 1.12 (RBVI, University of California, San Francisco, CA, USA), and Discovery Studio 4.5 (Accelrys, San Diego, CA, USA).

5.3.10. Calculation of pharmacokinetic parameters

The drug likeness properties of the compounds were predicted using the Molinspiration online toolkit (http://www.molinspiration.com/cgi-bin/properties). Orally active drugs should comply with these widely utilized drug likeness properties to prove their pharmaceutical fidelity. In this study, molecular descriptors such as miLogP, the number of hydrogen-bond donors, the number of hydrogen-bond acceptors, the molecular mass of the compounds, TPSA (topological polar surface area), the number of rotatable bonds, and violations of Lipinski's rule of five (Lipinski et al. 2001) were calculated. According to a previously described method (Zhao et al. 2002), absorption (% ABS) was calculated using the following formula:

$$\% \text{ ABS} = 109 - (0.345 \times \text{TPSA})$$

5.3.11. Prediction of toxicological properties

Since toxicity is a major concern for using any drug, toxicological properties of the compounds were predicted with the admetSAR online toolkit (http://lmmd.ecust.edu.cn:8000/), which is reported to be an important and useful predictor in drug discovery. Ames toxicity, carcinogenic properties, acute oral toxicity, rat acute toxicity, and inhibitory effects on hERG (human ether-a-go-go-related gene) were predicted.

5.3.12. Density functional theory (DFT) calculation

All compounds were fully optimized by DFT employing Becke's three-parameter hybrid model, Lee–Yang–Parr (B3LYP) correlation functional method at the 6–31G (d,p) level, using Gaussian09 software. Electronic energies (E), enthalpy (H), Gibbs free energies (G), dipole moments, and frontier molecular orbital energies were also investigated using the same level of theory. HOMO (highest occupied molecular orbital energy)–LUMO (lowest unoccupied molecular orbital energy) gaps of each compound were calculated by subtracting the LUMO energy (εLUMO) value from the corresponding HOMO energy (εHOMO) value of the compound. The hardness (η) and softness (S) of each compound were calculated from the energies of frontier HOMO and LUMO according to the following equations:

$$\eta = [\varepsilon HOMO - \varepsilon LUMO]/2$$

$$S = 1/\eta$$

5.3.13. Statistical analysis

Data are expressed as means ± standard error (SE). Results were analyzed using a Student's *t* test with IBM SPSS Statistics 24 (IBM Corporation, Armonk, NY, USA). Values of $p < 0.05$ and $p < 0.01$ were considered statistically significant.

5.4. Results and discussion

5.4.1. Anti-inflammatory effects

As shown in **Figure 5.2**, OP compounds inhibited albumin denaturation in a dose-dependent manner. They all showed strong inhibitory effects, and the results were found to be significant compared to ketorolac, a non-steroidal anti-inflammatory drug (NSAID). Out of all compounds, NA showed the best effects followed by NC, INB, NB, and GN. The IC_{50} values for NA, NC, INB, NB, and GN were 0.26, 0.37, 0.42, 0.54, and 1.02 µM, respectively. However, ketorolac at a 200 µM concentration inhibited only 52% albumin denaturation. Since cellular proteins are denatured due to inflammation, the drugs showing inhibitory action against protein denaturation seem to be effective for treating inflammation (Rauf et al. 2015). For this purpose, OP compounds might be a suitable candidate for further studies. Next, they were tested on LPS-stimulated RAW 264.7 cells and were found to have stronger effects on nitrite accumulation in culture supernatants. Firstly, all the compounds were assessed for their cytotoxicity on RAW 264.7 cells through the MTT assay. Most of the compounds at tested concentrations did not inhibit cell proliferation; rather, they induced cell proliferation to some extent. However, NB and INB at 12 µM concentration significantly inhibited cell proliferation but with a slight deviation (approximately 3–5%) from the control group. Hence, NB and INB at 12 µM concentration were used in the subsequent nitrite assay. The standard drug, ketorolac, at 200 µM concentration did not show cytotoxicity on RAW 264.7 cells, and showed a significant effect on nitrite formation in the supernatant with 26% inhibition compared to the cells treated only with LPS. However, OP compounds exerted stronger and concentration-dependent inhibitory effects on nitrite formation than that of ketorolac (**Figure 5.3**).

NC showed the highest inhibitory effects with an IC_{50} value 2.4 µM followed by NA, NB, INB, and GN (whose IC_{50} values were 3.2, 5.4, 6.2, and 7.0 µM, respectively) (**Table 5.1**). They also inhibited COX-2 activity dose-dependently in LPS-induced RAW 264.7 cells, and the IC_{50} values for NA, NB, NC, INB, and GN were 11.74, 17.90, 15.45, 23.78, and 24.03 µM, respectively (**Figure 5.4**). In LPS-treated macrophage cells, two major pro-inflammatory mediators, NO and PGE_2 are produced from L-arginine and arachidonic acid, respectively, and these reactions are catalyzed by transcriptional activation of the inducible nitric oxide synthase (iNOS) and COX-2 genes, respectively (Zhou et al. 2008, Kacem et al. 2015). Importantly, iNOS and COX-2 are downstream signaling components of PAK1 (Song et al. 2002, Nguyen et al. 2017a). Hence, it can be assumed here that OP compounds firstly inhibit PAK1, and subsequently, suppress the catalytic activities of iNOS and COX-2. Taken together, OP components could protect cellular proteins and reduce the formation of NO and PGE_2 in inflamed tissues, and therefore, they could be utilized as herbal drugs for treating inflammation and other related disorders.

5.4.2. α-Glucosidase and acetylcholinesterase (AChE) inhibitory effects

The anti-diabetic effects of OP compounds were evaluated by testing their yeast α-glucosidase inhibitory activities. The enzyme α-glucosidase, secreted in the small intestine, is essential for carbohydrate digestion and the subsequent increase in postprandial blood glucose levels. An abnormal increase in postprandial blood glucose level is thought to be a major reason for T2D progression (Kasturi et al. 2017). Hence, α-glucosidase inhibitors are recommended as an oral anti-diabetic drug which can retard carbohydrate degradation, thus delaying and reducing the level of postprandial hyperglycemia (Kasturi et al. 2017). Apart from these factors, α-glucosidase inhibitors

might also provide other health benefits such as moderating plasma triglyceride levels with cardiovascular disorders and hypertension risks through reducing glucose toxicity and improved insulin response (Benalla et al. 2010). All compounds tested showed stronger inhibition of *in vitro* α-glucosidase activity than the positive control quercetin (IC_{50} = 6.65 µM). NA and NC inhibited significantly with IC_{50} values of 3.77 and 4.09 µM, respectively (**Figure 5.5**), whereas the IC_{50} values for NB, INB, and GN were 5.66, 5.12, and 5.40 µM, respectively. These findings indicate that OP compounds can act as anti-diabetic drugs for treating T2D.

Like α-glucosidase inhibition, all compounds showed suppressive effects on electric eel AChE enzyme activity when tested *in vitro* (**Figure 5.5**). INB and NA inhibited AChE strongly compared to the standard drug donepezil (IC_{50} = 8.13 µM), with IC_{50} values of 7.23 and 7.77 µM, respectively. GN, NB, and NC also inhibited AChE, but with lower effects than donepezil. The IC_{50} values for GN, NB, and NC were 12.34, 15.09, and 15.70 µM, respectively. AChE is localized in synaptic gaps of the central and peripheral nervous system and is responsible for the breakdown of acetylcholine (ACh). Thus, AChE terminates nerve impulses through the loss of basal forebrain cholinergic neurons and by reducing the level of the neurotransmitter ACh, which is characteristic of AD as a chronic neurodegenerative disorder (Machado et al. 2015, Khan et al. 2018). Inhibition of AChE increases cholinergic functions, and hence, it is the therapeutic target for not only managing AD, but also for moderating other disorders such as myasthenia gravis, glaucoma, and Lewy body dementia (Khan et al. 2018). Since synthetic AChE inhibitors have some adverse effects, such as hepatotoxicity and gastrointestinal complaints, OP compounds reported here could be

utilized successfully as natural-product-derived drugs for treating AD and other cholinergic dysfunctions.

5.4.3. Molecular docking study

To understand the mechanisms of α-glucosidase and AChE inhibition by OP compounds, as well as the binding mode inside the binding pocket of the enzymes, and to confirm the experimental results, molecular docking simulations were performed in this study. All the compounds were docked to the crystal structure of isomaltase (PDB ID: 3A4A) which has strong similarity to α-glucosidase. They showed promising binding affinities with variable free binding energies ranging from −7.1 to −9.9 kcal/mol, clarifying their wide-spectrum structural and functional features. Except for GN, all other compounds could be embedded into the same binding pocket of 3A4A (**Figure 5.6**). The results in terms of binding energy, non-bonded interactions, and bond distance are presented in **Table 5.2**. According to the binding affinities, the compounds could be ranked as NC > NA > INB > NB > GN. However, the experimental results revealed their rank as NA > NC > INB > NB > GN. Both the docking simulation and the experimental results demonstrated NA and NC as the most active α-glucosidase inhibitors. The three-dimensional structures of non-bonded interactions of the three best OP compounds with 3A4A are presented in **Figure 5.7**. All compounds showed different types of non-bonded interactions such as hydrogen bonding, hydrophobic bonding, and electrostatic bonding with several residues of the active site or close to the active site. NA and NC showed one hydrogen-bond interaction with the active site residue Asp352, whereas INB formed two hydrogen bonds with two different catalytic residues, Asp352 and Glu277. On the other hand,

NB and GN did not interact with the active-site residues, but they interacted with other residues close to the catalytic cleft.

When the compounds were docked with AChE (PDB ID: 4EY7), they showed almost similar binding energies ranging from −11.0 to −11.5 kcal/mol. NC and INB showed identical binding affinity (−11.0 kcal/mol), but the highest binding affinity was demonstrated by NA, followed by GN and NB. The free binding energies for NA, GN, and NB were −11.5, −11.3, and −11.2 kcal/mol, respectively (**Table 5.2**). On the other hand, NA was found to be the second highest AChE inhibitor after INB through *in vitro* experiments. However, all compounds could bind to the same pocket of AChE with similar orientation (**Figure 5.6**). Non-bonded interactions of all compounds with different protein residues are presented in **Table 5.2**. In AChE, Trp86 is termed as the choline-binding site residue which interacts with the ligand through hydrophobic interactions (Azam et al. 2014). Surprisingly, all tested compounds showed hydrophobic interactions with Trp86 with π–σ, π–π stacked, or π–alkyl bond formation. NB and NC interacted with AChE via the formation of two and three hydrogen bonds, respectively, with the catalytic residues Tyr72 and Phe295. These two residues were found to be involved in donepezil binding (PDB ID: 4EY7). INB interacted with one catalytic residue Phe295 along with another residue Asp74 which is close to the catalytic pocket. However, NA and GN did not interact with any catalytic residues, but they interacted with the close residues of catalytic site. NA interacted with AChE only through hydrophobic bonds, whereas GN formed two hydrogen bonds with AChE backbone residues Gln291 and Tyr124 (**Figure 5.7**).

The free binding energies, binding modes, and interactions of OP compounds with α-glucosidase and AChE protein calculated from this *in silico* study demonstrate that these compounds might show promising interactions with the target proteins, and thus, could slow carbohydrate breakdown in the small intestine and the catabolism of ACh in synaptic cleft. In accordance with the experimental findings, the *in silico* studies indicate that major components of OP could act as herbal drugs for treating T2D and AD, although further investigations are warranted to explore their in-depth mechanism of action.

5.4.4. Pharmacokinetic and toxicological properties

Pharmacokinetic properties (PKs) are thought to be important in drug development, since they determine the characteristic features for a successful oral drug which is promptly and completely absorbed from the gastrointestinal tract, distributed to the site of action, metabolized well, and eliminated in a suitable manner without causing any detrimental effects. That is why many drugs under clinical trial fail to commercialize due to having poor PKs. PKs depend on the chemical descriptors of the molecule. Computational predictions are currently used in drug discovery programs to explore absorption, distribution, metabolism, excretion, and toxicity (ADMET) profiling of new drug candidates with the clear aim of selecting only drug-like compounds having optimal PKs (Azam et al. 2016). The Molinspiration online property calculation toolkit was used here to screen ADMET properties of OP compounds as future drug candidates based on Lipinski's rule of five (Lipinski et al. 2001). The results are presented in **Table 5.3**. According to this rule, orally administered drugs should have a molecular weight of <500 amu, a LogP value ≤ 5, five or fewer hydrogen-bond donor sites, and ten or fewer hydrogen-bond acceptor

sites. Drug candidates violating one of the above rules may have problems with bioavailability. Interestingly, none of the OP compounds violate these rules, and hence, all may have good oral bioavailability.

Additionally, based on Veber's rule, orally bioavailable drugs should have the number of rotatable bonds below or equal to 10, and TPSA values ≤ 140 $Å^2$ (Veber et al. 2002). The number of rotatable bonds is thought be a good descriptor for suitable drugs, whereas TPSA is involved in passive molecular transport of drugs through membranes. All OP compounds have a number of rotatable bonds lower than 10 and TPSA values lower than 140 $Å^2$. According to Zhao et al. (2002), the calculated percentage of absorption for OP compounds ranged from 72.01–78.99%.

Toxicological properties of OP components were also predicted using the admetSAR server. The results demonstrated that none of the compounds posed a risk of Ames toxicity and carcinogenicity (**Table 5.4**). However, all of the compounds were found to be weak inhibitors for the hERG and showed weak rat acute toxicity with a median lethal dose (LD_{50}) of 3.1399 mol/kg. As per the predicted acute oral toxicity values, all the compounds lie in "class III". Compounds of this class have LD_{50} values greater than 500 mg/kg but less than 5000 mg/kg and are generally considered suitable from a druggable point of view (Chander et al. 2016). Thus, OP compounds are qualified for use as promising drugs with good oral bioavailability and safety features.

5.4.5. Density functional theory (DFT)-based computations

DFT-based computation has, indeed, the potential of becoming a very important tool in computer-aided drug design (CADD) with the aim of developing new drugs for new targets, and thus, for medicinal chemistry (Sulpizi et al. 2002). DFT-

based scoring functions for molecular descriptors might play an important role in quantitative structure–activity relationship (QSAR), pharmacology, genomics, drug design, toxicology, proteomics, analytical chemistry, virtual screening, and so forth. Global and local descriptors of DFT may also significantly correlate computed and experimental drug activities. In this investigation, DFT calculations of OP compounds were carried out to understand the structural features, reactive nature, and sites of the compounds essential for biological activities, which enable the design of new drugs with potential effects, as well as attractive materials with applications in industry. The results are presented in **Table 5.5**, which includes changes in electronic energy, enthalpy, and Gibbs free energy, as well as dipole moment, εHOMO, εLUMO, hardness, and softness. Greater negative values of thermodynamic properties indicate improved thermodynamic features of the compounds. Dipole moment is the indicator of drug–receptor interaction, which facilitates hydrogen-bond interactions (Lien et al. 1982). All OP compounds show comparatively higher dipole moments ranging from 2.235–5.228 Debey, and NC has the highest dipole moment (5.228 Debey) which agrees with its experimental interaction with the target receptors used in this study.

According to the frontier molecular orbital theory, HOMO and LUMO energies play important roles in the chemical reactivity and kinetic stability features of drugs (Khan et al. 2017). The energy gap of HOMO–LUMO also determines the hardness and softness of drugs. Large gaps denote a hard molecule and small gaps signify a soft molecule (Azam et al. 2017). The reactivity of drugs increases with their softness. All the OP compounds show relatively low HOMO–LUMO energy gaps ranging from 0.1599–0.1684 Hartree and high softness ranging from 11.8715–12.4564 Hartree, demonstrating that they have a strong reactive nature with their targets. Frontier

orbitals are displayed in **Figure 5.8**, which reflect the localization pattern of frontier molecular orbitals in OP compounds. Their localization in different positions demonstrate their structural and functional diversity. However, in all compounds, the frontier molecular orbitals are located mostly in aromatic moieties not in the geranyl side chain, which clarifies the active role of aromatic moieties during the interaction with their target receptors.

5.5. Conclusion

In summary, it was found that the prenylated flavonoids of OP significantly inhibited albumin denaturation *in vitro*, demonstrating their protective effects on cellular proteins from destruction due to chronic inflammation. Moreover, OP compounds reduced nitrite accumulation and COX-2 activity significantly in an inflammatory model of LPS-stimulated RAW 264.7 cells. All compounds inhibited α-glucosidase and acetylcholinesterase enzyme activity in a dose-dependent fashion, which correlate with the findings of their molecular docking simulations. They could strongly bind to the active site or close allosteric sites of α-glucosidase and acetylcholinesterase protein receptors. Pharmacokinetics and toxicological properties revealed their drug-like properties, confirming them as safe drug sources. Global reactivity descriptors determined from DFT-based computations confirmed that OP compounds have a strong reactive nature showing low HOMO–LUMO energy gaps. However, the potential pharmacological properties of OP components as anti-inflammatory, anti-diabetic, and anti-Alzheimer's drugs described might also be attributed to their PAK1-inhibiting actions. Collectively, this investigation allows the

conclusion that OP components might be novel and safe drug sources for the treatment of inflammation, diabetes, and AD.

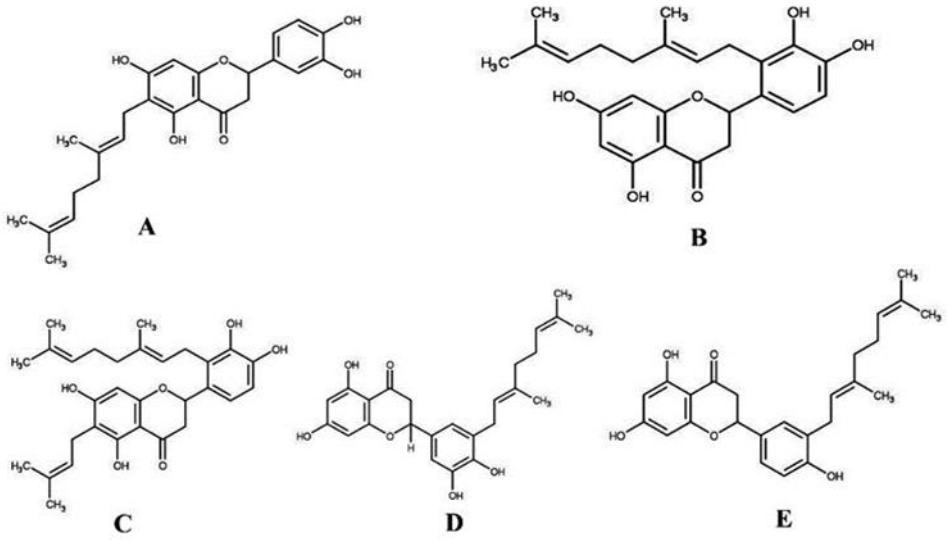

Figure 5.1. Chemical structures of the purified compounds from Okinawa propolis. (**A**) Nymphaeol-A (NA), (**B**) nymphaeol-B (NB), (**C**) nymphaeol-C (NC), (**D**) isonymphaeol-B (INB), and (**E**) 3′-geranyl-naringenin (GN).

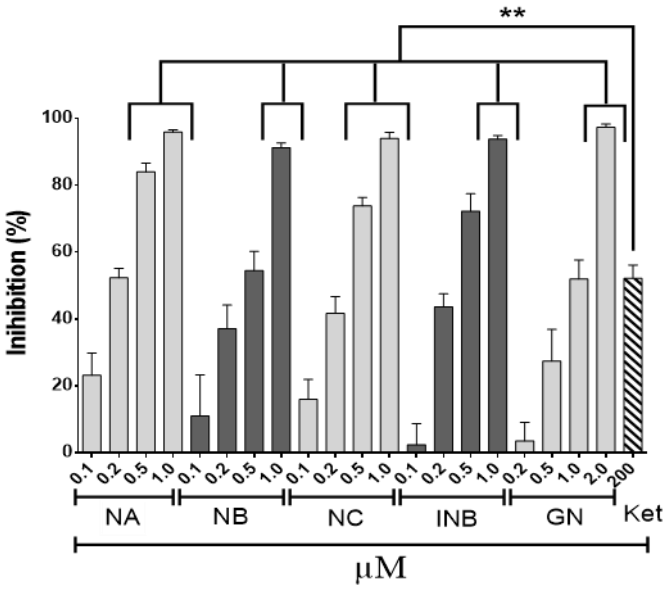

Figure 5.2. Inhibitory effects of Okinawa propolis (OP) compounds on albumin denaturation *in vitro*. Ketorolac (Ket) was used as a control, and asterisks indicate significant differences compared to the positive control (** $p < 0.01$).

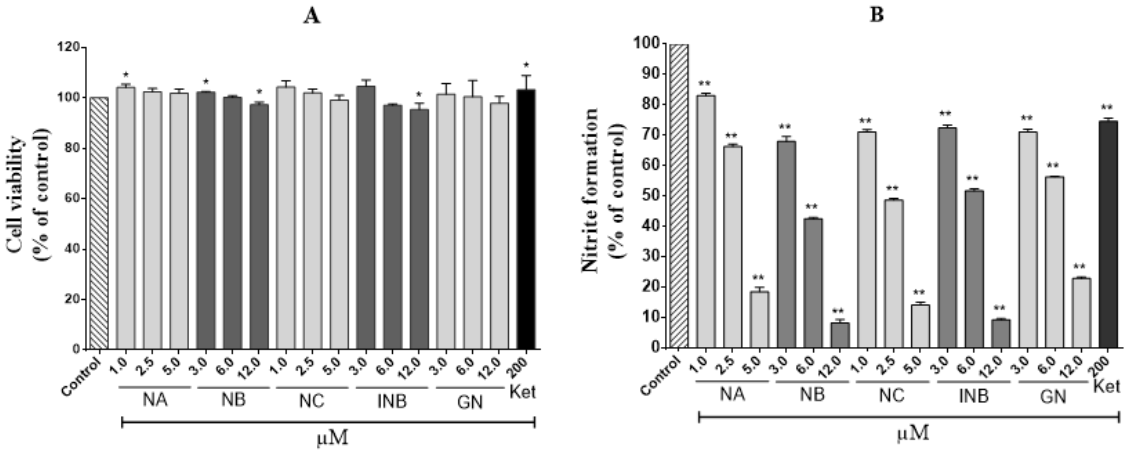

Figure 5.3. Effects of different compounds on RAW 264.7 cell viability (**A**) and on nitrite formation (**B**) in lipopolysaccharide (LPS)-stimulated RAW 264.7 cells. Ketorolac (Ket) was used as a standard drug. Asterisks indicate significant differences compared to the control (* $p < 0.05$; ** $p < 0.01$).

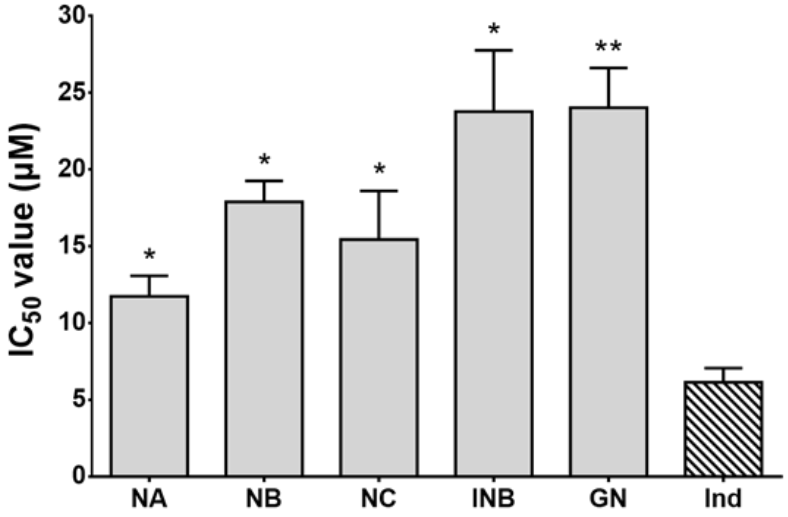

Figure 5.4. Cyclooxygenase-2 (COX-2) inhibitory effects of Okinawa propolis (OP) compounds. Results are expressed as means ± SE of three repeated experiments. Indomethacin (Ind) was used as a standard inhibitor. Asterisks indicate significant differences compared to the positive control (* $p < 0.05$; ** $p < 0.01$).

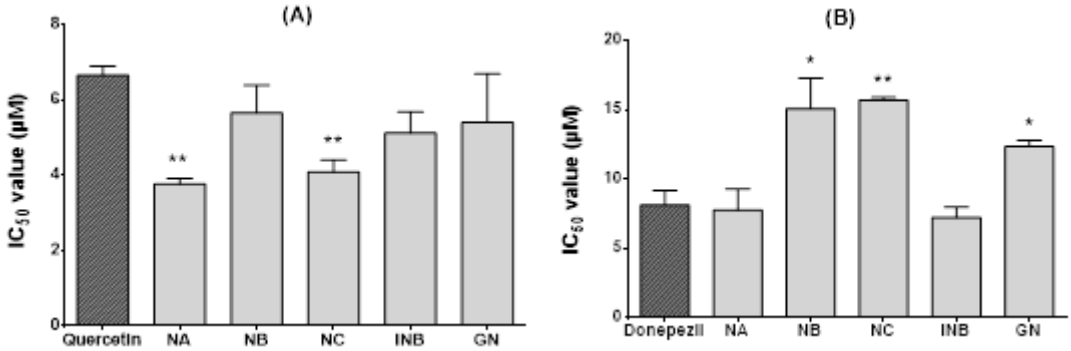

Figure 5.5. The α-glucosidase (**A**) and acetylcholinesterase (**B**) inhibitory effects of different Okinawa propolis (OP) compounds. Data represent means ± SE of three experiments. Asterisks indicate significant differences compared to the positive control (* $p < 0.05$; ** $p < 0.01$).

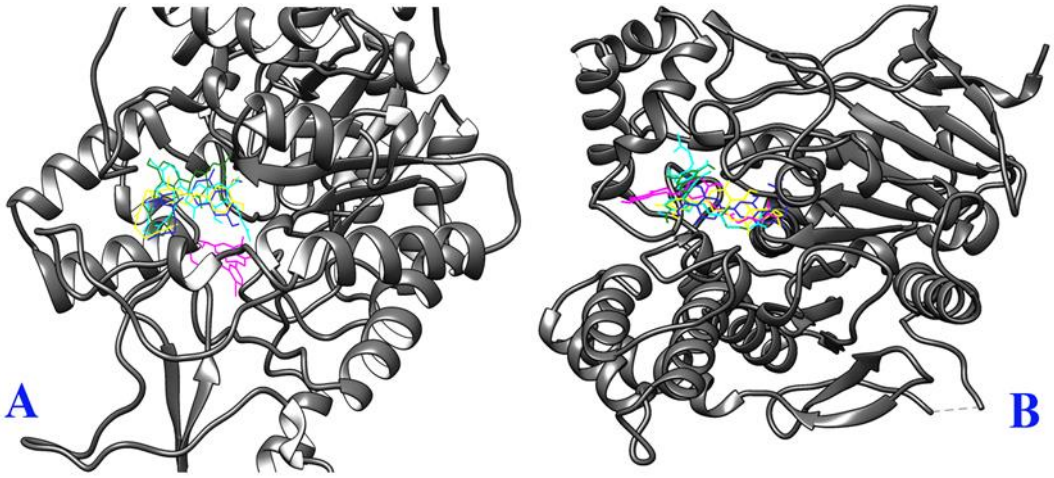

Figure 5.6. Binding orientations of Okinawa propolis (OP) compounds within α-glucosidase (PDB ID: 3A4A) and acetylcholinesterase (PDB ID: 4EY7) protein receptors. (A) Binding orientation within 3A4A (nymphaeol-A (NA) = yellow; nymphaeol-B (NB) = green; nymphaeol-C (NC) = cyan; isonymphaeol-B (INB) = blue; 3′-geranyl-naringenin (GN) = magenta), and (B) binding orientation within 4EY7 (NA = yellow; NB = green; NC = cyan; INB = blue; GN = magenta).

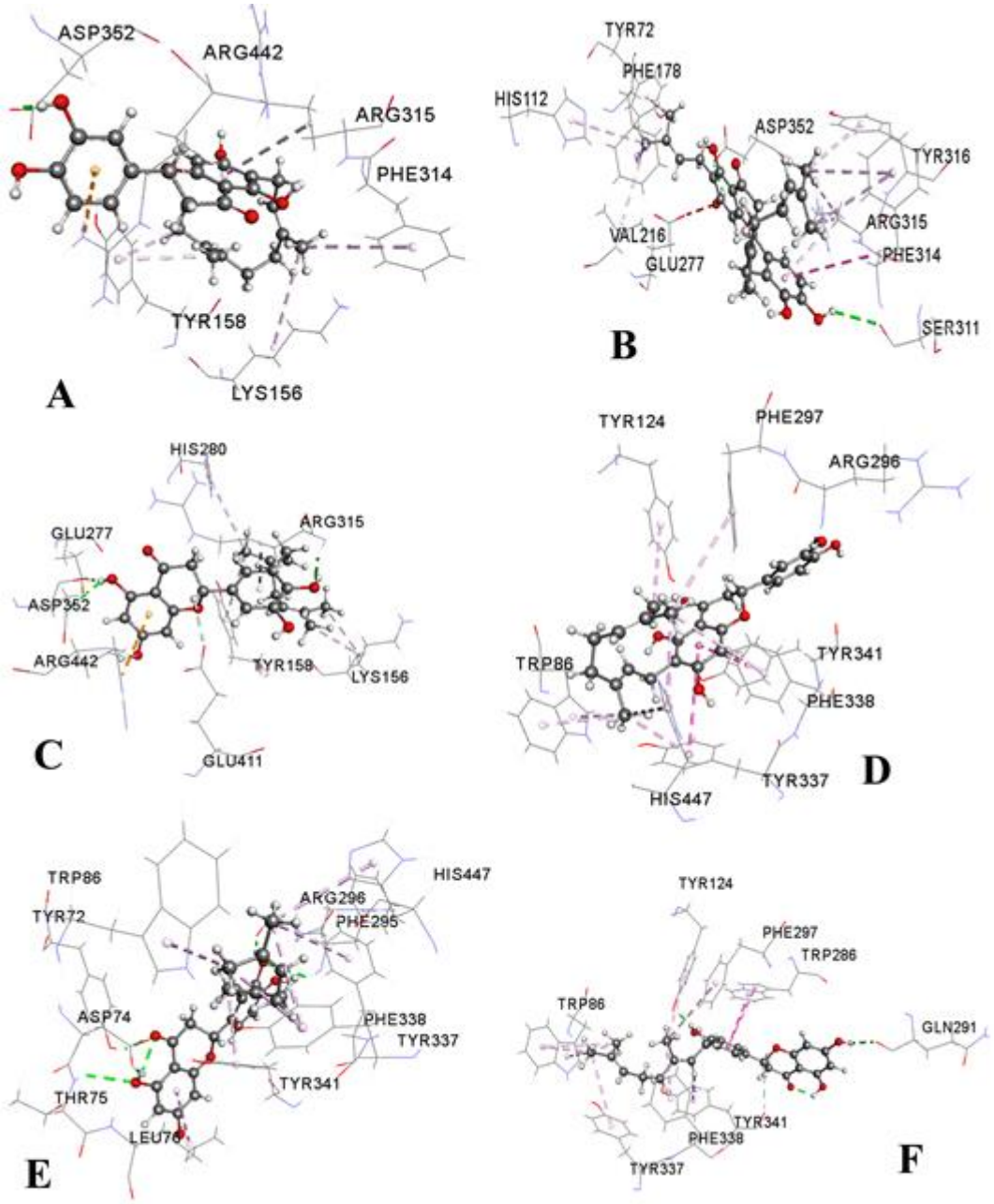

Figure 5.7. Non-bonded interactions of the best-docked compounds with α-glucosidase (PDB ID: 3A4A) and acetylcholinesterase (PDB ID: 4EY7) proteins. (**A**) Nymphaeol-A (NA) with 3A4A, (**B**) nymphaeol-C (NC) with 3A4A, (**C**) isonymphaeol-B (INB) with 3A4A, (**D**) NA with 4EY7, (**E**) nymphaeol-B (NB) with 4EY7, and (**F**) 3′-geranyl-naringenin (GN) with 4EY7.

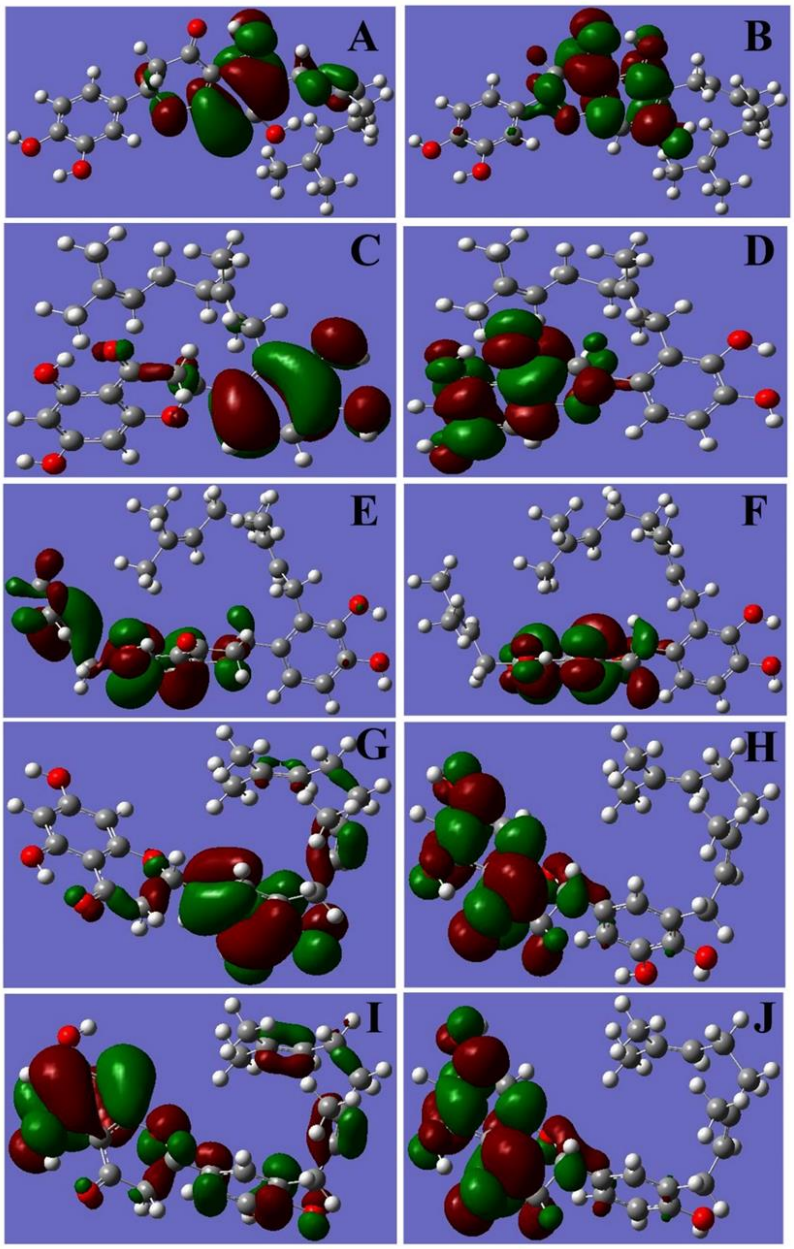

Figure 5.8. Visualization of frontier molecular orbitals of Okinawa propolis (OP) compounds. **A**, **B** – HOMO and LUMO of nymphaeol A (NA); **C**, **D** – HOMO and LUMO of nymphaeol B (NB); **E**, **F** – HOMO and LUMO of nymphaeol C (NC); **G**, **H** – HOMO and LUMO of isonymphaeol B (INB); **I**, **J** – HOMO and LUMO of 3´-geranyl-naringenin (GN). HOMO = highest occupied molecular orbital; LUMO = lowest unoccupied molecular orbital.

Table 5.1. IC_{50} values of nitrite inhibition by different compounds. NA: nymphaeol-A; NB: nymphaeol-B; NC: nymphaeol-C; INB: isonymphaeol-B; GN: 3′-geranyl-naringenin.

Compound	**Nitrite Inhibition** (IC_{50} value, μM)
NA	3.2
NB	5.4
NC	2.4
INB	6.2
GN	7.0

Table 5.2. Binding affinity and binding interactions of Okinawa propolis (OP) compounds with α-glucosidase (PDB ID: 3A4A) and acetylcholinesterase (PDB ID: 4EY7) proteins.

Compound	Binding Affinity (kcal/mol)	Hydrogen Bonds	Hydrophobic Bonds					Electrostatic Bonds
			π–σ	π–π Stacked	π–Alkyl	Alkyl	Amide–π Stacked	
3A4A								
NA	−9.3	Asp^{352} (1.92)	Tyr^{158} (3.56)		Arg^{315} (4.88) Tyr^{158} (4.11) Phe^{314} (4.97)	Lys^{156} (5.05)		Arg^{442} (4.67)
NB	−8.7	Gln^{353} (2.20) Arg^{315} (3.50)	Arg^{315} (3.98)	Phe^{303} (4.62)	Tyr^{158} (4.36) Phe^{314} (5.10) Phe^{314} (4.89)	Arg^{315} (5.18) Arg^{315} (4.42)		
NC	−9.9	Ser^{311} (2.82) Asp^{352} (2.17)	Phe^{178} (3.71)		Arg^{315} (4.51) Tyr^{72} (4.51) His^{112} (4.90) Phe^{314} (5.00) Phe^{314} (4.96) Tyr^{316} (5.02)	Arg^{315} (4.36) Arg^{315} (4.37) Val^{216} (4.33)	Phe^{314} (5.83) Arg^{315} (5.83)	
INB	−9.2	Glu^{277} (2.24) Asp^{352} (2.60) Arg^{315} (2.21)			Arg^{315} (3.85) Tyr^{158} (4.73) His^{280} (5.32)	Lys^{156} (3.47) Lys^{156} (4.03)		Arg^{442} (4.07)
GN	−7.1	Lys^{466} (2.44) Pro^{467} (2.31) Trp^{36} (2.19)		Trp^{36} (5.38)	Phe^{469} (4.97) Tyr^{470} (4.63)			

Table 5.2. (*continued*)

Compound	Binding Affinity (kcal/mol)	Hydrogen Bonds	Hydrophobic Bonds					Electrostatic Bonds
			π–σ	π–π Stacked	π–Alkyl	Alkyl	Amide–π Stacked	
4EY7								
NA	−11.5		Trp^{86} (3.97)	Tyr^{337} (5.41) Tyr^{341} (4.00)	Trp^{86} (4.05), Tyr^{124} (4.93), Phe^{297} (5.23), Tyr^{337} (3.95), Phe^{338} (4.79), His^{447} (5.43), His^{447} (4.46)			
NB	−11.2	Asp^{74} (2.02) Arg^{296} (1.86) Tyr^{72} (2.05) Thr^{75} (2.77) Phe^{295} (2.77)	Tyr^{341} (3.67)		Leu^{76} (4.61), Trp^{86} (4.57), Tyr^{337} (4.02), Tyr^{337} (4.52), Phe^{338} (5.36), His^{447} (4.60)			
NC	−11.0	Ser^{293} (2.17) Tyr^{72} (2.07) Tyr^{72} (2.02) Phe^{295} (2.69) Arg^{296} (2.31) Arg^{296} (2.29)	Tyr^{341} (3.73)		Leu^{76} (4.86), Trp^{86} (4.63), Tyr^{337} (4.41), Tyr^{337} (4.02), Phe^{338} (5.29), His^{447} (4.57)			
INB	−11.0	Asp^{74} (2.00) Phe^{295} (1.88)	Trp^{86} (3.89)	Tyr^{337} (5.10) Trp^{286} (4.01) Tyr^{341} (4.72) Trp^{286} (5.32)	Trp^{86} (4.57), Trp^{86} (5.07), Tyr^{337} (5.39), His^{447} (4.71)			
GN	−11.3	Gln^{291} (2.29) Tyr^{124} (1.89)	Tyr^{341} (3.75) Trp^{86} (3.78) Trp^{86} (3.88) Trp^{86} (3.94)	Trp^{286} (3.92) Trp^{286} (4.98)	Trp^{86} (5.04), Tyr^{124} (5.35), Phe^{297} (5.36), Tyr^{337} (4.91), Phe^{338} (4.64)			

Values in the bracket indicate the bond distance (Å).

Table 5.3. Physicochemical properties of the compounds for good oral bioavailability.

Compound	% ABS	TPSA (Å^2)	MW	MiLogP	HBD	HBA	n-ROTB	Lipinski's Violation
Rule	-	-	<500	≤5	<5	<10	≤10	≤1
NA	72.01	107.22	424.49	5.52	4	6	6	1
NB	72.01	107.22	424.49	5.49	4	6	6	1
NC	72.01	107.22	492.61	7.53	4	6	8	1
INB	72.01	107.22	424.49	5.49	4	6	6	1
GN	78.99	86.99	408.49	6.21	3	5	6	1

% ABS = Percentage of absorption; TPSA = topological polar surface area; MW = molecular weight; MiLogP = logarithm of compound partition coefficient between *n*-octanol and water; HBD = number of hydrogen-bond donors; HBA = number of hydrogen-bond acceptors; n-ROTB = number of rotatable bonds.

Table 5.4. Toxicological properties of the compounds.

Parameters	Compound				
	NA	**NB**	**NC**	**INB**	**GN**
Ames toxicity	Non Ames toxic	Non Ames toxic	Non Ames toxic	Non Ames toxic	Non Ames toxic
Carcinogens	Non-carcinogenic	Non-carcinogenic	Non-carcinogenic	Non-carcinogenic	Non-carcinogenic
Acute oral toxicity	III	III	III	III	III
Rat acute toxicity	3.1399	3.1399	3.1399	3.1399	3.1399
hERG [a]	Weak inhibitor	Weak inhibitor	Weak inhibitor	Weak inhibitor	Weak inhibitor
Carcinogenicity (Three-class)	Not required	Not required	Not required	Not required	Not required

[a] Human ether-a-go-go-related gene.

Table 5.5. Results of quantum chemical calculations and thermodynamic properties of the compounds.

Compound	Electronic Energy (Hartree)	Enthalpy (Hartree)	Gibbs Free Energy (Hartree)	Dipole Moment (Debye)	εHOMO (Hartree)	εLUMO (Hartree)	Gap (Hartree)	η	S
NA	−1420.38	−1420.38	−1420.48	3.337	−0.2097	−0.0465	0.1632	0.08161	12.2526
NB	−1420.37	−1420.37	−1420.47	3.168	−0.2107	−0.0502	0.1605	0.08028	12.4564
NC	−1615.60	−1615.60	−1615.72	5.228	−0.2090	−0.0489	0.1600	0.08004	12.4929
INB	−1420.38	−1420.38	−1420.47	2.235	−0.2135	−0.0536	0.1599	0.07995	12.5078
GN	−1345.16	−1345.16	−1345.25	4.959	−0.2207	−0.0522	0.1684	0.08423	11.8715

εHOMO = energy of HOMO; εLUMO = energy of LUMO; η = hardness; S = softness.

CHAPTER-VI

General Conclusion

The basis of modern medicine or allopathy lies in traditional therapeutic systems which date back to the existence of human civilization. Traditional therapeutic systems emerged with the abundant use of natural products (NPs). In modern medicine, the goals of using NPs as therapeutic agents are: 1) to isolate biologically active compounds for direct use as drugs and 2) to discover leads for developing novel drugs with higher potentiality through semi-synthesis approaches. This study was designed with different Okinawan NPs collected from terrestrial and marine sources with the major goals of purifying their bioactive components and studying their chemopreventive activities including anti-inflammatory, anti-cancer, anti-diabetic, and anti-Alzheimer's effects. The findings from this investigation are concluded as the followings:

1) Five major compounds purified from *Alpinia zerumbet* var. *excelsa* (*Alpinia*) leaves, 5,6-dehydrokawain (DK), dihydro-5,6-dehydrokawain (DDK), (*E*)-5-methoxy-8-(4-methoxy-2-oxo-2*H*-pyran-6-yl)-7-phenyl-1-styryl-2-oxabicyclo[4.2.0]oct-4-en-3-one (AS-2), kaempferol 3-O-*β*-D-glucuronide (KOG), and quercetin 3-O-*β*-D-glucuronide (QOG), could be promising chemopreventive and therapeutic agents for inflammatory disorders since they were found to inhibit albumin denaturation, proteinase activity, and the formation of inflammatory mediators NO (nitric oxide) and PGE_2 (prostaglandin E2). In addition, they can be utilized in cosmetic formulations as safe de-pigmenting agents.

2) Bioactive compounds from the leaves of *Ardisia sieboldii*, 2-methyl-5-(8*Z*-heptadecenyl) resorcinol (**1**), 5-(8*Z*-heptadecenyl) resorcinol (**2**), and ardisiaquinone A (**3**), showed notable cytotoxicity against a panel of cancer cells

and on the brine shrimps, demonstrating their potential cancer chemoprevention effects. Compounds **1**–**3** can also be utilized in prevention and treatment of inflammation since they were found to inhibit albumin denaturation, NO production in RAW 264.7 cells, and COX-2 (cyclooxygenase-2) enzyme activity.

3) Desulfated saponin from marine sea cucumber *Holothuria atra*, desulfated echinoside B (DEB), was found to have promising cytotoxic effects on both cancer cells and brine shrimps compared to the sulfated saponin frondoside A (FRA) purified from *Cucumaria frondosa*. *In silico* studies demonstrates that DEB could inhibit the oncogenic kinase PAK1 (p21-activated kinase 1) and thus could function as cancer chemoprevention drug.

4) Major compounds of Okinawa propolis (OP), nymphaeol-A, nymphaeol-B, nymphaeol-C, isonymphaeol-B, and 3′-geranyl-naringenin, showed promising therapeutic and chemopreventive potentials on inflammation, type 2 diabetes, and Alzheimer's disease (AD). They inhibited albumin denaturation, nitrite accumulation, and COX-2 enzyme activity. They also strongly suppressed the *in vitro* activity of two major enzymes, α-glucosidase and acetylcholinesterase responsible for type-2 diabetes and AD, respectively.

Taken together, bioactive compounds from *Alpinia*, *A. sieboldii*, sea cucumber, and OP might exert chemopreventive and therapeutic effects on inflammation, skin pigmentation, cancer, type 2 diabetes, and Alzheimer's disease. All of these data provide a scientific evidence for understanding their health benefits as traditional medicines, and hence, they could be exploited for developing herbal drugs or functional foods.

Literature Cited

Abagyan R, Totrov M, Kuznetsov R. ICM - A new method for protein modeling and design: applications to docking and structure prediction from the distorted native conformation. *J Comput Chem.* **1994**, 15, 488–506.

Abdel-Salam IM, Ashmawy AM, Hilal AM, Eldahshan OA, Ashour M. Chemical composition of aqueous-ethanol extract of *Luffa cylindrica* leaves and its effect on representation of caspase 8, caspase 3 and the proliferation marker Ki67 in intrinsic molecular sub-types of breast cancer *in vitro*. *Chem Biodivers*. **2018**, 15, e1800045.

Abdel-Salam IM, Awadein NE, Ashour M. Cytotoxicity of *Luffa cylindrica* (L.) M. Roem. extract against circulating cancer stem cells in hepatocellular carcinoma. *J Ethnopharmacol*. **2019**, 229, 89–96.

Adams M, Berset C, Kessler M, Hamburger M. Medicinal herbs for the treatment of rheumatic disorders–a survey of European herbals from the 16th and 17th century. *J Ethnopharmacol*. **2009**, 1213, 343–359.

Afrapoli FM, Asghari B, Saeidnia S, Ajani Y, Mirjani M, Malmir M, Baza RD, Hadjiakhoondi A, Salehi P, Hamburger M, et al. *In vitro* α-glucosidase inhibitory activity of phenolic constituents from aerial parts of *Polygonum hyrcanicum*. *J Pharm Sci*. **2012**, 20, 1–6.

Ahn MR, Bae JY, Jeong DH, Takahashi H, Uto Y, Maruta H. Both triazolyl ester of ketorolac (15K) and YM155 inhibit the embryonic angiogenesis *in ovo* (fertilized eggs) via their common PAK1-survivin/VEGF signaling pathway. *Drug Discov Ther*. **2017**, 11, 300–306.

Akihisa T, Higo N, Tokuda H, Ukiya M, Akazawa H, Tochigi Y, Kimura Y, Suzuki T, Nishino H. Cucurbitane-type triterpenoids from the fruits of *Momordica*

charantia and their cancer chemopreventive effects. *J Nat Prod*. **2007**, 70, 1233–1239.

Akiyama H, Barger S, Barnum S, Bradt B, Bauer J, Cole GM, Cooper NR, Eikelenboom P, Emmerling M, Fiebich BL. et al. Inflammation and Alzheimer's disease. *Neurobiol Aging*. **2000**, 21, 383–421.

Alam F, Islam A, Haryo Sasongko T, Hua Gan S. Type 2 diabetes mellitus and Alzheimer's disease: Bridging the pathophysiology and management. *Curr Pharm Des*. **2016**, 22, 4430–4442.

Andres M, Park JH, Wimbush M, Zhu XH, Chang KI, Ichikawa H. Study of the Kuroshio/Ryukyu current system based on satellite-altimeter and *in situ* measurements. *J Oceanogr*. **2008**, 64, 937–950.

Anjaneyulu ASR, Raju KVS. A new triterpene glycoside from the sea cucumber *Holothuria atra* off Mandapam Coast. *Indian J Chem*. **1996**, 35B, 810–814.

Aramoto M, Ishigaki C, Shinzato T, Asato I, Wu L. Plants distribution on the main island in subtropical Okinawa. *Kyushu J. Forest Res-Jpn*. **2006**, 59, 60–64.

Arodola OA, Soliman ME. Quantum mechanics implementation in drug-design workflows: does it really help?. *Drug Des Devel Ther*. **2017**, 11, 2551.

Azam F, Alabdullah NH, Ehmedat HM, Abulifa AR, Taban I, Upadhyayula S. NSAIDs as potential treatment option for preventing amyloid β toxicity in Alzheimer's disease: An investigation by docking, molecular dynamics, and DFT studies. *J Biomol Struct Dyn*. **2017**, 36, 2099–2117.

Azam F, Amer AM, Abulifa AR, Elzwawi MM. Ginger components as new leads for the design and development of novel multi-targeted anti-Alzheimer's drugs: A computational investigation. *Drug Des Dev Ther*. **2014**, 8, 2045.

Azam F, Mohamed N, Alhussen F. Molecular interaction studies of green tea catechins as multitarget drug candidates for the treatment of Parkinson's disease: Computational and structural insights. *Netw Comput Neural Syst*. **2016**, 26, 97–115.

Baharara J, Amini E, Nikdel N, Salek-Abdollahi F. The cytotoxicity of dacarbazine potentiated by sea cucumber saponin in resistant B16F10 melanoma cells through apoptosis induction. *Avicenna J Med Biotechnol*. **2016**, 8, 112.

Balandrin MF, Klocke JA, Wurtele ES, Bollinger WH. Natural plant chemicals: sources of industrial and medicinal materials. *Science*. **1985**, 228, 1154–1160.

Balupuri A, Balasubramanian PK, Cho SJ. Molecular docking studies of p21-activated kinase-1 (PAK1) inhibitors. *J Chosun Nat Sci*. **2016**, 9, 161–165.

Bao L, Wang M, Zhao F, Zhao Y, Liu H. Two new resorcinol derivatives with strong cytotoxicity from the roots of *Ardisia brevicaulis* Diels. *Chem Biodivers*. **2010**, 7, 2901–2907.

Be Tu PT, Nguyen BC, Tawata S, Yun CY, Kim EG, Maruta H. The serum/PDGF-dependent" melanogenic" role of the minute level of the oncogenic kinase PAK1 in melanoma cells proven by the highly sensitive kinase assay. *Drug Discov Ther*. **2016**, 10, 314–322.

Be Tu PT, Tawata S. Anti-obesity effects of hispidin and *Alpinia zerumbet* bioactives in 3T3-L1 adipocytes. *Molecules*. **2014**, 19, 16656–16671.

Be Tu PT, Tawata S. Anti-oxidant, anti-aging, and anti-melanogenic properties of the essential oils from two varieties of *Alpinia zerumbet*. *Molecules*. **2015**, 20, 16723–16740.

Benalla W, Bellahcen S, Bnouham M. Antidiabetic medicinal plants as a source of alpha glucosidase inhibitors. *Curr Diabetes Rev*. **2010**, 6, 247–254.

Blunden G. Biologically active compounds from marine organisms. *Phytother Res*. **2001**, 15, 89–94.

Brady GP, Stouten PF. Fast prediction and visualization of protein binding pockets with PASS. *J Comput Aided Mol Des*. **2000**, 14, 383–401.

Brenner M, Hearing VJ. The protective role of melanin against UV damage in human skin. *Photochem Photobiol*. **2008**, 539–549.

Briganti S, Camera E, Picardo M. Chemical and instrumental approaches to treat hyperpigmentation. *Pigment Cell Melanoma Res*. **2003**, 16, 101–110.

Briskin DP. Medicinal plants and phytomedicines: linking plant biochemistry and physiology to human health. *Plant Physiol*. **2000**, 124, 507–514.

Broom GM, Shaw IC, Rucklidge JJ. The ketogenic diet as a potential treatment and prevention Strategy for Alzheimer's disease. *Nutrition*. **2018**, 118–121.

Burg RW, Miller BM, Baker EE, Birnbaum J, Currie SA, Hartman R, Kong Y-L, Monaghan RL, Olson G, Putter I, et al. Avermectins, new family of potent anthelmintic agents: Producing organism and fermentation. *Antimicrob Agents Chemother*. **1979**, 15, 361–367.

Campos PM, Horinouchi CDDS, Prudente ADS, Cechinel-Filho V, Cabrini DDA, Otuki MF. Effect of a *Garcinia gardneriana* (Planchon and Triana) Zappi hydroalcoholic extract on melanogenesis in B16F10 melanoma cells. *J Ethnopharmacol*. **2013**, 148, 199–204.

Cattaneo A, Cattane N, Galluzzi S, Provasi S, Lopizzo N, Festari C, Ferrari C, Guerra UP, Paghera B, Muscio C, et al. Association of brain amyloidosis with pro-

inflammatory gut bacterial taxa and peripheral inflammation markers in cognitively impaired elderly. *Neurobiol Aging*. **2017**, 49, 60–68.

Chan EWC, Lim YY, Wong SK, Lim KK, Tan SP, Lianto FS, Yong MY. Effects of different drying methods on the antioxidant properties of leaves and tea of ginger species. *Food Chem*. **2009**, 113, 166–172.

Chan YY, Kim KH, Cheah SH. Inhibitory effects of *Sargassum polycystum* on tyrosinase activity and melanin formation in B16F10 murine melanoma cells. *J Ethnopharmacol*. **2011**, 137, 1183–1188.

Chander S, Wang P, Ashok P, Yang LM, Zheng YT, Murugesan S. Rational design, synthesis, anti-HIV-1 RT and antimicrobial activity of novel 3-(6-methoxy-3, 4-dihydroquinolin-1(2H)-yl)-1-(piperazin-1-yl)propan-1-one derivatives. *Bioorg Chem*. **2016**, 67, 75–83.

Chatterjee P, Chandra S, Dey P, Bhattacharya S. Evaluation of anti-inflammatory effects of green tea and black tea: a comparative *in vitro* study. *J Adv Pharm Technol Res*. **2012**, 3, 136–138.

Chaudhary A, King WG, Mattaliano MD, Frost JA, Diaz B, Morrison DK, Cobb MH, Marshall MS, Brugge JS. Phosphatidylinositol 3-kinase regulates Raf1 through PAK phosphorylation of serine 338. *Curr Biol*. **2000**, 10, 551–554.

Chen CP, Lin CC, Namaba T. Screening of Taiwanese crude drugs for antibacterial activity against *Streptococcus mutans*. *J Ethnopharmacol*. **1989**, 27, 285–295.

Chen C, Pipoly JJ. Myrsinaceae. In: Flora of China; Ed. Wu Z, Raven PH; Beijing and Missouri Botanical Garden Press, St. Louis: Science Press; **1996**, 1–38.

Chen IS, Chang CT, Sheen WS, Teng CM, Tsai IL, Duh CY, Ko FN. Coumarins and antiplatelet aggregation constituents from Formosan *Peucedanum japonicum*. *Phytochemistry*. **1996**, 412, 525–530.

Chen L, Morrow JK, Tran HT, Phatak SS, Du-Cuny L, Zhang S. From laptop to benchtop to bedside: structure-based drug design on protein targets. *Curr Pharm Des*. **2012**, 18, 1217–1239.

Chen LP, Zhao F, Wang Y, Zhao LL, Li QP, Liu HW. Antitumor effect of resorcinol derivatives from the roots of *Ardisia brevicaulis* by inducing apoptosis. *J Asian Nat Prod Res*. **2011**, 13, 734–743.

Cheng F, Li W, Zhou Y, Shen J, Wu Z, Liu G, Lee PW, Tang Y. admetSAR: A comprehensive source and free tool for assessment of chemical ADMET properties. *J Chem Inf Model*. **2012**, 52, 3099–3105.

Cho H, Yun CW, Park WK, Kong JY, Kim KS, Park Y, Lee S, Kim BK. Modulation of the activity of pro-inflammatory enzymes, COX-2 and iNOS, by chrysin derivatives. *Pharmacol Res*. **2004**, 49, 37–43.

Chompoo J, Upadhyay A, Gima S, Fukuta M, Tawata S. Antiatherogenic properties of acetone extract of *Alpinia zerumbet* seeds. *Molecules*. **2012**, 17, 6237–6248.

Chompoo J, Upadhyay A, Kishimoto W, Makise T, Tawata S. Advanced glycation end products inhibitors from *Alpinia zerumbet* rhizomes. *Food Chem*. **2011**, 129, 709–715.

Chonpathompikunlert P, Wattanathorn J, Muchimapura S. Piperine, the main alkaloid of Thai black pepper, protects against neurodegeneration and cognitive impairment in animal model of cognitive deficit like condition of Alzheimer's disease. *Food Chem Toxicol*. **2010**, 48, 798–802.

Cole JC, Murray CW, Nissink JW, Taylor RD, Taylor R. Comparing protein-ligand docking programs is difficult. *Proteins*. **2005**, 60, 325–332.

Coleman JW. Nitric oxide in immunity and inflammation. *Int Immunopharmacol*. **2001**, 1, 1397–1406.

Colotta F, Allavena P, Sica A, Garlanda C, Mantovani A. Cancer-related inflammation, the seventh hallmark of cancer: links to genetic instability. *Carcinogenesis*. **2009**, 30, 1073–1081.

Cotran RS, Kumar V, Collins T, Robbins SL. Robbins pathologic basis of disease, 6th ed. Philadelphia: WB Saunders. **1999**, 54–92.

Cowman PF, Parravicini V, Kulbicki M, Floeter SR. The biogeography of tropical reef fishes: Endemism and provinciality through time. *Biol Rev*. **2017**, 92, 2112–2130.

Cragg GM, Newman DJ. Biodiversity: A continuing source of novel drug leads. *Pure Appl Chem.* **2005**, 77, 7–24.

da Cunha GH, de Moraes MO, Fechine FV, Bezerra FAF, Silveira ER, Canuto KM, de Moraes MEA. Vasorelaxant and antihypertensive effects of methanolic fraction of the essential oil of *Alpinia zerumbet*. *Vasc Pharmacol*. **2013**, 58, 337–345.

Darden T, York D, Pedersen L. Particle mesh Ewald: An $N\cdot\log(N)$ method for Ewald sums in large systems. *J Chem Phys*. **1993**, 98, 10089–10092.

Das SN, Chatterjee S. Long term toxicity study of ART-400. *Indian Indg Med*. **1995**, 16, 117–123.

de Mejía EG, Ramírez-Mares MV. Ardisia: health-promoting properties and toxicity of phytochemicals and extracts. *Toxicol Mech Methods*. **2011**, 21, 667–674.

Dhinakaran DI, Lipton AP. Bioactive compounds from *Holothuria atra* of Indian ocean. *SpringerPlus.* **2014**, 3, 673.

Druker BJ, Lydon NB. Lessons learned from the development of an Abl tyrosine kinase inhibitor for chronic myelogenous leukemia. *J Clin Invest*. **2000**, 105, 3–7.

Duke JA, Godwin MJB, duCellier J, Duke PNK. Hand book of Medicinal Herbs, 2nd edn. CRC Press: Washington, DC. **2002**

Dundas J, Ouyang Z, Tseng J, Binkowski A, Turpaz Y, Liang J. CASTp: computed atlas of surface topography of proteins with structural and topographical mapping of functionally annotated residues. *Nucleic Acids Res*. **2006**, 34, W116–118.

El-Gabalawy H, Guenther LC, Bernstein CN. Epidemiology of Immune-Mediated Inflammatory Diseases: Incidence, Prevalence, Natural History, and Comorbidities. *J Rheumatol Suppl*. **2010**, 85, 2–10.

Ellman GL, Courtney KD, Andres V, Featherstone RM. A new and rapid colorimetric determination of acetylcholinesterase activity. *Biochem Pharmacol*. **1961**, 7, 88–95.

Ewing T, Makino S, Skillman AG, Kuntz ID. DOCK 4.0: Search strategies for automated molecular docking of flexible molecule databases. *J Comput Aided Mol Des*. **2001**, 15, 411–428.

Fawole OA, Amoo SO, Ndhlala AR, Light ME, Finnie JF, Van Staden J. Antiinflammatory, anticholinesterase, antioxidant and phytochemical properties of medicinal plants used for pain-related ailments in South Africa. *J Ethnopharmacol*. **2010**, 127, 235–241.

Fernández SS, Ribeiro SM. Nutrition and Alzheimer disease. *Clin Geriatr Med*. **2018**, 34, 677–697.

Ferreira LG, Dos Santos RN, Oliva G, Andricopulo AD. Molecular docking and structure-based drug design strategies. *Molecules*. **2015**, 2, 13384–13421.

Findlay GH, Morrison JG, Simson IW. Exogenous ochronosis and pigmented colloid milium from hydroquinone bleaching creams. *Br J Dermatol*. **1975**, 93, 613–622.

Foryst-Ludwig A, Naumann M. P21-activated Kinase 1 activates the nuclear factor κB (NF-κB)-inducing kinase-IκB kinases NF-κB pathway and proinflammatory cytokines in *Helicobacter pylori* infection. *J Biol Chem*. **2000**, 275, 39779–39785.

Fosslien E. Biochemistry of cyclooxygenase (COX)-2 inhibitors and molecular pathology of COX-2 in neoplasia. *Crit Rev Clin Lab Sci*. **2000**, 37, 431–502.

Friesner RA, Banks JL, Murphy RB, Halgren TA, Klicic JJ, Mainz DT, Repasky MP, Knoll EH, Shelley M, Perry JK, et al. Glide: a new approach for rapid, accurate docking and scoring. 1. Method and assessment of docking accuracy. *J Med Chem*. **2004**, 47, 1739–1749.

Frisch MJ, Trucks GW, Schlegel HB, Scuseria GE, Robb MA, Cheeseman JR, Scalmani G, Barone V, Mennucci B, Petersson G, et al. Gaussian 09, Revision A. 02; Gaussian. Inc.: Wallingford, CT, USA, **2009**, p. 200.

Frost JA, Steen H, Shapiro P, Lewis T, Ahn N, Shaw PE, Cobb MH. Cross-cascade activation of ERKs and ternary complex factors by Rho family proteins. *EMBO J*. **1997**, 16, 6426–6438.

Fujita T, Nishimura H, Kaburagi K, Mizutani J. Plant growth inhibiting α-pyrones from *Alpinia speciosa*. *Phytochem*. **1994**, 36, 23–27.

Fukuyama Y, Kiriyama Y, Kodama M, Iwaki H, Hosozawa A, Matsui K. Naturally occurring 5-lipoxygenase inhibitors. VI. Structures of ardisiaquinones D, E, and F from *Ardisia sieboldii*. *Chem Pharm Bull (Tokyo)*. **1995**, 43, 1391–1394.

Fukuyama Y, Kiriyama Y, Kodama M, Iwaki H, Hosozawa S, Aki S. Total synthesis of ardisiaquinone A, a potent 5-lipoxygenase inhibitor, isolated from *Ardisia sieboldii*, and degree of 5-lipoxygenase inhibitory activity of its derivatives. *Chem Pharm Bull (Tokyo)*. **1994**, 42, 2211–2213.

Garcia A, Fulton Jr JE. The combination of glycolic acid and hydroquinone or kojic acid for the treatment of melasma and related conditions. *Dermatol Surg*. **1996**, 22, 443–447.

Gasparini L, Netzer WJ, Greengard P, Xu H. Does insulin dysfunction play a role in Alzheimer's disease? *Trends Pharmacol Sci*. **2002**, 23, 288–293.

Govindappa M, Channabasava R, Sowmya DV, Meenakshi J, Shreevidya MR, Lavanya A, Santoyo G, Sadananda TS. Phytochemical screening, antimicrobial and *in vitro* anti-inflammatory activity of endophytic extracts from *Loranthus* sp. *Pharmacogn J*. **2011**, 3, 82–90.

Grivennikov SI, Greten FR, Karin M. Immunity, Inflammation, and Cancer. *Cell*. **2010**, 140, 883–899.

Grover JK, Yadav SP. Pharmacological actions and potential uses of *Momordica charantia*: a review. *J Ethnopharmacol*. **2004**, 93, 123–132.

Guerard F, Decourcelle N, Sabourin C, Floch-laizet C, Le Grel L, Le Floch P, Gourlay F, Le Delezir R, Jaouen P, Bourseau P. Recent developments of marine

ingredients for food and nutraceutical applications: A review. *J Sci Hal Aquat*. **2011**, 2, 21–27.

Guo Z. The modification of natural products for medical use. *Acta Pharm Sin B*. **2017**, 7, 119–136.

Gupta SC, Hevia D, Patchva S, Park B, Koh W, Aggarwal BB. Upsides and downsides of reactive oxygen species for cancer: The roles of reactive oxygen species in tumorigenesis, prevention, and therapy. *Antioxid Redox Signal*. **2012**, 16, 1295–1322.

Ha YM, Chung SW, Song S, Lee H, Suh H, Chung HY. 4-(6-Hydroxy-2-naphthyl)-1,3-bezendiol: a potent, new tyrosinase inhibitor. *Biol Pharm Bull*. **2007**, 30, 1711–1715.

Hamalainen M. Inducible nitric oxide synthase as a target of anti-inflammatory treatment modalities. Academic dissertation, University of Tampere, Finland. **2008**.

Hardy J, Allsop D. Amyloid deposition as the central event in the etiology of Alzheimer's disease. *Trends Pharmacol Sci*. **1991**, 12, 383–388.

Hassan NM, Alhossary AA, Mu Y, Kwoh CK. Protein-ligand blind docking using QuickVina-W with inter-process spatio-temporal integration. *Sci Rep*. **2017**, 7, 15451.

He Y, Yue Y, Zheng X, Zhang K, Chen S, Du Z. Curcumin, inflammation, and chronic diseases: how are they linked?. *Molecules*. **2015**, 20, 9183–9213.

He Z, Guo JL, McBride JD, Narasimhan S, Kim H, Changolkar L, Zhang B, Gathagan RJ, Yue C, Dengler C, et al. Amyloid-β plaques enhance Alzheimer's brain tau-

seeded pathologies by facilitating neuritic plaque tau aggregation. *Nat Med*. **2018**, 24, 29–38.

Hearing VJ, Tsukamato K. Enzymatic control of pigmentation in mammals. *FASEB J*. **1991**, 5, 2902–2909.

Herman WH. The global burden of diabetes: an overview. In: Diabetes Mellitus in Developing Countries and Underserved Communities; Ed. Dagogo-Jack S, Springer, Cham; **2017**, 1–5.

Herschman HR. Prostaglandin synthase 2. *Biochim Biophys Acta*. **1996**. 1299, 125–140.

Hidalgo GV. Comparative analysis of the natural products of three sea cucumber species: *Holothuria grisea*, *Synaptula reciprocans* and *Holothuria manningí*. Master's Thesis, University of Aberdeen, Aberdeen, Scotland, September **2013**.

Hirabara SM, Gorjao R, Vinolo MA, Rodrigues AC, Nachbar RT, Curi R. Molecular targets related to inflammation and insulin resistance and potential interventions. *BioMed Res Int*. **2012**, doi:10.1155/2012/379024

Hisamoto M, Kikuzaki H, Ohigashi H, Nakatani N. Antioxidant compounds from the leaves of *Peucedanum japonicum* thunb. *J Agric Food Chem*. **2003**, 5118, 5255–5261.

Hokama T, Binns C. Declining longevity advantage and low birthweight in Okinawa. *Asia-Pac J Public Health*. **2008**, 20, 95–101.

Hokawa S. Chouju wo sasaeta no shokuseikatsu. In: *Okinawa no Chouju (in Japanese)*; Eds. Sho H & Yamamoto S. Center for Academic Societies, Japan, Toyonaka, **1996**, 31–48.

Horgen FD, Guinaudeau H, Pezzuto JM, Soejarto DD, Farnsworth NR, Agcaoili F, De Los Reyes G, Edrada RA. Isolation and structure elucidation of ardisenone: a new, cytotoxic alkenylphenol from *Ardisia iwahigensis*. *J Nat Prod*. **1997**, 60, 533–535.

Hu XQ, Wang YM, Wang JF, Xue Y, Li ZJ, Nagao K, Yanagita T, Xue CH. Dietary saponins of sea cucumber alleviate orotic acid-induced fatty liver in rats via PPARα and SREBP-1c signaling. *Lipids Health Dis*. **2010**, 9, 25.

Hughes TP, Bellwood DR, Connolly SR. Biodiversity hotspots, centres of endemicity, and the conservation of coral reefs. *Ecol Lett*. **2002**, 5, 775–784.

Hung CL, Chen CC. Computational approaches for drug discovery. *Drug Dev Res*. **2014**, 75, 412–418.

Huynh N, He H. p21-activated kinase family: promising new drug targets. *Res Rep Biochem*. **2015**, 5, 119–128.

Innami S, Tabata K, Shimizu J, Kusunoki K, Ishida H, Matsuguma M, Wada M, Sugiyama N, Kondo M. Dried green leaf powders of Jew's mellow (*Corchorus*), persimmon (*Diosphyros kaki*) and sweet potato (*Ipomoea batatas* Poir) lower hepatic cholesterol concentration and increase fecal bile acid excretion in rats fed a cholesterol-free diet. *Plant Foods Hum Nutr*. **1998**, 52, 55–66.

Jain AN. Surflex: fully automatic flexible molecular docking using a molecular similarity-based search engine. *J Med Chem*. **2003**, 46, 499–511.

Janakiram NB, Mohammed A, Rao CV. Sea cucumbers metabolites as potent anti-cancer agents. *Mar Drugs*. **2015**, 13, 2909–2923.

Jhoti H, Rees S, Solari R. High-throughput screening and structure-based approaches to hit discovery: Is there a clear winner? *Expert Opin Drug Discov*. **2013**, 8, 1449–1453.

Ji S, Fattahi A, Raffel N, Hoffmann I, Beckmann MW, Dittrich R, Schrauder M. Antioxidant effect of aqueous extract of four plants with therapeutic potential on gynecological diseases; semen persicae, *Leonurus cardiaca*, *Hedyotis diffusa*, and *Curcuma zedoaria*. *Eur J Med Res*. **2017**, 22, 50.

Jones G, Willett R, Glen R, Leach AR, Taylor R. Development and validation of a genetic algorithm for flexible docking. *J Mol Biol*. **1997**, 267, 727–748.

Joppa LN, Visconti P, Jenkins CN, Pimm SL. Achieving the convention on biological diversity's goals for plant conservation. *Science*. **2013**, 341, 1100–1103.

Jorgensen WL. The many roles of computation in drug discovery. *Science*. **2004**, 303, 1813–1818.

Kacem M, Simon G, Leschiera R, Misery L, ElFeki A, Lebonvallet N. Antioxidant and anti-inflammatory effects of *Ruta chalepensis* L. extracts on LPS-stimulated RAW 264.7 cells. *In Vitro Cell Dev Biol: Anim*. **2015**, 51, 128–141.

Kanaoka S, Takai T, Yoshida A. Cyclooxygenase-2 and tumor biology. *Adv Clin Chem.* **2007**, 43, 59–78.

Kardos N, Demain AL. Penicillin: the medicine with the greatest impact on therapeutic outcomes. *Appl Microbiol Biotechnol*. **2011**, 92, 677.

Karpov AS, Amiri P, Bellamacina C, Bellance MH, Breitenstein W, Daniel D, Denay R, Fabbro D, Fernandez C, Galuba I. et al. Optimization of a dibenzodiazepine hit to a potent and selective allosteric PAK1 inhibitor. *ACS Med Chem Lett*. **2015**, 6, 776–781.

Kastenholz MA, Pastor M, Cruciani G, Haaksma EE, Fox T. GRID/CPCA: a new computational tool to design selective ligands. *J Med Chem*. **2000**, 43, 3033–3044.

Kasturi S, Surarapu S, Uppalanchi S, Anireddy JS, Dwivedi S, Anantaraju HS, Perumal Y, Sigalapalli DK, Babu BN, Ethiraj KS. Synthesis and α-glucosidase inhibition activity of dihydroxy pyrrolidines. *Bioorg Med Chem Lett*. **2017**, 27, 2818–2823.

Katiyar C, Gupta A, Kanjilal S, Katiyar S. Drug discovery from plant sources: An integrated approach. *Ayu*. **2012**, 33, 10.

Kaur A, Pathak DP, Sharma V, Narasimhan B, Sharma P, Mathur R, Wakode S. Synthesis, biological evaluation and docking study of N-(2-(3, 4, 5-trimethoxybenzyl) benzoxazole-5-yl) benzamide derivatives as selective COX-2 inhibitor and anti-inflammatory agents. *Bioorg Chem*. **2018**, 81, 191–202.

Kawai T, Akira S. Signaling to NF-κB by Toll-like receptors. *Trends in Mol Med*. **2007**, 13, 460–469.

Kawamori T, Rao CV, Seibert K, Reddy BS. Chemopreventive activity of celecoxib, a specific cyclooxygenase-2 inhibitor, against colon carcinogenesis. *Cancer Res.* **1998**, 58, 409–412.

Khaled M, Larribere L, Bille K, Aberdam E, Ortonne JP, Ballotti R, Bertolotto C. Glycogen synthase kinase 3β is activated by cAMP and plays an active role in the regulation of melanogenesis. *J Biol Chem*. **2002**, 277, 33690–33697.

Khan AM, Shawon J, Halim MA. Multiple receptor conformers based molecular docking study of fluorine enhanced ethionamide with mycobacterium enoyl ACP reductase (InhA). *J Mol Graph Model*. **2017**, 77, 386–398.

Khan H, Amin S, Kamal MA, Patel S. Flavonoids as acetylcholinesterase inhibitors: Current therapeutic standing and future prospects. *Biomed Pharmacother*. **2018**, 101, 860–870.

Kichina JV, Goc A, Al-Husein B, Somanath PR, Kandel ES. PAK1 as a therapeutic target. *Expert Opin Ther Targets*. **2010**, 14, 703–725.

Kiew PL, Don MM. Jewel of the seabed: Sea cucumbers as nutritional and drug candidates. *Int J Food Sci Nutr*. **2012**, 63, 616–636.

Kim HE, Ishihara A, Lee SG. The effects of Caffeoylserotonin on inhibition of melanogenesis through the downregulation of MITF via the reduction of intracellular cAMP and acceleration of ERK activation in B16 murine melanoma cells. *BMB Rep*. **2012**, 724–729.

Kim KJ, Lee MS, Jo K, Hwang JK. Piperidine alkaloids from *Piper retrofractum* Vahl. protect against high-fat diet-induced obesity by regulating lipid metabolism and activating AMP-activated protein kinase. *Biochem Biophys Res Commun*. **2011**, 411, 219–225

Kim M, Shin S, Lee J-A, Park D, Lee J, Jung E. Inhibition of melanogenesis by *Gaillardia aristata* flower extract. *BMC Complement Altern Med*. **2015**, 15, 449.

Kim SK, Himaya SW. Triterpene glycosides from sea cucumbers and their biological activities. *Adv Food Nutr Res*. **2012**, 65, 297–319.

Kim SY, Park JY, Park PS, Bang SH, Lee KM, Lee YR, Jang YH, Kim MJ, Chun W, Heo MY, et al. Flavonoid glycosides as acetylcholinesterase inhibitors from the whole plants of *Persicaria thunbergii*. *Nat Prod Sci*. **2014**, 20, 191–195.

Kimura K, Lee JH, Lee IS, Lee HS, Park KH, Chiba S. Two potent competitive inhibitors discriminating alpha-glucosidase family I from family II. *Carbohydr Res*. **2004**, 339, 1035–1040.

King H, Nicholas NS, Wells CM. Role of p-21-activated kinases in cancer progression. *Int Rev Cell Mol Biol*. **2014**, 309, 347–387.

Kinghorn AD. Drug discovery from natural products. In: Foye's Principles of Medicinal Chemistry; Ed. Lemke TL, Williams DA; Philadelphia, PA, USA: Wolters Kluwer/Williams & Wilkins; **2008**, 12–25.

Kitagawa I, Kobayashi M, Inamoto T, Fuchida M, Kyogoku Y. Structures of echinosides A and B, antifungal lanostane-oligosides from the sea cucumber *Actinopyga echinites* (JAEGER). *Chem Pharm Bull (Tokyo)*. **1985**, 33, 5214–5224.

Kitai Y, Hayashi K, Otsuka M, Nishiwaki H, Senoo T, Ishii T, Sakane G, Sugiura M, Tamura H. New sesquiterpene lactone dimer, uvedafolin, extracted from eight yacon leaf varieties (*Smallanthus sonchifolius*): cytotoxicity in HeLa, HL-60, and Murine B16-F10 melanoma cell lines. *J Agric Food Chem*. **2015**, 63, 10856–10861.

Kizaki K. Geology and tectonics of the Ryukyu Islands. *Tectonophysics*. **1986**, 125, 193–207.

Kobayashi H, de Mejía E. The genus *Ardisia*: a novel source of health-promoting compounds and phytopharmaceuticals. *J Ethnopharmacol*. **2005**, 96, 347–354.

Kobayashi JI. Search for new bioactive marine natural products and application to drug development. *Chem Pharm Bull (Tokyo)*. **2016**, 64, 1079–1083.

Kolb H, Mandrup-Poulsen T. The global diabetes epidemic as a consequence of lifestyle-induced low-grade inflammation. *Diabetologia*. **2010**, 53, 10–20.

Krieger E, Darden T, Nabuurs SB, Finkelstein A, Vriend G. Making optimal use of empirical energy functions: Force-field parameterization in crystal space. *Proteins*. **2004**, 57, 678–683.

Krieger F, Fierz B, Bieri O, Drewello M, Kiefhaber T. Dynamics of unfolded polypeptide chains as model for the earliest steps in protein folding. *J Mol Biol*. **2003**, 332, 265–274.

Kroner Z. The relationship between Alzheimer's disease and diabetes: Type 3 diabetes? *Altern Med Rev*. **2009**, 14, 373–379.

Kubo I, Nitoda T, Nihei KI. Effects of quercetin on mushroom tyrosinase and B16-F10 melanoma cells. *Molecules*. **2007**, 12, 1045–1056.

Kumar R, Gururaj AE, Barnes CJ. p21-activated kinases in cancer. *Nat Rev Cancer*. **2006**, 6, 459.

Kumar R, Sanawar R, Li X, Li F. Structure, biochemistry, and biology of PAK kinases. *Gene*. **2017**, 605, 20–31.

Kumar S, Narwal S, Kumar V, Prakash O. α-Glucosidase inhibitors from plants: A natural approach to treat diabetes. *Pharmacogn Rev*. **2011**, 5, 19.

Kumazawa S, Murase M, Momose N, Fukumoto S. Analysis of antioxidant prenylflavonoids in different parts of *Macaranga tanarius*, the plant origin of Okinawan propolis. *Asian Pac J Trop Med*. **2014**, 7, 16–20.

Kumazawa S, Ueda R, Hamasaka T, Fukumoto S, Fujimoto T, Nakayama T. Antioxidant prenylated flavonoids from propolis collected in Okinawa, Japan. *J Agric Food Chem.* **2007**, 55, 7722–7725.

Kuntz ID, Blaney JM, Oatley SJ, Langridge R, Ferrin TE. A geometric approach to macromolecule-ligand interactions. *J Mol Biol*. **1982**, 161, 269–288.

Kurata R, Adachi M, Yamakawa O, Yoshimoto M. Growth suppression of human cancer cells by polyphenolics from sweet potato (*Ipomoea batatas* L.) leaves. *J Agric Food Chem*. **2007**, 55, 185–190.

Labib MB, Sharkawi SM, El-Daly M. Design, synthesis of novel isoindoline hybrids as COX-2 inhibitors: anti-inflammatory, analgesic activities and docking study. *Bioorg Chem*. **2018**, 80, 70–80.

Lavecchia A, Di Giovanni C. Virtual screening strategies in drug discovery: A critical review. *Curr Med Chem*. **2013**, 20, 2839–2860.

Lebovitz HE. α-Glucosidase inhibitors. *Endocrinol Metab Clin North*. **1997**, 26, 539–551.

Lechner M, Lirk P, Rieder J. Inducible nitric oxide synthase (iNOS) in tumor biology: the two sides of the same coin. In: Seminars in cancer biology (Vol. 15, No. 4, p. 277–289). Academic Press. **2005**.

Lee J, Yang G, Lee K, Lee MH, Eom JW, Ham I, Choi HY. Anti-inflammatory effect of *Prunus yedoensis* through inhibition of nuclear factor-κB in macrophages. *BMC Complement Altern Med.* **2013**, 13, 92.

Lee JH, Jang JY, Park C, Kim BW, Choi YH, Choi BT. Curcumin suppresses alpha-melanocyte stimulating hormone-stimulated melanogenesis in B16F10 cells. *Int J Mol Med.* **2010**, 26, 101–106.

Lee KK, Choi JD. The effects of *Areca catechu* L extract on anti-aging. *Int J Cosmet Sci*. **1999**, 21, 285–295.

Lee MY, Choi DS, Lee MK, Lee HW, Park TS, Kim DM, Chung CH, Kim DK, Kim IJ, Jang HC. et al. Comparison of acarbose and voglibose in diabetes patients who are inadequately controlled with basal insulin treatment: randomized, parallel, open-label, active-controlled study. *J Korean Med Sci*. **2014**, 29, 90–97.

Lee W, Crawford JJ, Aliagas I, Murray LJ, Tay S, Wang W, Heise CE, Hoeflich KP, La H, Mathieu S, et al. Synthesis and evaluation of a series of 4-azaindole-containing p21-activated kinase-1 inhibitors. *Bioorg Med Chem Lett.* **2016**, 26, 3518–3524.

Levitt DG, Banaszak LJ. POCKET: a computer graphics method for identifying and displaying protein cavities and their surrounding amino acids. *J Mol Graph*. **1992**, 10, 229–234.

Licciulli S, Maksimoska J, Zhou C, Troutman S, Kota S, Liu Q, Duron S, Campbell, D, Chernoff J, Field J. et al. FRAX597, a small molecule inhibitor of the p21-activated kinases, inhibits tumorigenesis of neurofibromatosis type 2 (NF2)-associated Schwannomas. *J Biol Chem.* **2013**, 288, 29105–29114.

Lien EJ, Guo ZR, Li RL, Su CT. Use of dipole moment as a parameter in drug-receptor interaction and quantitative structure-activity relationship studies. *J Pharm Sci*. **1982**, 71, 641–655.

Lipinski CA, Lombardo F, Dominy BW, Feeney PJ. Experimental and computational approaches to estimate solubility and permeability in drug discovery and development settings. *Adv Drug Deliv Rev*. **2001**, 46, 3–26.

Liu H, Zhao F, Yang R, Wang M, Zheng M, Zhao Y, Zhang X, Qiu F, Wang H. Dimeric 1, 4-benzoquinone derivatives and a resorcinol derivative from *Ardisia gigantifolia*. *Phytochemistry*. **2009**, 70, 773–778.

Lockemann G. Friedrich Wilhelm Serturner, the discoverer of morphine. *J Chem Ed*. **1951**, 28, 279.

Lontchi-Yimagou E, Sobngwi E, Matsha TE, Kengne AP. Diabetes mellitus and inflammation. *Curr Diabetes Rep*. **2013**, 13, 435–444.

López-Vallejo F, Caulfield T, Martínez-Mayorga K, Giulianotti MA, Houghten RA, Nefzi A, Medina-Franco JL. Integrating virtual screening and combinatorial chemistry for accelerated drug discovery. *Comb Chem High Throughput Screen*. **2011**, 14, 475–487.

Lowenstein CJ, Padalko E. iNOS (NOS2) at a glance. *J Cell Sci*. **2004**, 117, 2865–2867.

Luyen BTT, Tai BH, Thao NR, Yang SY, Cuong NM. A new phenylpropanoid and an alkylglycoside from *Piper retrofractum* leaves with their antioxidant and α-glucosidase inhibitory activity. *Bioorg Med Chem Lett*. **2014**, 24, 4120–4124.

Macalino SJ, Gosu V, Hong S, Choi S. Role of computer-aided drug design in modern drug discovery. *Arch Pharm Res*. **2015**, 38, 1686–16701.

Machado LP, Carvalho LR, Young MC, Cardoso-Lopes EM, Centeno DC, Zambotti-Villela L, Colepicolo P, Yokoya NS. Evaluation of acetylcholinesterase inhibitory activity of Brazilian red macroalgae organic extracts. *Rev Bras Farmacogn*. **2015**, 25, 657–662.

Maeda R, Ida T, Ihara H, Sakamoto T. Induction of apoptosis in MCF-7 cells by β-1,3-xylooligosaccharides prepared from *Caulerpa lentillifera*. *Biosci Biotechnol Biochem*. **2012**, 76, 1032–1034.

Maier JA, Martinez C, Kasavajhala K, Wickstrom L, Hauser KE, Simmerling C. ff14SB: Improving the accuracy of protein side chain and backbone parameters from ff99SB. *J Chem Theory Comput*. **2015**, 11, 3696–3713.

Mallbris L, Akre O, Granath F, Yin L, Lindelöf B, Ekbom A, Ståhle-Bäckdahl M. Increased risk for cardiovascular mortality in psoriasis inpatients but not in outpatients. *Eur J Epidemiol.* **2004**, 19, 225–230.

Mancuso C, Santangelo R. Alzheimer's disease and gut microbiota modifications: the long way between preclinical studies and clinical evidence. *Pharmacol Res*. **2018**, 129, 329–336.

Mangiaterra G, Laudadio E, Cometti M, Mobbili G, Minnelli C, Massaccesi L, Citterio, B, Biavasco F, Galeazzi R. Inhibitors of multidrug efflux pumps of *Pseudomonas aeruginosa* from natural sources: An *in silico* high-throughput virtual screening and *in vitro* validation. *Med Chem Res.* **2017**. 26, 414–430.

Maruta H, Ahn MR. From bench (laboratory) to bed (hospital/home): How to explore effective natural and synthetic PAK1-blockers/longevity-promoters for cancer therapy. *Eur J Med Chem*. **2017**, 142, 229–243.

Maruta H, Be Tu PT, Ahn MR. Natural or synthetic ant-melanogenic compounds that block the PDGFR-EGFR-PAK1-MITF-Tyrosinase signaling pathway. *J Dermatol Res Ther*. **2017**, 3, 048.

Maruta H. Herbal therapeutics that block the oncogenic kinase PAK1: a practical approach towards PAK1-dependent diseases and longevity. *Phytother Res*. **2014**, 28, 656–672.

Masoumi J, Abbasloui M, Parvan R, Mohammadnejad D, Pavon-Djavid G, Barzegari A, Abdolalizadeh J. Apelin, a promising target for Alzheimer disease prevention and treatment. *Neuropeptides*. **2018**, 70, 76–86.

Matanjun P, Mohamed S, Muhammad K, Mustapha NM. Comparison of cardiovascular protective effects of tropical seaweeds, *Kappaphycus alvarezii*, *Caulerpa lentillifera*, and *Sargassum polycystum* on high-cholesterol/high-fat diet in rats. *J Med Food*. **2010**, 13, 792–800.

Matanjun P, Mohamed S, Mustapha NM, Muhammad K. Nutrient content of tropical edible seaweeds, *Eucheuma cottonii*, *Caulerpa lentillifera* and *Sargassum polycystum*. *J Appl Phycol*. **2009**, 21, 75–80.

Matsuda H, Ninomiya K, Morikawa T, Daisuke Y, Yamaguchi I, Yoshikawa M. Hepatoprotective amide constituents from the fruit of *Piper chaba*: structural requirements, mode of action, and new amides. *Bioorgan Med Chem*. **2009**, 17, 7313–7323.

Matsunami K, Otsuka H. Okinawan subtropical plants as a promising resource for novel chemical treasury. *Chem Pharm Bull (Tokyo).* **2018**, 66, 519–526.

McConkey BJ, Sobolev V, Edelman M. The performance of current methods in ligand-protein docking. *Curr Sci*. **2002**, 83, 845–855.

Medzhitov R. Origin and physiological roles of inflammation. *Nature*. **2008**, 454, 428.

Medzhitov R. Toll-like receptors and innate immunity. *Nat Rev Immunol*. **2001**, 1, 135–145.

Meng XY, Zhang HX, Mezei M, Cui M. Molecular docking: a powerful approach for structure-based drug discovery. *Curr Comput-Aided Drug Des*. **2011**, 7, 146–157.

Meyer BN, Ferrigni NR, Putnam JE, Jacobsen LB, Nichols DE, McLaughlin JL. Brine shrimp: a convenient general bioassay for active plant constituents. *Planta Med*. **1982**, 45, 31–34.

Mezei M. A new method for mapping macromolecular topography. *J Mol Graph Model*. **2003**, 21, 463–472.

Miller AH, Malteic V, Raison CL. Inflammation and its discontents: the role of cytokines in the pathophysiology of major depression. *Biol Psychiatry*. **2009**, 65, 732–741.

Miller LH, Su X. Artemisinin: Discovery from the Chinese herbal garden. *Cell*. **2011**, 146, 855–858.

Mishra BB, Tiwari VK. Natural products: an evolving role in future drug discovery. *Eur J Med Chem*. **2011**, 46, 4769–807.

Miura T, Itoh C, Iwamoto N, Kato M, Kawai M, Park SR, Suzuki I. Hypoglycemic activity of the fruit of the *Momordica charantia* in type 2 diabetic mice. *J Nutr Sci Vitaminol*. **2001**, 47, 340–344.

Moghadam FD, Baharara J, Balanezhad SZ, Jalali M, Amini E. Effect of *Holothuria leucospilota* extracted saponin on maturation of mice oocyte and granulosa cells. *Res Pharm Sci*. **2016**, 11, 130.

Molla SG, Motaal AA, Hefnawy HE, Fishawy AE. Cytotoxic activity of phenolic constituents from *Echinochloa crus-galli* against four human cancer cell lines. *Rev Bras Farmacogn*. **2016**, 26, 62–67.

Molli PR, Li DQ, Murray BW, Rayala SK, Kumar R. PAK signaling in oncogenesis. *Oncogene*. **2009**, 28, 2545.

Moreira PI. Alzheimer's disease and diabetes: An integrative view of the role of mitochondria, oxidative stress, and insulin. *J Alzheimers Dis*. **2012**, 30, S199–S215.

Morris GM, Goodsell DS, Halliday R, Huey R, Hart WE, Belew RK, Olson AJ. Automated docking using a Lamarckian genetic algorithm and an empirical binding free energy function. *J Comput Chem*. **1998**, 19, 1639–1662.

Moses H, Dorsey ER, Matheson DH, Thier SO. Financial anatomy of biomedical research. *Jama*. **2005**, 294, 1333–1342.

Multhoff G, Molls M, Radons J. Chronic inflammation in cancer development. *Front Immunol*. **2012**, 2, 98.

Myers S, Baker A. Drug discovery - an operating model for a new era. *Nat Biotechnol*. **2001**, 19, 727–730.

Nagai M, Tani M, Kishimoto Y, Iizuka M, Saita E, Toyozaki M, Kamiya T, Ikeguchi M, Kondo K. Sweet potato (*Ipomoea batatas* L.) leaves suppressed oxidation of low density lipoprotein (LDL) *in vitro* and in human subjects. *J Clin Biochem Nutr*. **2011**, 48, 203–208.

Nagamine R, Ueno S, Tsubata M, Yamaguchi K, Takagaki K, Hira T, Hara H, Tsuda T. Dietary sweet potato (*Ipomoea batatas* L.) leaf extract attenuates hyperglycemia by enhancing the secretion of glucagon-like peptide-1 (GLP-1). *Food Funct*. **2014**, 5, 2309–2316.

Nagata H, Takekoshi S, Takeyama R, Homma T, Yoshiyuki Osamura R. Quercetin enhances melanogenesis by increasing the activity and synthesis of tyrosinase

in human melanoma cells and in normal human melanocytes. *Pigment Cell Res*. **2004**, 17, 66–73.

Nakajima M, Shinoda I, Fukuwatari Y, Hayasawa H. Arbutin increases the pigmentation of cultured human melanocytes through mechanisms other than the induction of tyrosinase activity. *Pigment Cell Res*. **1998**, 11, 12–17.

Nalivaeva NN, Turner AJ. AChE and the amyloid precursor protein (APP)–Cross-talk in Alzheimer's disease. *Chem Biol Interact*. **2016**, 259, 301–306.

Ndontsa BL, Tala MF, Talontsi FM, Wabo HK, Tene M, Laatsch H, Tane P. New cytotoxic alkylbenzoquinone derivatives from leaves and stem of *Ardisia kivuensis* (Myrsinaceae). *Phytochem Lett*. **2012**, 5, 463–466.

Nguyen BCQ, Kim SA, Won SM, Park SK, Uto Y, Maruta H. 1, 2, 3-Triazolyl ester of ketorolac (15K): Boosting both heat-endurance and lifespan of *C. elegans* by down-regulating PAK1 at nM levels. *Drug Discov Ther*. **2018**, 12, 92–96.

Nguyen BCQ, Taira N, Maruta H, Tawata S. Artepillin C and other herbal PAK1-blockers: effects on hair cell proliferation and related PAK1-dependent biological function in cell culture. *Phytother Res*. **2016**, 30, 120–127.

Nguyen BCQ, Taira N, Tawata S. Several herbal compounds in Okinawa plants directly inhibit the oncogenic/aging kinase PAK1. *Drug Discov Ther*. **2014**, 8, 238–244.

Nguyen BCQ, Takahashi H, Uto Y, Shahinozzaman MD, Tawata S, Maruta H. 1,2,3-Triazolyl ester of Ketorolac: A "click chemistry"-based highly potent PAK1-blocking cancer-killer. *Eur J Med Chem*. **2017**a, 126, 270–276.

Nguyen BCQ, Yoshimura K, Kumazawa S, Tawata S, Maruta H. Frondoside A from sea cucumber and nymphaeols from Okinawa propolis: Natural anti-cancer

agents that selectively inhibit PAK1 *in vitro*. *Drug Discov Ther*. **2017**b, 11, 110–114.

Nguyen VT, Ueng JP, Tsai GJ. Proximate composition, total phenolic content, and antioxidant activity of Seagrape (*Caulerpa lentillifera*). *J Food Sci*. **2011**, 76, C950–C958.

Niazi S, Purohit M, Sonawani A, Niazi JH. Revealing the molecular interactions of aptamers that specifically bind to the extracellular domain of HER2 cancer biomarker protein: An *in silico* assessment. *J Mol Graph Model*. **2018**, 83, 112–121.

Nugara RN, Inafuku M, Takara K, Iwasaki H, Oku H. Pteryxin: a coumarin in *Peucedanum japonicum* Thunb leaves exerts antiobesity activity through modulation of adipogenic gene network. *Nutrition*. **2014**, 30, 1177–1184.

Ogawa H, Sakaki S, Yoshihira K, Natori S. The structures of ardisiaquinones A, B and C, bis (benzoquinonyl)-olefine derivatives from *Ardisia sieboldii* miquel. *Tetrahedron Lett*. **1968**, 9, 1387–1392.

Omar YM, Abdu-Allah HH, Abdel-Moty SG. Synthesis, biological evaluation and docking study of 1, 3, 4-thiadiazole-thiazolidinone hybrids as anti-inflammatory agents with dual inhibition of COX-2 and 15-LOX. *Bioorg Chem*. **2018**, 80, 461–471.

Osman NI, Sidik NJ, Awal A, Adam NA, Rezali NI. *In vitro* xanthine oxidase and albumin denaturation inhibition assay of *Barringtonia racemosa* L. and total phenolic content analysis for potential anti-inflammatory use in gouty arthritis. *J Intercult Ethnopharmacol*. **2016**, 5, 343–349.

Ou-Yang SS, Lu JY, Kong XQ, Liang ZJ, Luo C, Jiang H. Computational drug discovery. *Acta Pharmacol Sin*. **2012**, 33, 1131.

Parveen M, Ahmad F, Malla AM, Azaz S, Alam M, Basudan OA, Silva MR, Silva PSP. Acetylcholinesterase and cytotoxic activity of chemical constituents of *Clutia lanceolata* leaves and its molecular docking study. *Nat Prod Bioprospect*. **2016**, 6, 267–278.

Paul DJ, Laure NB, Guru SK, Khan IA, Ajit SK, Vishwakarma RA, Pierre T. Antiproliferative and antimicrobial activities of alkylbenzoquinone derivatives from *Ardisia kivuensis*. *Pharm Biol*. **2014**, 52, 392–397.

Pawelec G, Goldeck D, Derhovanessian E. Inflammation, ageing and chronic disease. *Curr Opin Immunol*. **2014**, 29, 23–28.

Phiel CJ, Wilson CA, Lee VM, Klein PS. GSK-3alpha regulates production of Alzheimer's disease amyloid-beta peptides. *Nature*. **2003**, 423, 435–439.

Pripp AH. Docking and virtual screening of ACE inhibitory dipeptides. *Eur Food Res Technol*. **2007**, 225, 589–592.

Radu M, Semenova G, Kosoff R, Chernoff J. PAK signalling during the development and progression of cancer. *Nat Rev Cancer*. **2014**, 14, 13.

Raghupathi W, Raghupathi V. An Empirical Study of Chronic Diseases in the United States: A Visual Analytics Approach to Public Health. *Int J Env Res Public Health*. **2018**, 15, 431.

Raman A, Lau C. Anti-diabetic properties and phytochemistry of *Momordica charantia* L.(Cucurbitaceae). *Phytomedicine*. **1996**, 2, 349–362.

Rarey M, Kramer B, Lengauer T, Klebe G. A fast flexible docking method using an incremental construction algorithm. *J Mol Biol*. **1996**, 261, 470–489.

Rauf A, Khan R, Khan H, Tokuda H. Cytotoxic, antitumour-promoting and inhibition of protein denaturation effects of flavonoids, isolated from *Potentilla evestita* Th. Wolf. *Nat Prod Res*. **2015**, 29, 1775–1778.

Rayan A, Raiyn J, Falah M. Nature is the best source of anticancer drugs: Indexing natural products for their anticancer bioactivity. *PloS One*. **2017**, 12, e0187925.

Razzaghi-Asl N, Mirzayi S, Mahnam K, Sepehri S. Identification of COX-2 inhibitors via structure-based virtual screening and molecular dynamics simulation. *J Mol Graph Model.* **2018**, 83, 138–152.

Reger MA, Watson GS, Green PS, Wilkinson CW, Baker LD, Cholerton B, Fishel MA, Plymate SR, Breitner JCS, DeGroodt W, et al. Intranasal insulin improves cognition and modulates beta-amyloid in early AD. *Neurology*. **2008**, 70, 440–448.

Reitz C, Brayne C, Mayeux R. Epidemiology of Alzheimer disease. *Nat Rev Neurol*. **2011**, 7, 137–52.

Reuter S, Gupta SC, Chaturvedi MM, Aggarwal BB. Oxidative stress, inflammation, and cancer: How are they linked? *Free Radic Biol Med*. **2010**, 49, 1603–1616.

Ricciotti E, Fitzgerald GA. Prostaglandins and inflammation. *Arterioscler Thromb Vasc Biol*. **2011**, 31, 986–1000.

Ridzwan BH. *Sea Cucumbers, A Malaysian Heritage*, 1st ed.; Research Centre of International Islamic University Malaysia (IIUM): Kuala Lumpur Wilayah Persekutuan, Malaysia, **2007**, ISBN 9789833855117.

Riley PA. Melanogenesis and melanoma. *Pigment Cell Res*. **2003**, 16, 548–552.

Roberts CM, Mittermeier CG, Schueler FW. Marine biodiversity hotspots and conservation priorities for tropical reefs. *Science*. **2002**, 295, 1280–1285.

Roses AD. Commentary on “a roadmap for the prevention of dementia: The inaugural Leon Thal Symposium.” An impending prevention clinical trial for Alzheimer’s disease: Roadmaps and realities. *Alzheimers Dement*. **2008**, 4, 164–166.

Ruhsam M, Hollingsworth PM. Authentication of eleutherococcus and rhodiola herbal supplement products in the United Kingdom. *J Pharm Biomed Anal*. **2017**, 149, 403–409.

Sadleir KR, Kandalepas PC, Buggia-Prévot V, Nicholson DA, Thinakaran G, Vassar R. Presynaptic dystrophic neurites surrounding amyloid plaques are sites of microtubule disruption, BACE1 elevation, and increased Ab generation in Alzheimer’s disease. *Acta Neuropathol*. **2016**, 132, 235–256.

Salen P, De Lorgeril M. The Okinawan diet: a modern view of an ancestral healthy lifestyle. In: Healthy Agriculture, Healthy Nutrition, Healthy People; Karger Publishers; **2011**, 102, 114–123.

Sarfaraj HM, Sheeba F, Saba A, Mohd S. Marine natural products: A lead for anti-cancer. *Indian J Mar Sci*. **2012**, 41, 27–39.

Saso L, Valentini G, Casini ML, Grippa E, Gatto MT, Leone MG, Silvestrini B. Inhibition of heat-induced denaturation of albumin by nonsteroidal antiinflammatory drugs (NSAIDs): pharmacological implications. *Arch Pharmacol Res*. **2001**, 24, 150–158.

Sato T, Hanyu H, Hirao K, Kanetaka H, Sakurai H, Iwamoto T. Efficacy of PPAR- γ agonist pioglitazone in mild Alzheimer disease. *Neurobiol Aging*. **2011**, 32, 1626–1633.

Seo SY, Sharma VK, Sharma N. Mushroom tyrosinase: recent prospects. *J Agric Food Chem*. **2003**, 51, 2837–2853.

Shahinozzaman M, Ishii T, Gima S, Ngyuen BCQ, Hossain MA, Tawata S. Anti-inflammatory and anti-melanogenic effects of major leaf components of *Alpinia zerumbet* var. *excelsa*. *Phcog Mag.* **2018**a, 14, 578–586.

Shahinozzaman M, Ishii T, Takano R, Halim M, Hossain M, Tawata S. Cytotoxic desulfated saponin from *Holothuria atra* predicted to have high binding affinity to the oncogenic kinase PAK1: A combined *in vitro* and *in silico* study. *Sci Pharm*. **2018**b, 86, p. 32.

Shahinozzaman M, Taira N, Ishii T, Halim M, Hossain M, Tawata S. Anti-inflammatory, anti-diabetic, and anti-Alzheimer's effects of prenylated flavonoids from Okinawa propolis: an investigation by experimental and computational studies. *Molecules*. **2018**c, 23, p. 2479.

Sharma JN, Al-Omran A, Parvathy SS. Role of nitric oxide in inflammatory diseases. *Inflammopharmacology*. **2007**, 15, 252–259.

Shekhar C. *In silico* pharmacology: computer-aided methods could transform drug development. *Chem Biol*. **2008**, 15, 413–414.

Shimabukuro K. Syokubutsu zenkoku taikai kinenshi Okinawa no seibutsu *(in Japanese)* [Commemoration of nationwide convention of Okinawan plants and organism]. *Okinawa seibutsu kyoiku kenkyukai* / *Okinawan Society of biological educational study*. **1984**, 23–32.

Shinjo S, Yamamoto S. Okinawa no choujushoku; shokeikatsu no jikkentekikenshou. In: *Okinawa no Chouju (in Japanese)*; Eds. Sho H & Yamamoto S. Center for Academic Societies, Japan, Toyonaka, **1999**, 79–103.

Shoelson SE, Lee J, Goldfine AB. Inflammation and insulin resistance. *J Clin Invest.* **2006**, 116, 1793–1801.

Shroder H, Vila J, Marrugat J, Covas MI. Low energy density diets are associated with favorable nutrient intake profile and adequacy in free-living elderly men and women. *J Nutr*. **2008**, 138, 1476–1481.

Sliwoski G, Kothiwale S, Meiler J, Lowe EW. Computational methods in drug discovery. *Pharmacol Rev*. **2014**, 66, 334–395.

Smith EM, Grosser T, Wang M, Yu Y, FitzGerald GA. Prostanoids in health and disease. *J Lipid Res.* **2009**, 50, S423–428.

Solis PN, Wright CW, Anderson MM, Gupta MP, Phillipson JD. A microwell cytotoxicity assay using *Artemia salina* (brine shrimp). *Planta Med*. **1993**, 59, 250–252.

Song CM, Lim SJ, Tong JC. Recent advances in computer-aided drug design. *Brief. Bioinformatics*. **2009**, 10, 579–591.

Song YS, Park EH, Hur GM, Ryu YS, Lee YS, Lee JY, Kim YM, Jin C. Caffeic acid phenethyl ester inhibits nitric oxide synthase gene expression and enzyme activity. *Cancer Lett*. **2002**, 175, 53–66.

Souli I, Jemni M, Rodríguez-Verástegui LL, Chaira N, Artés F, Ferchichi A. Phenolic composition profiling of Tunisian 10 varieties of common dates (*Phoenix dactylifera* L.) at tamar stage using LC-ESI-MS and antioxidant activity. *J Food Biochem*. **2018**, e12634.

Stanikunaite R, Khan SI, Trappe JM, Ross SA. Cyclooxygenase-2 inhibitory and antioxidant compounds from the truffle *Elaphomyces granulatus*. *Phytother Res*. **2009**, 23, 575–578.

Stanley M, Macauley SL, Holtzman DM. Changes in insulin and insulin signaling in Alzheimer's disease: Cause or consequence? *J Exp Med*. **2016**, 213, 1375–1385.

Stumpfe D, Ripphausen P, Bajorath J. Virtual compound screening in drug discovery. *Future Med Chem*. **2012**, 4, 593–602.

Sugawara T, Zaima N, Yamamoto A, Sakai S, Noguchi R, Hirata T. Isolation of sphingoid bases of sea cucumber cerberosides and their cytotoxicity against human colon cancer cells. *Biosci Biotechnol Biochem*. **2006**, 70, 2906–2912.

Sulpizi M, Folkers G, Rothlisberger U, Carloni P, Scapozza L. Applications of density functional theory-based methods in medicinal chemistry. *Quant Struct-Act Relat*. **2002**, 21, 173–181.

Sun J. Vitamin D: Anti-inflammatory effects to prevent and treat diseases. In: Vitamin D: Oxidative Stress, Immunity, and Aging; Ed. Gombart AF; CRC Press, Taylor & Francis Group: Boca Raton, FL, USA, **2012**, 307–316.

Surh Y-J, Chun K-S, Cha H-H, Han SS, Keum Y-S, Park K-K, Lee SS. Molecular mechanisms underlying chemopreventive activities of anti-inflammatory phytochemicals: down-regulation of COX-2 and iNOS through suppression of NF-κB activation. *Mutat Res Fundam Mol Mech Mutagen*. **2001**, 480, 243–268.

Taha M, Shah SA, Afifi M, Imran S, Sultan S, Rahim F, Khan KM. Synthesis, α-glucosidase inhibition and molecular docking study of coumarin based derivatives. *Bioorg Chem*. **2018**, 77, 586–592.

Taira N, Nguyen BCQ, Be Tu PT, Tawata S. Effect of Okinawa propolis on PAK1 activity, *Caenorhabditis elegans* longevity, melanogenesis, and growth of cancer cells. *J Agric Food Chem*. **2016**, 64, 5484–589.

Taira N, Nguyen BCQ, Tawata S. Hair growth promoting and anticancer effects of p21-activated kinase 1 (PAK1) inhibitors isolated from different parts of *Alpinia zerumbet*. *Molecules*. **2017**, 22, 132.

Tak PP, Firestein GS. NF-κB: a key role in inflammatory diseases. *J Clin Invest*. **2001**, 107, 7–11.

Takahashi M, Hirose N, Ohno S, Arakaki M, Wada K. Flavor characteristics and antioxidant capacities of hihatsumodoki (*Piper retrofractum* Vahl) fresh fruit at three edible maturity stages. *J Food Sci Technol*. **2018**, 55, 1295–1305.

Takeuchi N, Kasama T, Aida Y, Oki J, Maruyama I, Watanabe K, Tobinaga S. Pharmacological activities of the prenylcoumarins, developed from folk usage as a medicine of *Peucedanum japonicum* Thunb. *Chem Pharm Bull (Tokyo)*. **1991**, 396, 1415–1421.

Tamir S, Tannenbaum SR. The role of nitric oxide (NO) in the carcinogenic process. *Biochim Biophys Acta - Rev Cancer*. **1996**, 1288, F31–F36.

Tan JJ, Cong XJ, Hu LM, Wang CX, Jia L, Liang XJ. Therapeutic strategies underpinning the development of novel techniques for the treatment of HIV infection. *Drug Discov Today*. **2010**, 15, 186–197.

Tawata S, Fukuta M, Xuan TD, Deba F. Total utilization of tropical plants *Leucaena leucocephala* and *Alpinia zerumbet*. *J Pestic Sci*. **2008**, 33, 40–43.

Tawata S, Ota H. Okinawa no yakuso Hyakka: dare ni demo dekiru yakuso no riyoho: yasasi senzikata to nomikata (*in Japanese*) [Encyclopedia of Okinawan herbs:

Traditional usage of medicinal herbs: How to make decoction and drink herb gently]. *Naha syuppansya / Naha publishing company*. **1998**.

Teschke R, Xuan TD. A contributory role of shell ginger (*Alpinia zerumbet*) for human longevity in Okinawa, Japan?. *Nutrients*. **2018**, 10, 166.

The world health report 1998. Life in the 21st century: a vision for all. Geneva, World Health Organization, **1998**.

Thomford NE, Senthebane DA, Rowe A, Munro D, Seele P, Maroyi A, Dzobo K. Natural products for drug discovery in the 21st century: Innovations for novel drug discovery. *Int J Mol Sci.* **2018**, 19.

Tian F, Zhang XW, Tong YG, Yi YH, Zhang SL, Li L, Sun P, Lin L, Ding J. PE, a new sulfated saponin from sea cucumber, exhibits anti-angiogenic and anti-tumor activities *in vitro* and *in vivo*. *Cancer Biol Ther*. **2005**, 4, 874–884.

Tian X, Tang H, Lin H, Cheng G, Wang S, Zhang X. Saponins: The potential chemotherapeutic agents in pursuing new anti-glioblastoma drugs. *Mini Rev Med Chem*. **2013**, 13, 1709–1724.

Tomita Y, Maeda K, Tagami H. Mechanisms for hyperpigmentation in postinflammatory pigmentation, urticaria pigmentosa and sunburn. *Dermatology*. **1989**, 179, 49–53.

Trott O, Olson AJ. AutoDock Vina: improving the speed and accuracy of docking with a new scoring function, efficient optimization, and multithreading. *J Comput Chem*. **2010**, 31, 455–461.

Ueda K, Uemura D. Bioactive marine metabolites from Okinawan waters. In: Studies in natural products chemistry; Ed. Atta-ur-Rahman. Elsevier, **2008**, 57–100.

Upadhyay A, Chompoo J, Kishimoto W, Makise T, Tawata S. HIV-1 integrase and neuraminidase inhibitors from *Alpinia zerumbet*. *J Agric Food Chem*. **2011**, 59, 2857–2862.

Van Dyck S, Gerbaux P, Flammang P. Qualitative and quantitative saponin contents in five sea cucumbers from the Indian Ocean. *Mar Drugs*. **2010**, 8, 173–189.

Van Thanh N, Dang NH, van Kiem P, Cuong NX, Huong HT, van Minh C. A new triterpene glycoside from the sea cucumber *Holothuria scabra* collected in Vietnam. *ASEAN J Sci Technol Dev*. **2017**, 23, 253–259.

Veber DF, Johnson SR, Cheng HY, Smith BR, Ward KW, Kopple KD. Molecular properties that influence the oral bioavailability of drug candidates. *J Med Chem*. **2002**, 45, 2615–2623.

Veeresham C. Natural products derived from plants as a source of drugs. *J Adv Pharm Technol Res*. **2012**, 3, 200–201.

Vitale P, Tacconelli S, Perrone MG, Melerba P, Simone L, Scilimati A, Lavecchia A, Dovizio M, Marcantoni E, Bruno A, et al. Synthesis, pharmacological characterization, and docking analysis of a novel family of diarylisoxazoles as highly selective cyclooxygenase-1 (COX-1) inhibitors. *J Med Chem.* **2013**, 56, 4277–4299.

Wang J, Wu JW, Wang ZX. Structural insights into the autoactivation mechanism of p21-activated protein kinase. *Structure*. **2011**, 19, 1752–1761.

Wang Z, Sun H, Yao X, Li D, Xu L, Li Y, Tian S, Hou T. Comprehensive evaluation of ten docking programs on a diverse set of protein-ligand complexes: the prediction accuracy of sampling power and scoring power. *Phys Chem Chem Phys*. **2016**, 18, 12964–12975.

Weisberg E, Manley PW, Breitenstein W, Brüggen J, Cowan-Jacob SW, Ray A, Huntly B, Fabbro D, Fendrich G, Hall-Meyers E, et al. Characterization of AMN107, a selective inhibitor of native and mutant Bcr-Abl. *Cancer cell*. **2005**, 7, 129–141.

White KN, Reimer JD. Commensal Leucothoidae (Crustacea, Amphipoda) of the Ryukyu Archipelago, Japan. Part I: ascidian dwellers. *ZooKeys*. **2012**, 163, 13–55.

Willcox BJ, Willcox CD, Suzuki M. The Okinawa Way: How to improve your health and longevity dramatically. *Penguin UK*. **2013**.

Willcox BJ, Willcox DC, Todoriki H, Fujiyoshi A, Yano K, He Q, Curb JD, Suzuki M. Caloric restriction, the traditional Okinawan diet, and healthy aging. The diet of the world's longest-lived people and its potential impact on morbidity and life span. *Ann N Y Acad Sci*. **2007**, 1114, 434–455.

Willcox DC, Scapagnini G, Willcox BJ. Healthy aging diets other than the Mediterranean: a focus on the Okinawan diet. *Mech Ageing Dev*. **2014**, 136, 148–162.

Willcox DC, Willcox BJ, Todoriki H, Suzuki M. The Okinawan diet: Health implications of a low calorie, nutrient-dense, antioxidant-rich dietary pattern low in glycemic load. *J Am Coll Nutr*. **2009**, 28, 500S–516S.

Willcox DG, Willcox BJ, Suzuki M. The Okinawa Program. New York, Three Rivers Press, **2001**.

Wright GD. Opportunities for natural products in 21st century antibiotic discovery. *Nat Prod Rep*. **2017**, 34, 694–701.

Wu C. An important player in brine shrimp lethality bioassay: The solvent. *J Adv Pharm Technol Res*. **2014**, 5, 57–58.

Wu QY, Wong ZC, Wang C, Fung AH, Wong EO, Chan GK, Dong TT, Chen Y, Tsim KW. Isoorientin derived from *Gentiana veitchiorum* Hemsl. flowers inhibits melanogenesis by down-regulating MITF-induced tyrosinase expression. *Phytomedicine*. **2019**, 57, 129–136.

Xiang M, Cao Y, Fan W, Chen L, Mo Y. Computer-aided drug design: lead discovery and optimization. *Comb Chem High Throughput Screen*. **2012**, 15, 328–337.

Yang LK, Khoo-Beattie C, Goh KL, Chng BL, Yoganathan K, Lai YH, Butler MS. Ardisiaquinones from *Ardisia teysmanniana*. *Phytochemistry*. **2001**, 58, 1235–1238.

Yao H, Liu J, Xu S, Zhu Z, Xu J. The structural modification of natural products for novel drug discovery. *Expert Opin Drug Discovery*. **2017**, 12, 121–140.

Yatoo MI, Gopalakrishnan A, Saxena A, Parray OR, Tufani NA, Chakraborty S, Tiwari R, Dhama K, Iqbal HM. Anti-inflammatory drugs and herbs with special emphasis on herbal medicines for countering inflammatory diseases and disorders-a review. *Recent Pat Inflamm Allergy Drug Discov*. **2018**, 12, 39–58.

Ye DZ, Field J. PAK signaling in cancer. *Cell Logist*. **2012**, 2, 105–116.

Yoshikawa M, Shimada H, Matsuda H, Yamahara J, Murakami N. Bioactive constituents of Chinese natural medicines. I. New sesquiterpene ketones with vasorelaxant effect from chinese moxa, the processed leaves of *Artemisia argyi* LEVL. ET VANT.: Moxartenone and moxartenolide. *Chem Pharm Bull (Tokyo)*. **1996**, 44, 1656–1662.

Yoshimoto M, Yahara S, Okuno S, Islam MS, Ishiguro K, Yamakawa O. Antimutagenicity of mono-, di-, and tricaffeoylquinic acid derivatives isolated from sweet potato (*Ipomoea batatas* L.) leaf. *Biosci Biotechnol Biochem*. **2002**, 66, 2336–2341.

Yun SH, Park ES, Shin SW, Na YW, Han JY, Jeong JS, Shastina VV, Stonik VA, Park JI, Kwak JY. Stichoposide C induces apoptosis through the generation of ceramide in leukemia and colorectal cancer cells and shows *in vivo* antitumor activity. *Clin Cancer Res*. **2012**, 18, 5934–5948.

Zarghi A, Arfaei S. Selective COX-2 inhibitors: a review of their structure-activity relationships. *Iran J Pharm Res*. **2011**, 10, 655.

Zasada M, Dębowska R, Pasikowska M, Ostrowska B, Budzisz E. Efficacy of tri-active brightening and anti-aging complex in treatment of facial skin hyperpigmentation. *J Pharm Pharmacol*. **2016**, 4, 564–573.

Zhang S. Computer-aided drug discovery and development. *Methods Mol Biol*. **2011**, 716, 23–38.

Zhao YH, Abraham MH, Le J, Hersey A, Luscombe CN, Beck G, Sherborne B, Cooper I. Rate-limited steps of human oral absorption and QSAR studies. *Pharm Res*. **2002**, 19, 1446–1457.

Zheng Y, Wu FE. Resorcinol derivatives from Ardisia maculosa. *J Asian Nat Prod Res*. **2007**, 9, 545–549.

Zhou HY, Shin EM, Guo LY, Youn UJ, Bae K, Kang SS, Zou LB, Kim YS. Anti-inflammatory activity of 4-methoxyhonokiol is a function of the inhibition of iNOS and COX-2 expression in RAW 264.7 macrophages via NF-kappaB, JNK and p38 MAPK inactivation. *Eur J Pharmacol*. **2008**, 586, 340–349.

Zihad SM, Bhowmick N, Uddin SJ, Sifat N, Rahman M, Rouf R, Islam MT, Dev S, Hazni H, Aziz S, et al. Analgesic activity, chemical profiling and computational study on *Chrysopogon aciculatus*. *Front Pharmacol*. **2018**, 9, 1164.

Zou ZR, Yi YH, Wu HM, Wu JH, Liaw CC, Lee KH. Intercedensides A–C, three new cytotoxic triterpene glycosides from the sea cucumber *Mensamaria intercedens* Lampert. *J Nat Prod*. **2003**, 66, 1055–1060.